CONTRACTOR REPORT

SAND81-7112
Unlimited Release
UC-63c

Accelerated Aging of GaAs Concentrator Solar Cells

Paul E. Gregory
Varian Associates, Inc., Solid State Laboratory
611 Hansen Way, Palo Alto, CA 94303

Prepared by Sandia National Laboratories Albuquerque, New Mexico 87185
and Livermore, California 94550 for the United States Department of Energy
under Contract DE-AC04-76DP00789

Printed April 1982

When printing a copy of any digitized SAND Report, you are required to update the markings to current standards.

Issued by Sandia National Laboratories, operated for the United States Department of Energy by Sandia Corporation.
NOTICE: This report was prepared as an account of work sponsored by an agency of the United States Government. Neither the United States Government nor any agency thereof, nor any of their employees, nor any of their contractors, subcontractors, or their employees, makes any warranty, express or implied, or assumes any legal liability or responsibility for the accuracy, completeness, or usefulness of any information, apparatus, product, or process disclosed, or represents that its use would not infringe privately owned rights. Reference herein to any specific commercial product, process, or service by trade name, trademark, manufacturer, or otherwise, does not necessarily constitute or imply its endorsement, recommendation, or favoring by the United States Government, any agency thereof or any of their contractors or subcontractors. The views and opinions expressed herein do not necessarily state or reflect those of the United States Government, any agency thereof or any of their contractors or subcontractors.

Printed in the United States of America
Available from
National Technical Information Service
U.S. Department of Commerce
5285 Port Royal Road
Springfield, VA 22161

NTIS price codes
Printed copy: A07
Microfiche copy: A01

Distribution
Category UC-63c

SAND81-7112
Unlimited Distribution
Printed April 1982

ACCELERATED AGING OF GaAs CONCENTRATOR SOLAR CELLS

Paul E. Gregory
Varian Associates, Inc.
Solid State Laboratory
611 Hansen Way
Palo Alto, CA 94303

ABSTRACT

An accelerated aging study of AlGaAs/GaAs solar cells has been completed. The purpose of the study was to identify the possible degradation mechanisms of AlGaAs/GaAs solar cells in terrestrial applications. Thermal storage tests and accelerated AlGaAs corrosion studies were performed to provide an experimental basis for a statistical analysis of the estimated lifetime. Results of this study suggest that a properly designed and fabricated AlGaAs/GaAs solar cell can be mechanically rugged and environmentally stable with projected lifetimes exceeding 100 years.

Prepared for Sandia National Laboratories under Contract 13-5674.

TABLE OF CONTENTS

Section		Page
I.	INTRODUCTION	1
II.	THERMAL STORAGE TESTS OF SOLAR CELLS	3
	A. Test Procedures	3
	1. The Solar Cell and Its Package	3
	2. Equipment for Thermal Storage Tests	7
	3. Test Procedures	9
	B. Test Results and Analysis	12
	1. One-sun Performance Results	12
	2. Analysis of Test Results for Cell Lifetime	55
	3. Solar Cell Surface Degradation	78
III.	OTHER THERMAL STORAGE TESTS	94
	A. Ohmic Contacts	94
	1. Test Patterns	94
	2. Ohmic Contact Data Analysis	94
	3. Ohmic Contact Test Results	99
	B. Electromigration	103
IV.	CORROSION TESTS	105
V.	ROOF TESTS	118
VI.	SOLAR CELL FABRICATION	129
VII.	CONCLUSIONS AND RECOMMENDATIONS	132
	REFERENCES	135

I. INTRODUCTION

An accelerated aging study of AlGaAs/GaAs solar cells has been carried out. The purpose of the study was to identify the possible degradation mechanisms of GaAs solar cells in terrestrial applications. Two types of experiments were carried out for the study: thermal storage tests, and AlGaAs corrosion studies.

The thermal storage tests were performed in order to assess degradation mechanisms, such as diffusion, which are thermally activated. Groups of unpackaged GaAs solar cells were stored at temperatures far in excess of any likely operating temperature, and their response to one-sun illumination was periodically measured. The cells proved to be quite rugged; it was necessary to subject them to higher temperatures than had been expected. Groups of solar cells were stored at 400°C and 425°C in nitrogen ambient and 250°C and 320°C in air ambient, and were subjected to thermal cycling between 25°C and 400°C in nitrogen ambient. The tests at 400°C and 250°C were both continued for over 3000 hours.

A statistical analysis was performed on the results of the thermal stress tests in order to project an estimated cell lifetime at expected operating temperatures. The result obtained from the analysis was at a cell temperature of 100°C; the median lifetime for the cell output power to drop by 20% of its initial value is between 5700 and 30,000 years. These results indicate that thermally-excited failure mechanisms within the cell itself (not including the cell package) should <u>not</u> be a limitation for the use of GaAs solar cells in practical systems.

The AlGaAs corrosion experiments assessed the vulnerability of the high aluminum-content AlGaAs window layer to atmospheric corrosion. The AlGaAs layer is protected from the atmosphere in these cells by a 700 Å thick Si_3N_4 optical antireflection coating. It was found that it is necessary to deposit the Si_3N_4 with the cell held at 400°C or above for

the Si_3N_4 to be sufficiently dense to protect the AlGaAs. Furthermore, it was found that AlGaAs/GaAs cells produced by organometallic vapor phase epitaxy (OM) are much more resistant to AlGaAs corrosion than are cells produced by liquid phase epitaxy (LPE). Experiments seem to indicate that the greater corrosion resistance of the OM cells is caused by the AlGaAs layer being thinner on the OM cells than it is on the LPE cells.

The results of this study provide a good basis for belief that a properly-fabricated AlGaAs/GaAs solar cell is a rugged, environmentally-stable device.

II. THERMAL STORAGE TESTS OF SOLAR CELLS

Groups of solar cells were subjected to thermal storage tests in both nitrogen and air ambients, and to a thermal cycling test in nitrogen. The tests are intended to accelerate diffusion and any other thermally-activated degradation mechanisms.

In the following sections, we describe the cells used in the tests and the procedures and equipment used to carry out the tests. Finally, we present the results of the tests and analyze the results in order to extrapolate cell lifetime to temperatures at which the cells would normally operate.

A. Test Procedures

1. The Solar Cell and Its Package

The solar cell epitaxial structure, contact grid, and package are shown in Fig. 2-1a, b, and c, respectively. This solar cell has been under development at Varian for the last several years.[1] The cell is a GaAs p-n junction device which has a high aluminum-content AlGaAs window layer. The function of the AlGaAs window layer is to reduce the surface recombination greatly at the upper GaAs surface. The AlGaAs layer is subject to corrosion by the air, so it must be protected from the atmosphere. During processing, the AlGaAs is protected by a GaAs "cap" layer grown over it. Just before packaging the cell, the cap layer is etched off the active cell areas, and a Si_3N_4 layer, approximately 700 Å thick, is deposited on the cell surface. The Si_3N_4 has the dual function of protecting the AlGaAs from atmospheric attack, and of serving as an optical antireflection (AR) coating for the solar cell. The Si_3N_4 layer is deposited by rf plasma reaction of SiH_4 and N_2, with the solar cell held at 400°C in an LFE Model PND-301 deposition system. Usually,

Figure 2-1

SCHEMATIC CROSS-SECTION OF GaAs SOLAR CELL

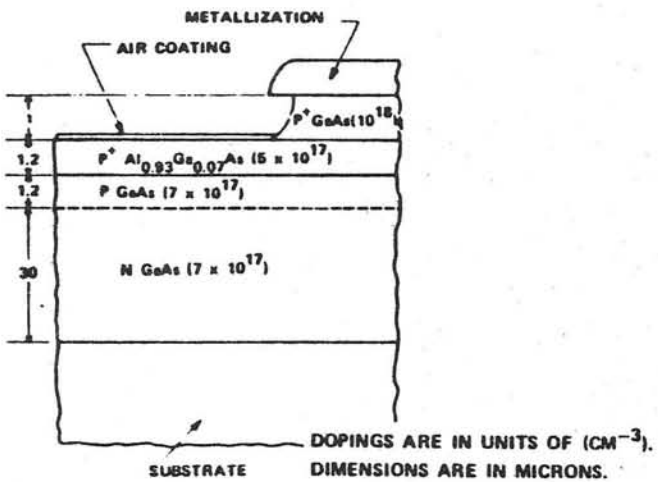

TOP GRID CONTACT PATTERN

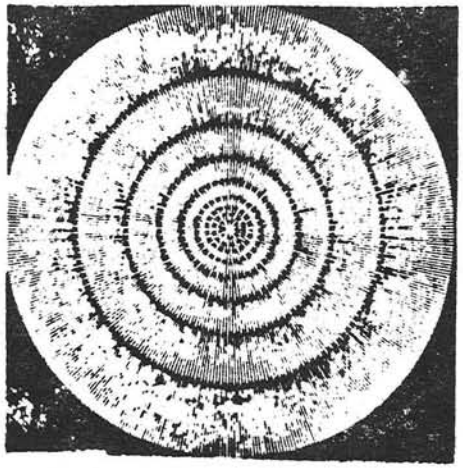

SOLAR CELL PACKAGE CROSS SECTION

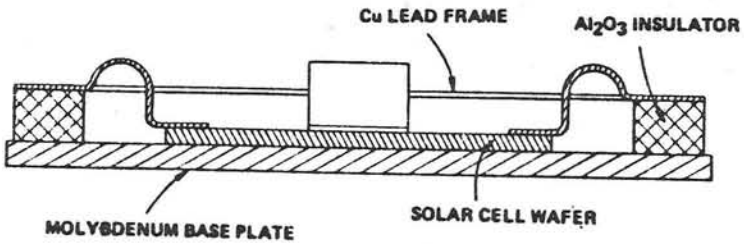

three cells are coated simultaneously along with a Si test piece. The quality of the AR coating is monitored by measuring the thickness and index of refraction of the Si_3N_4 on the Si test piece with an ellipsometer.

At the time this contract was begun, the GaAs and AlGaAs layers for Varian solar cells were usually grown by liquid phase epitaxy (LPE). An alternative growth technique, organometallic vapor phase epitaxy (OM-VPE, or just OM), had been under development at Varian for several years. Shortly after the accelerated aging program began, it became possible to routinely produce high-quality solar cells by OM. Since the thermal storage tests had begun with LPE cells, it was decided to continue to concentrate on LPE cells for those tests. All but two of the cells used in the thermal storage tests were LPE grown. Experiments to measure AlGaAs corrosion resistance, described in a later section, were performed on both LPE and OM cells, and the OM cells were found to have a greater corrosion resistance than the LPE cells. Partly as a result of those experiments, it was decided to produce only OM cells for future work. Both OM and LPE cells were delivered to Sandia under the cell delivery requirements for this contract.

The OM and LPE cells are similar in structure. The major differences are that the OM cells have Zn as a p-type dopant, while the LPE cells are Mg doped and the AlGaAs layer is typically 1500 Å thick in the OM cells versus 7000 Å in the LPE cells.

The front contact grid, seen in Fig. 2-1b, is a 1/3-inch radial pattern on a 0.36-inch square cell, and is formed by conventional photolithographic techniques. The front contact metal system, starting with the layer closest to the cell, is 300 Å Au/125 Å Mg/300 Å Au/1000 Å Ti-W/ 1500 Å Au. The back contact metal system is 100 Å Au/250 Å Sn/100 Å Au/ 1000 Å Ti-W/500 Å Au/4500 Å Ag. The contacts are alloyed in a belt furnace under a nitrogen atmosphere. The front contact series resistance is lowered by electroplating a 2-micron thick gold layer onto the grid pattern.

A cutaway of a packaged 1/3-inch cell is shown in Fig. 2-1c. The cell shown is soldered to a molybdenum baseplate using an Ag-Sn eutectic solder preform in a vacuum soldering station. The top contact is made by a gold-plated copper leadframe that is soldered to the cell corners with Pb-In paste solder (Indalloy #7). The leadframe soldering is done in a belt furnace. A similar package is used for 0.49-inch diameter cells, but has a metallized ceramic baseplate instead of the molybdenum baseplate. The ceramic baseplate provides electrical isolation between the cell and coolant water in the solar array.

The maximum temperature which the cell package can withstand is limited by the 180°C solidus temperature of the leadframe solder. It was originally hoped to develop a high-temperature cell package for the accelerated aging study by using Au-Ge solder, but we were unable to develop a technique for attaching the leadframe using Au-Ge solder. The Au-Ge eutectic temperature is 356°C. As discussed below, temperatures of 400°C or more were required to obtain a significant number of failed cells, so the Au-Ge solder would not have withstood the required temperatures anyway. Furthermore, results of a thermal storage test at 425°C with cells Au-Ge soldered (on the back side only) to ceramic trays showed that the solder itself can cause cell failures at high temperatures. Thus the thermal storage tests were limited to tests on unpackaged solar cells. The use of unpackaged cells means that the test results are valid for failure mechanisms intrinsic to the cell and are independent of any associated with a package.

The unpackaged solar cells were handled in two ways: completely loose cells, and cells soldered to ceramic trays. The ceramic trays were developed to minimize cell damage caused by handling of individual cells during testing, and to provide an easy means of identifying each cell. The ceramic trays were alumina substrates 2.5 inches x 1 inch x 0.02 inch thick with metallized areas to which the cells were soldered. The metallized areas were formed by painting on moly-manganese paste,

firing at 1400°C, and then plating up with nickel and gold. Five cells were soldered to each tray with Au-Ge solder.

After the test at 425°C had shown that the solder could cause the cells to short out, an aluminum cell holder was fabricated for handling the loose, unsoldered cells. Cells are placed in 0.4-inch square recessed areas in an aluminum block 2.6 x 1.2 inches by 0.25 inches thick, with space for ten cells per holder. These cell holders were used for the four loose cells stored at 425°C in nitrogen and the ten cells stored at 320°C in air.

2. Equipment for Thermal Storage Tests

For thermal storage of cells below 320°C, three Blue-M model IGF-146F-3 ovens were purchased. These are controlled atmosphere ovens, intended to be used with inert gases, such as nitrogen or argon. However, the testing at 400°C in nitrogen showed such a low failure rate that it was apparent that there was no point in testing cells at or below 320°C in nitrogen ambient. Therefore, one oven was connected to compressed air and used for the storage of ten cells in air at 320°C. (The connection to compressed air was necessary to provide the gas flow through the oven required for cooling internal oven seals.)

A small Blue-M oven Model OV-8A was used to store cells at 250°C in air. For the tests at 400°C and 425°C, the cells were stored in roll-on Marshall furnaces which had previously been used for LPE growth reactors. Figure 2-2 shows roll-on furnaces similar to those used in this work. The cylindrical furnace is mounted on wheels which roll in tracks, allowing the furnace to roll on and off the quartz tube. The cells under test are placed in the quartz tube on a graphite boat or in the aluminum cell holder. The nitrogen ambient gas (from the building nitrogen gas lines) flows through the quartz tube and out through an

Figure 2-2

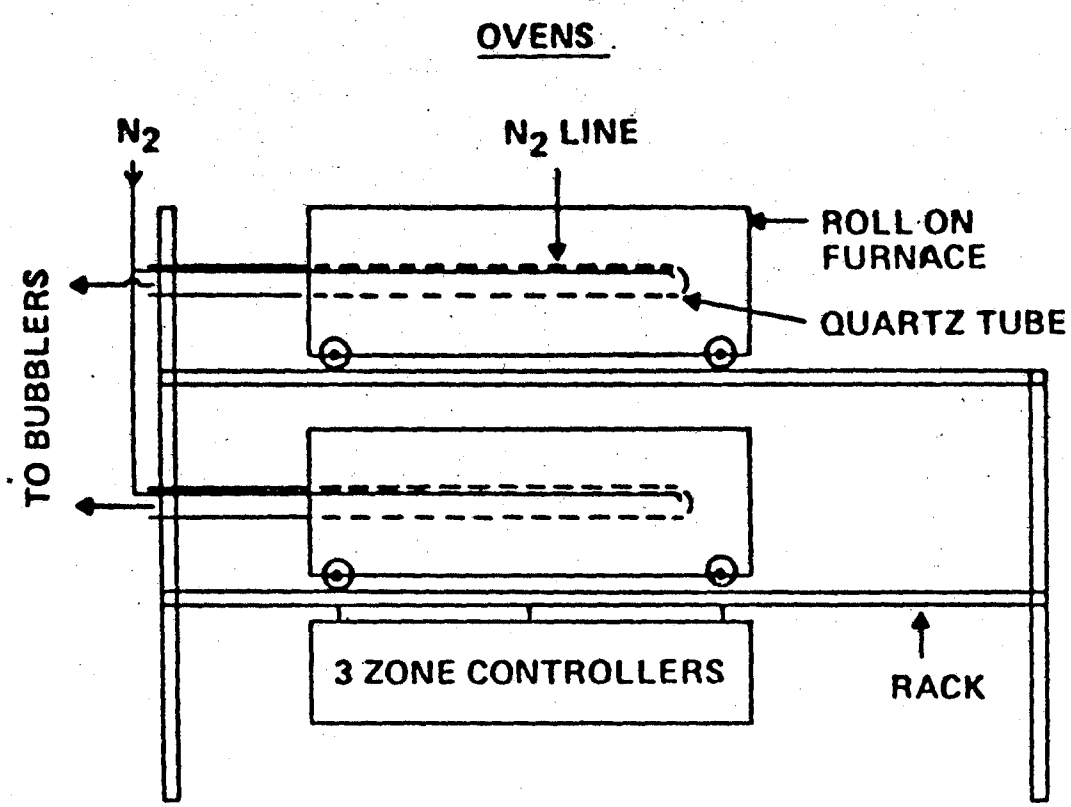
OVENS
N_2
N_2 LINE
ROLL ON FURNACE
QUARTZ TUBE
TO BUBBLERS
3 ZONE CONTROLLERS
RACK

oil-filled bubbler, which prevents back flow of air. The furnaces were controlled by a Leeds and Northrup controller on one furnace and a Eurotherm three-zone controller on the other furnace. Sample temperature was monitored by a chromel-alumel thermocouple placed near the solar cells.

The lower furnace shown in Fig. 2-2 was modified to be used for thermal cycling tests. The furnace was fitted with a drive motor to roll it on and off the quartz tube. A timing motor, relays, and microswitches were used to provide the logic required to periodically drive the furnace on or off the tube and stop it in the proper place. A fan positioned to blow air over the portion of the quartz tube containing the cells was wired to turn on when the furnace rolled off the tube, in order to cool the cells more quickly. Figure 2-3 shows a plot of the thermocouple output, measuring the temperature at the cell position during temperature cycling. One cycle takes approximatley 1/2 hour. A cycle counter increments each time the furnace rolls onto the tube.

It was originally planned to extend the temperature range of the cycling test to below ambient temperature by switching from the house nitrogen supply to chilled nitrogen blow-off gas from a nearby liquid nitrogen tank each time the furnace rolled off the tube. However, this would have required a more complex timing cycle to control the nitrogen flow and to prewarm the quartz tube to evaporate any condensation on it. It was decided that the modifications required for this would delay the experiment enough that results could not be obtained within the contract period. Therefore, testing was done within the range 25°C to 400°C.

3. Test Procedures

Since the cells used in these tests were unpackaged, testing of the cells was restricted to measurements at one-sun light intensity. Testing of unpackaged cells at high concentration levels is very difficult because the reliable contacts capable of conducting several amps

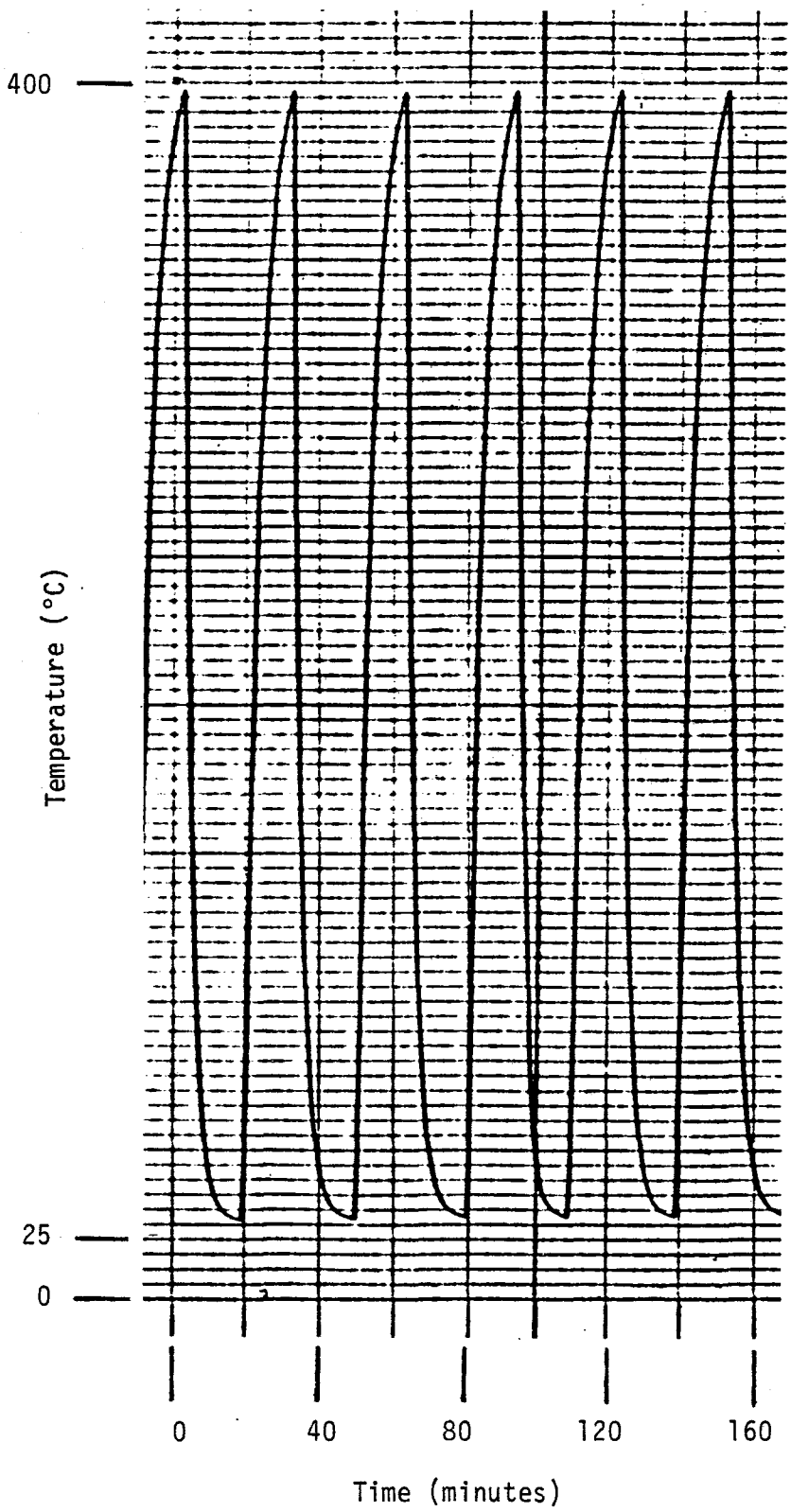

Fig. 2-3 Temperature vs. time for thermal cycling oven.

required for testing at concentration are difficult to achieve with pressure contacts on unpackaged cells. Periodically, the cells were returned to room temperature and one-sun measurements of cell I-V characteristics were made using a Spectrolab model XT-10 solar simulator. This light source is a xenon lamp whose spectrum is modified to simulate a terrestrial solar spectrum by use of dichroic filters and a filter consisting of a thin layer of water sandwiched between two glass plates. The light intensity at the cell under test was kept at ~900 W/m^2.

It was originally planned to measure the cell characteristics under computer control, but it proved to be impractical to locate the computer and solar simulator in the same room. Therefore, the cell I-V characteristics were displayed on a Tektronix curve tracer and photographed. The photographed I-V curve was analyzed by digitizing it on a plotter which input the data into an HP-9835 computer. The computer program then found the peak power point by interpolating between the digitized points with a spline fit. The program then saved the open circuit voltage, short circuit current, voltage and current at peak power point, peak power and fill factor on a disk file for further analysis. This method of analyzing the I-V characteristics no doubt introduced some inaccuracies into the data, but the accuracy was sufficient for the aging study. The main drawback of this technique was the large amount of time required to digitize the I-V curves.

After the cell I-V characteristics were measured, the condition of the cell surface was recorded by making a photomicrograph of the center of each cell's active area. The center of the cell was chosen for this measurement because it is easy to locate, and it is necessary to photograph the same area on the cell for each test.

B. Test Results and Analysis

Groups of solar cells were stored in nitrogen ambient at 400° and 425°C and in air ambient at 250° and 320°C, and one group of cells was cycled between 25° and 400°C in nitrogen. In the following section, we present the results of one-sun measurements made on the cells during the testing. In the next section, the measurements are analyzed to extract a cell lifetime extrapolated to normal cell operating conditions. Finally, the results of cosmetic evaluation of the cell surface during the testing are presented and discussed.

1. One-sun Performance Results

a. High Temperature Storage in Nitrogen

Nine LPE-grown cells were stored at 386-400°C in nitrogen; five of them were soldered to a ceramic tray and four were kept loose. Figures 2-4 through 2-9 show the data generated from the one-sun I-V curves for this group of cells. The figures show open circuit voltage (V_{oc}), short circuit current (I_{sc}), voltage at the peak power point (V_{pk-pwr}) current at the peak power point, peak power output, and fill factor versus the total thermal storage time. The values shown in Figs. 2-4 through 2-9 are normalized to the initial value of each parameter for each cell, measured before any thermal storage had taken place. The normalized values are plotted so that changes from the initial cell characteristics are readily apparent. For the purposes of this accelerated aging study, we have defined cell failure to occur when one of the measured cell parameters drops below 80% of its initial value. Thus, any line which drops below 80 in Figs. 2-4 through 2-9 indicates that the cell has failed with respect to the parameter plotted on that figure. "Tray 1" through "Tray 5" are the names adopted for the cells soldered to trays, while "HRF 6" etc., are the names of the cells that were kept loose. After over 3000 hours at 400°C, each cell failed with respect to at least one parameter.

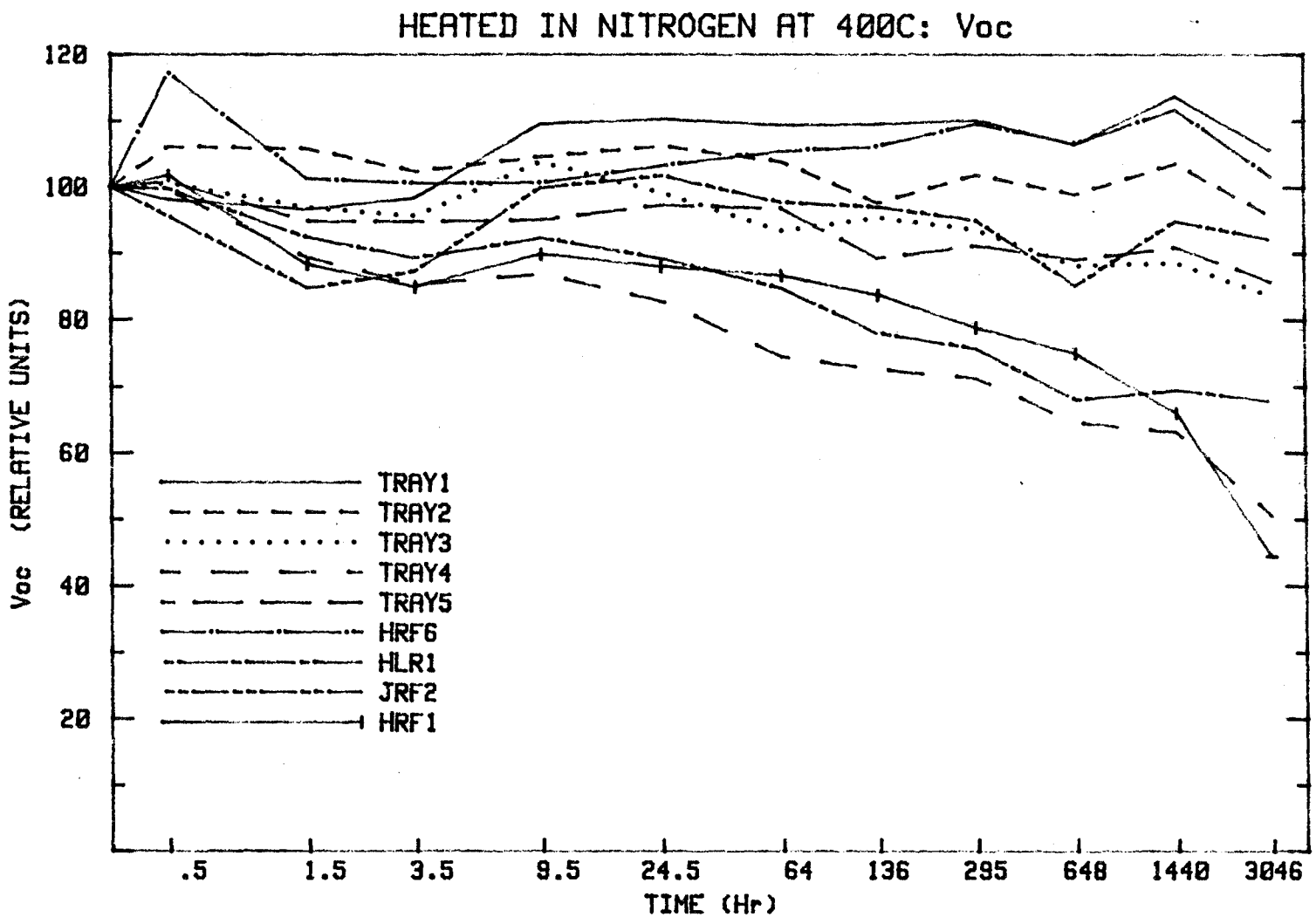

Fig. 2-4 Normalized open circuit voltage versus thermal storage time for cells stored at 400°C in nitrogen.

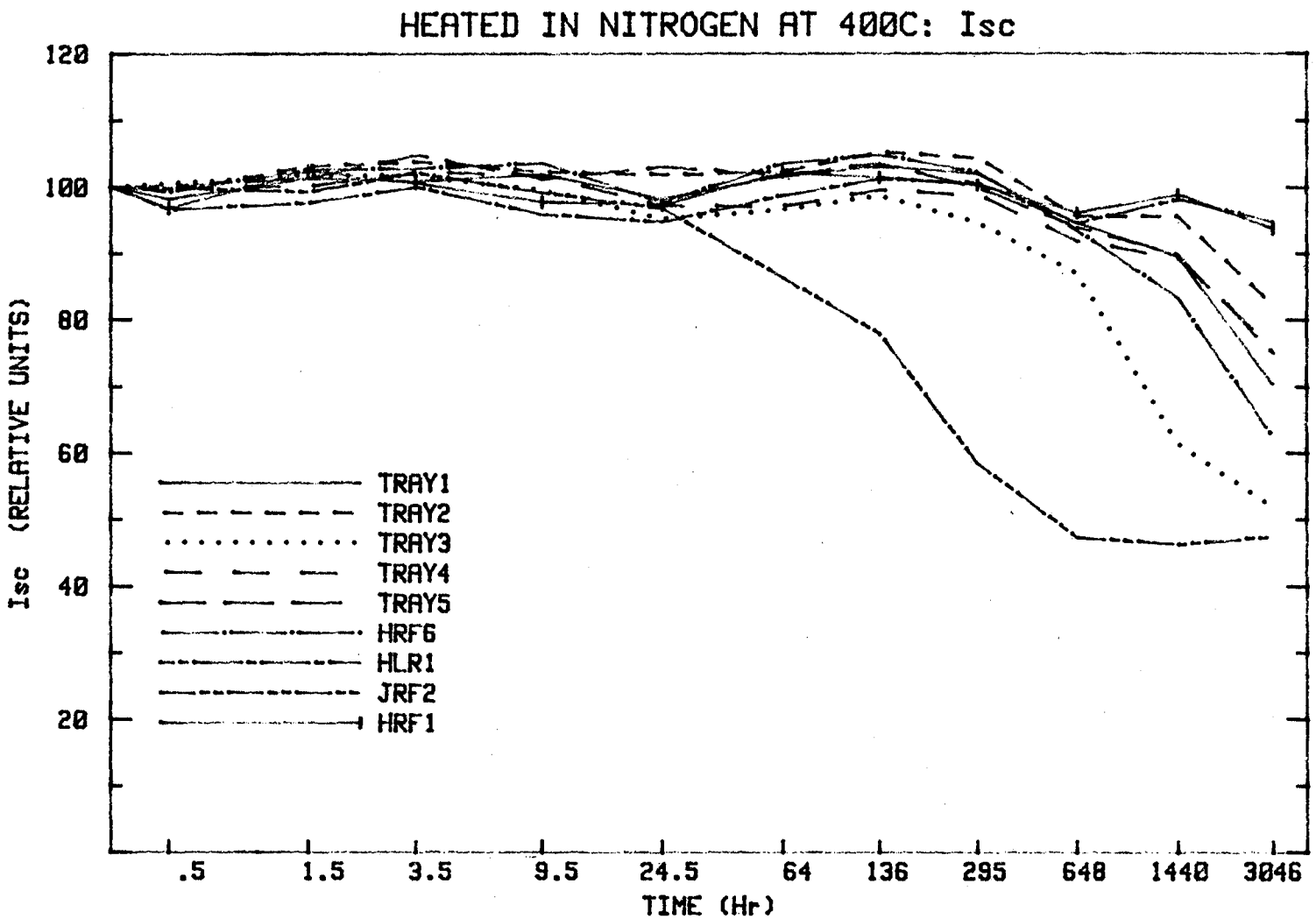

Fig. 2-5 Normalized short circuit current versus thermal storage time for cells stored at 400°C in nitrogen.

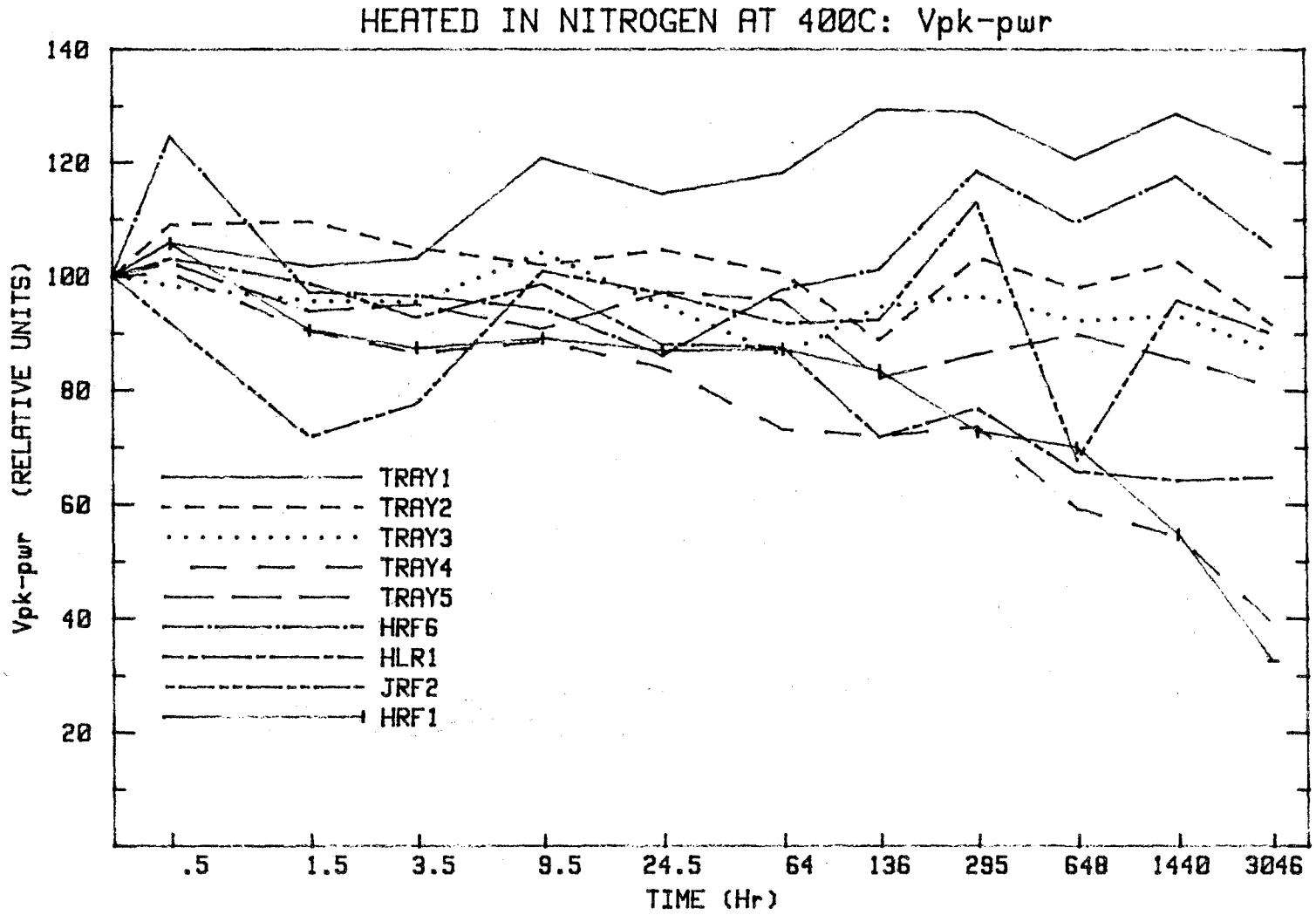

Fig. 2-6 Normalized voltage at peak power point versus thermal storage time for cells stored at 400°C in nitrogen.

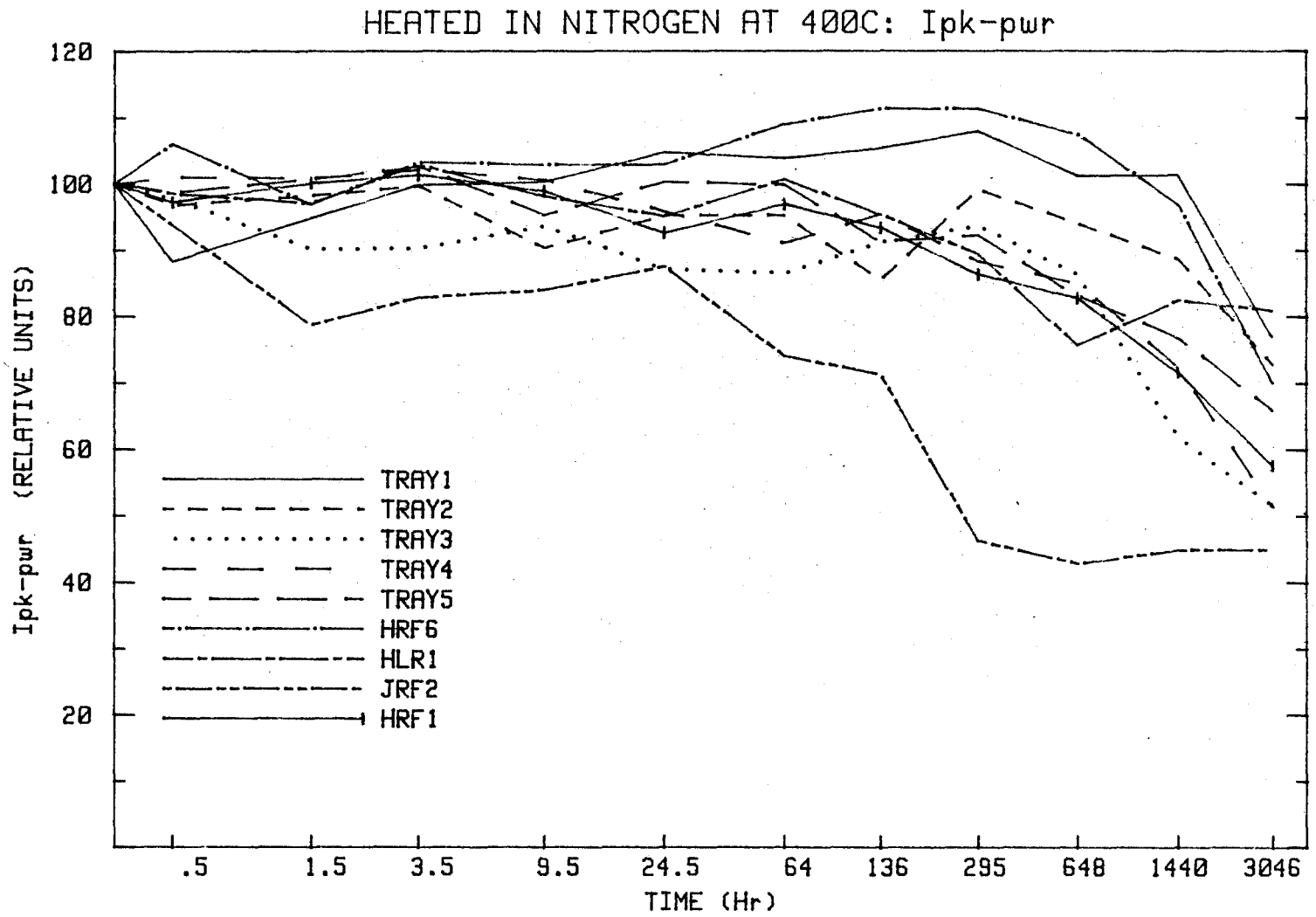

Fig. 2-7 Normalized current at peak power point versus thermal storage time for cells stored at 400°C in nitrogen.

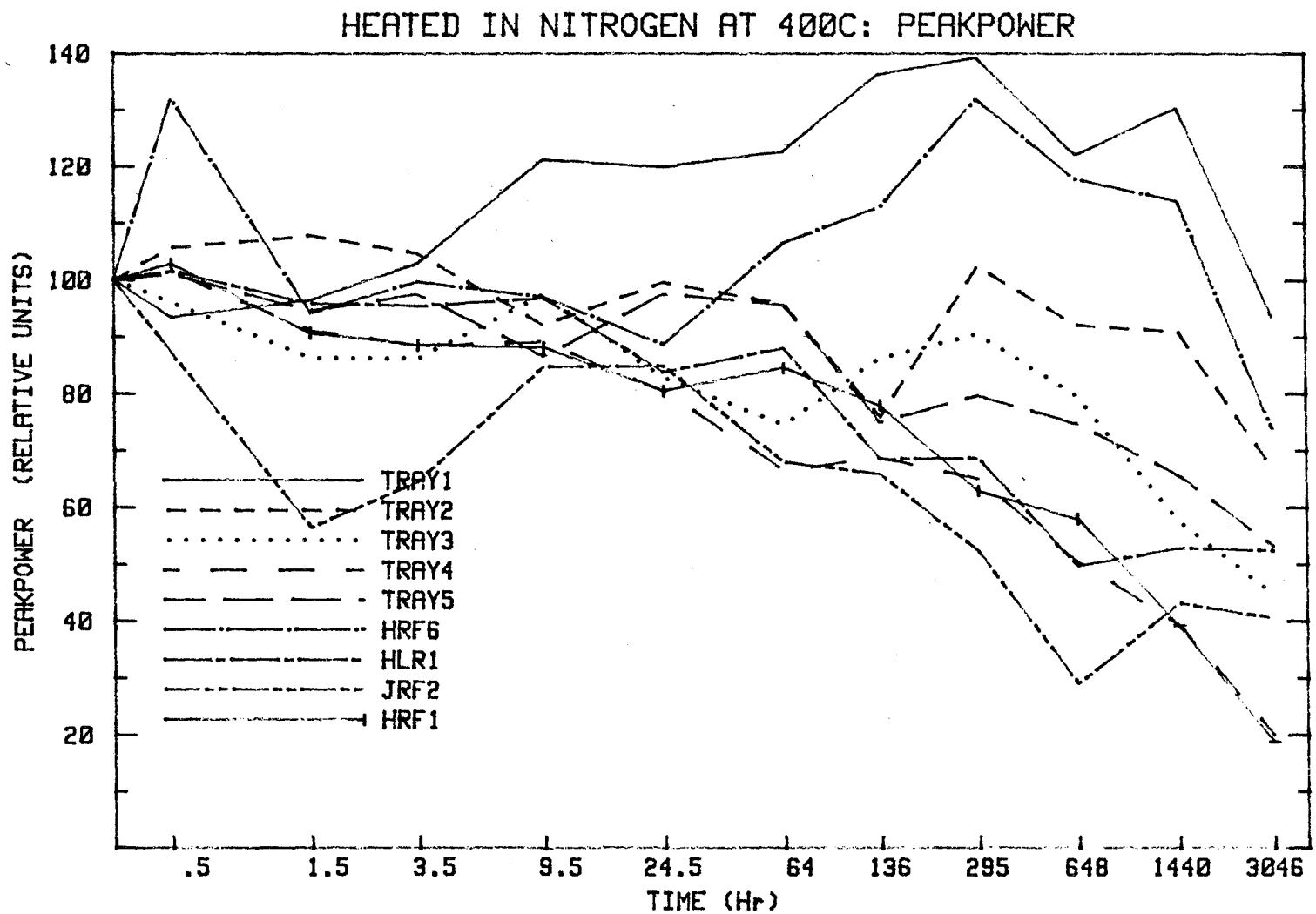

Fig. 2-8 Normalized peak power output versus thermal storage time for cells stored at 400°C in nitrogen.

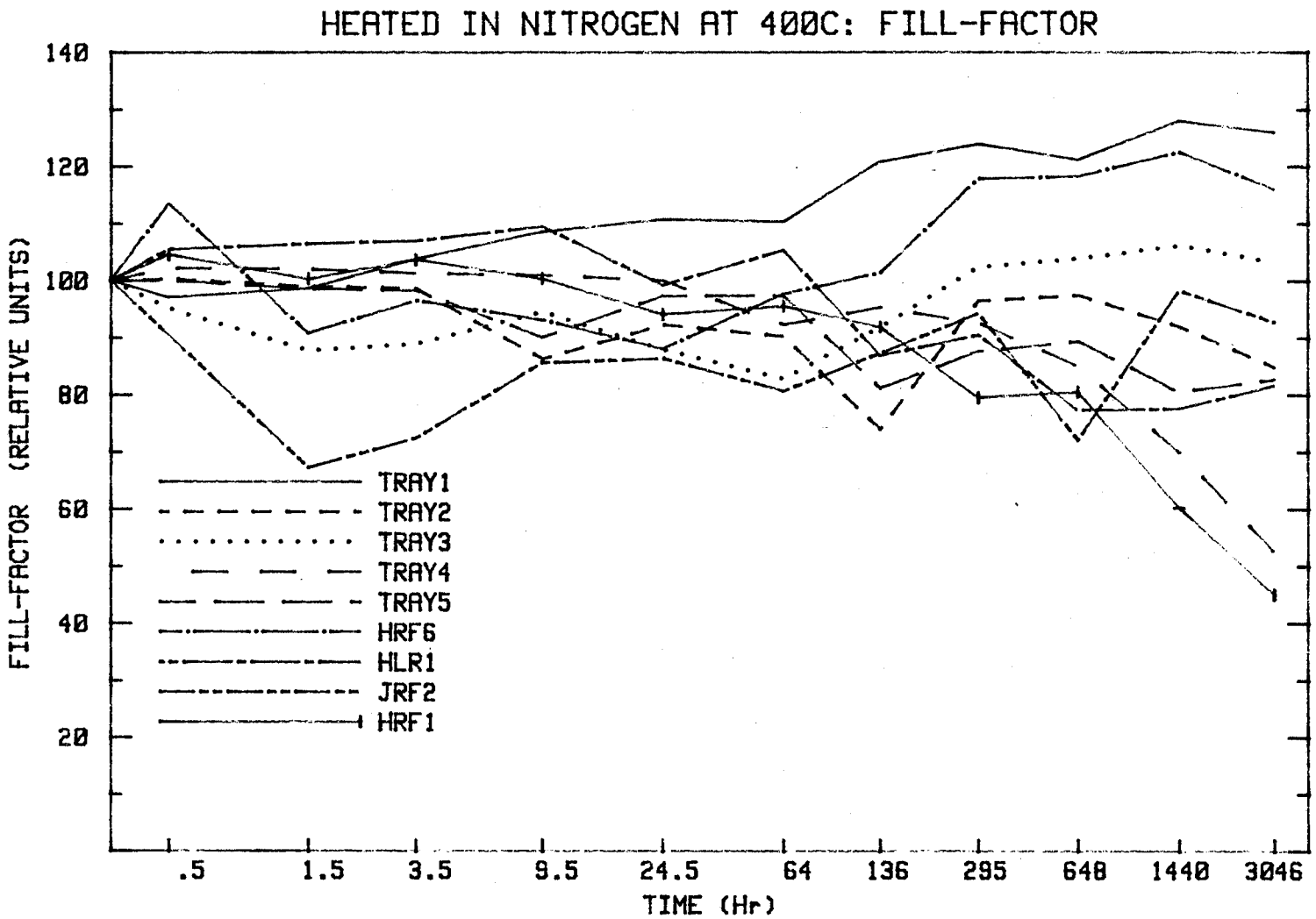

Fig. 2-9 Normalized fill factor versus thermal storage time for cells stored at 400°C in nitrogen.

The data of Figs. 2-4 through 2-9 shows quite a wide scatter. Some of the scatter is probably due to errors in digitizing the I-V curves. The 400°C test was the first test started, and the I-V curves were recorded on a small scale that makes accurate digitizing difficult. The I-V curves for the other tests were recorded on a larger scale. Other likely sources of scatter in the data are variations in the quality of the contacts to the cell and fluctuations in the solar simulator output. Contact to the cell front is made by probing the corner of the grid pattern. Contact to the back is made by probing the metallized ceramic to which the cell is soldered. This is usually an adequate contact, but sometimes a poor contact is made. The simulator light output is measured with a reference cell and is kept close to 900 W/m^2, but short-term fluctuations of several percent occur frequently.

Figures 2-10 through 2-13 show the un-normalized values of V_{oc}, I_{sc}, V_{pk-pwr} and Peak power versus time for the cells in the 400°C test. These figures show that there was considerable variation in the initial output from these cells.

Ten LPE cells, soldered to two trays, were stored at 425°C in nitrogen. Figures 2-14 through 2-16 show normalized values of V_{oc}, I_{sc}, and peak power for these cells. As the figures show, these cells experienced catastrophic failure after one hour or less at 425°C. V_{oc} dropped drastically, while I_{sc} remained fairly constant for some of the cells. The I-V characteristic for the cells became linear, indicating that the cells were shorted out, although they did retain light sensitivity.

It was suspected that the Au-Ge solder used to solder the cells to their trays might have caused the cell failures, since the solder melts at 356°C, considerably below the 425°C storage temperature. To test this point, another test at 425°C in nitrogen ambient was carried out, with four LPE cells kept loose. For the tests through 267 hours, the cells were held on a graphite boat. For the test period 267 through 598 hours, the cells were kept in an aluminum holder in the furnace.

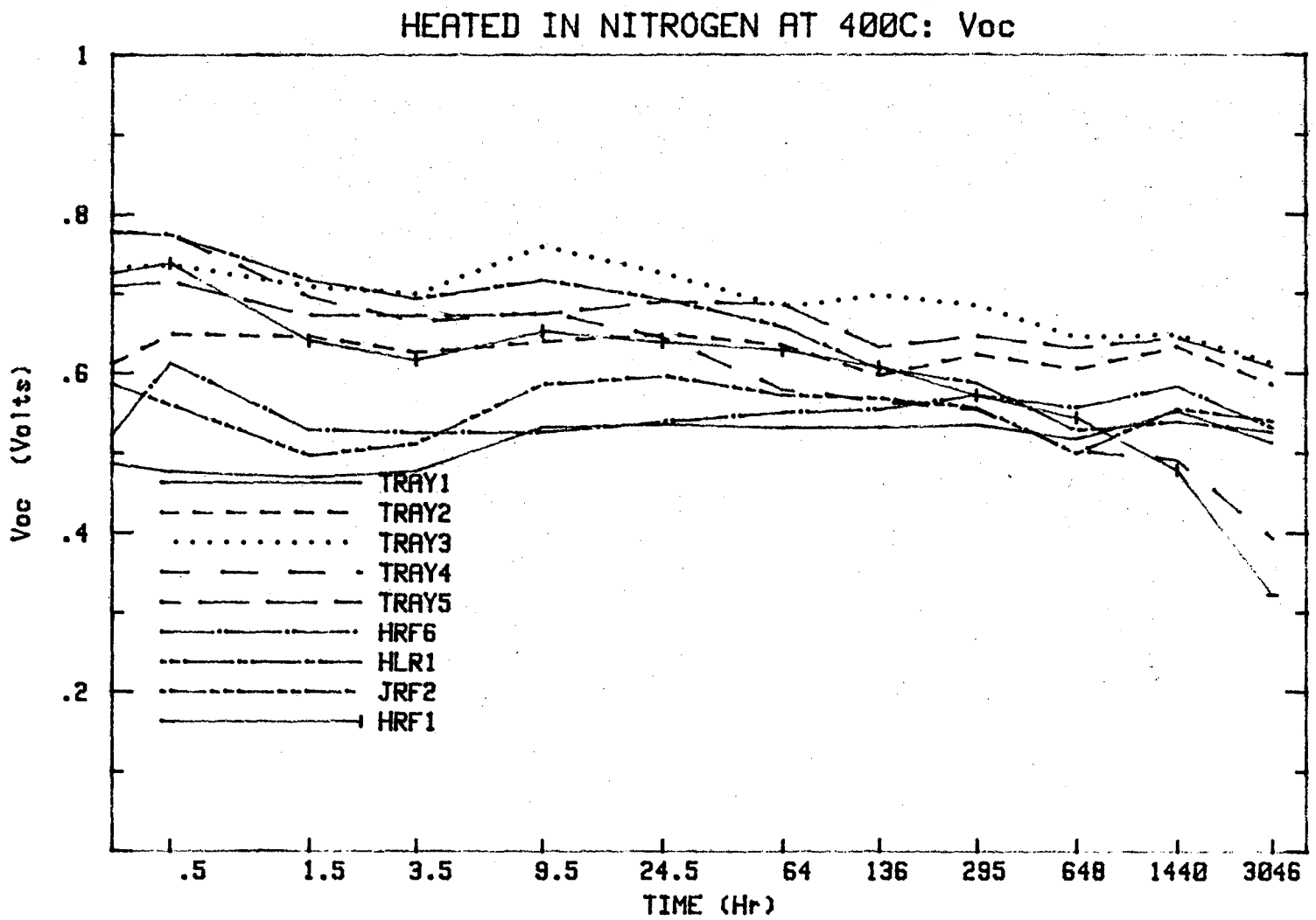

Fig. 2-10 Open circuit voltage versus thermal storage time for cells stored at 400°C in nitrogen.

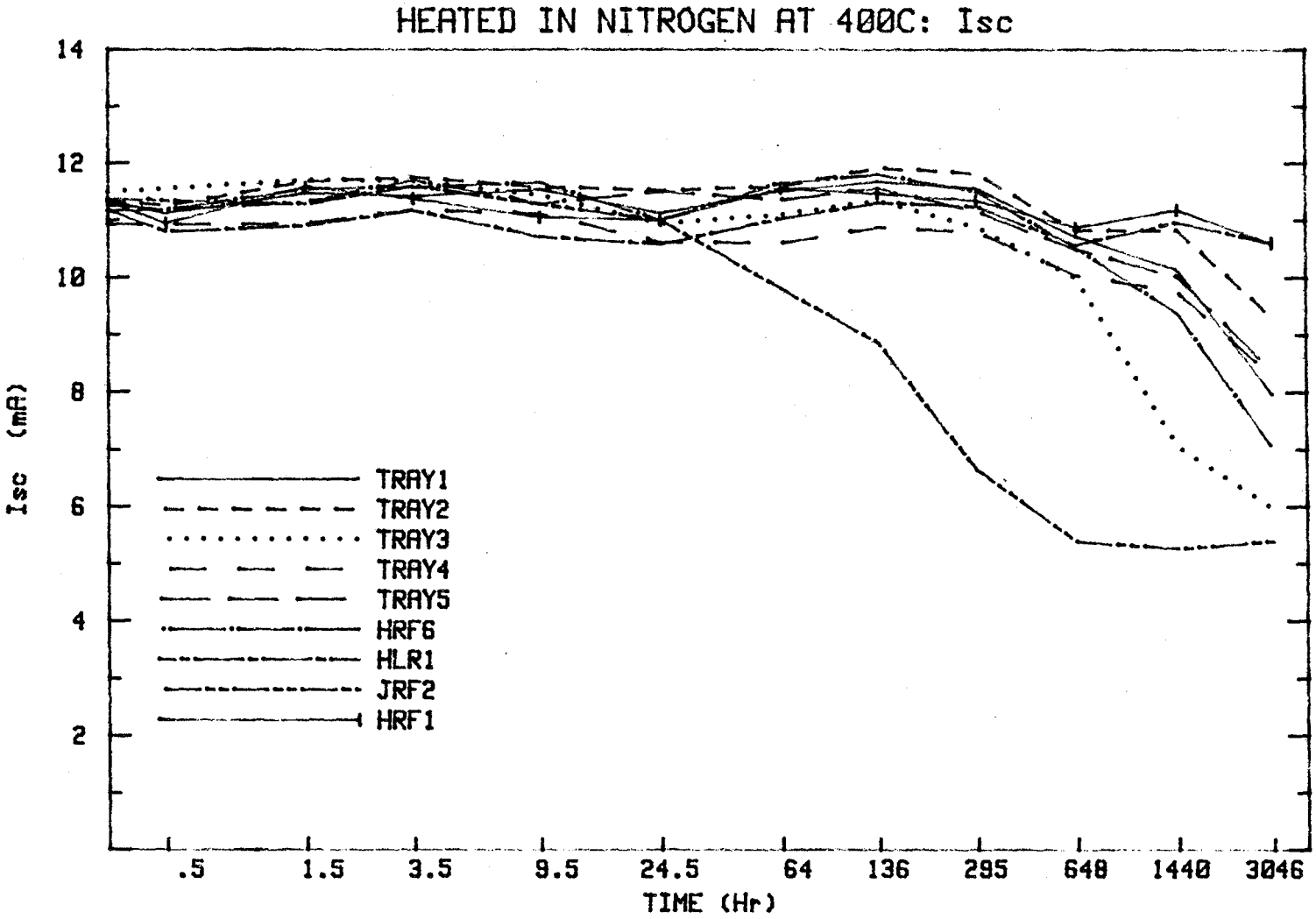

Fig. 2-11 Short circuit current versus thermal storage time for cells stored at 400°C in nitrogen.

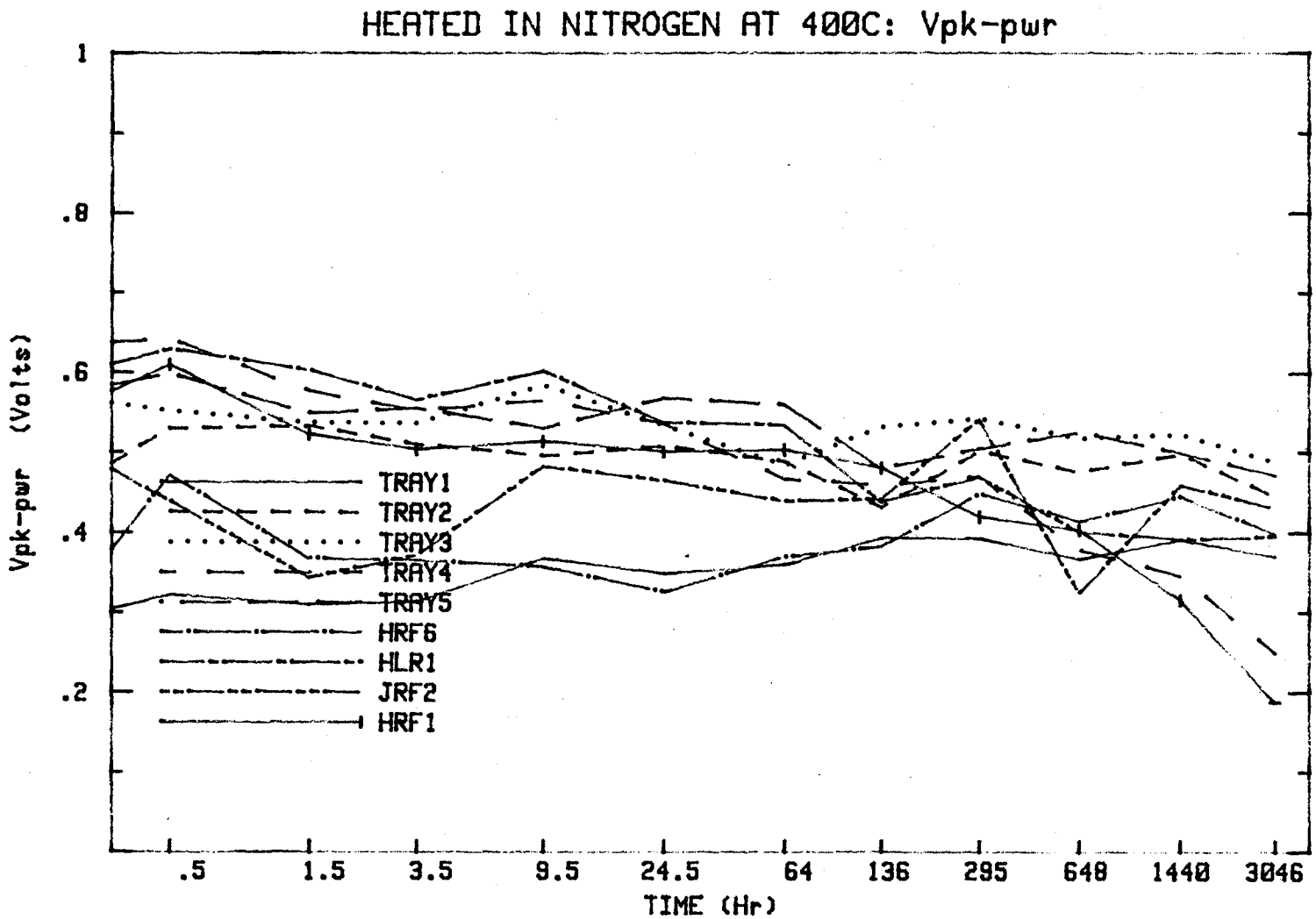

Fig. 2-12 Voltage at peak power point versus thermal storage time for cells stored at 400°C in nitrogen.

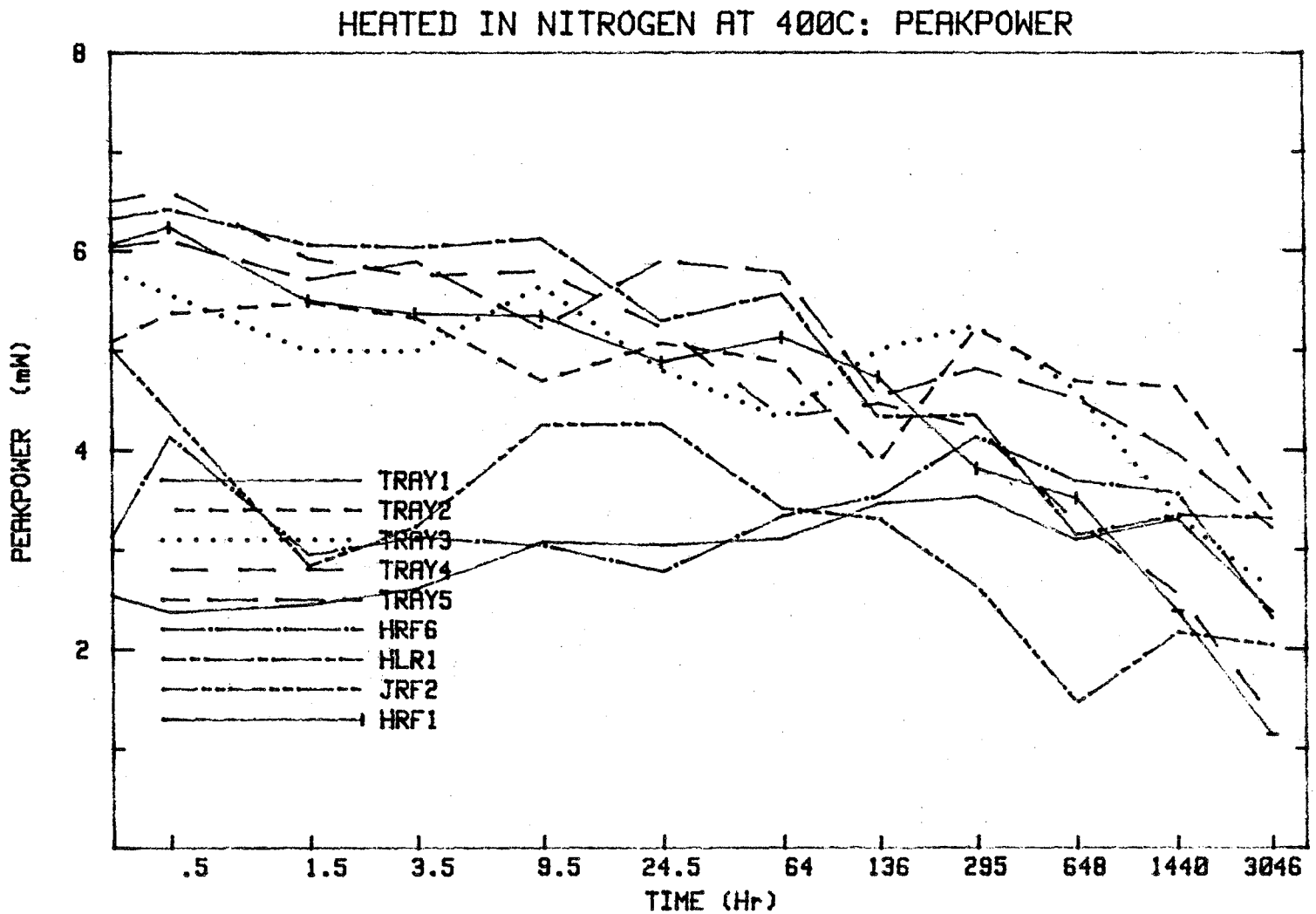

Fig. 2-13 Peak power output versus thermal storage time for cells stored at 400°C in nitrogen.

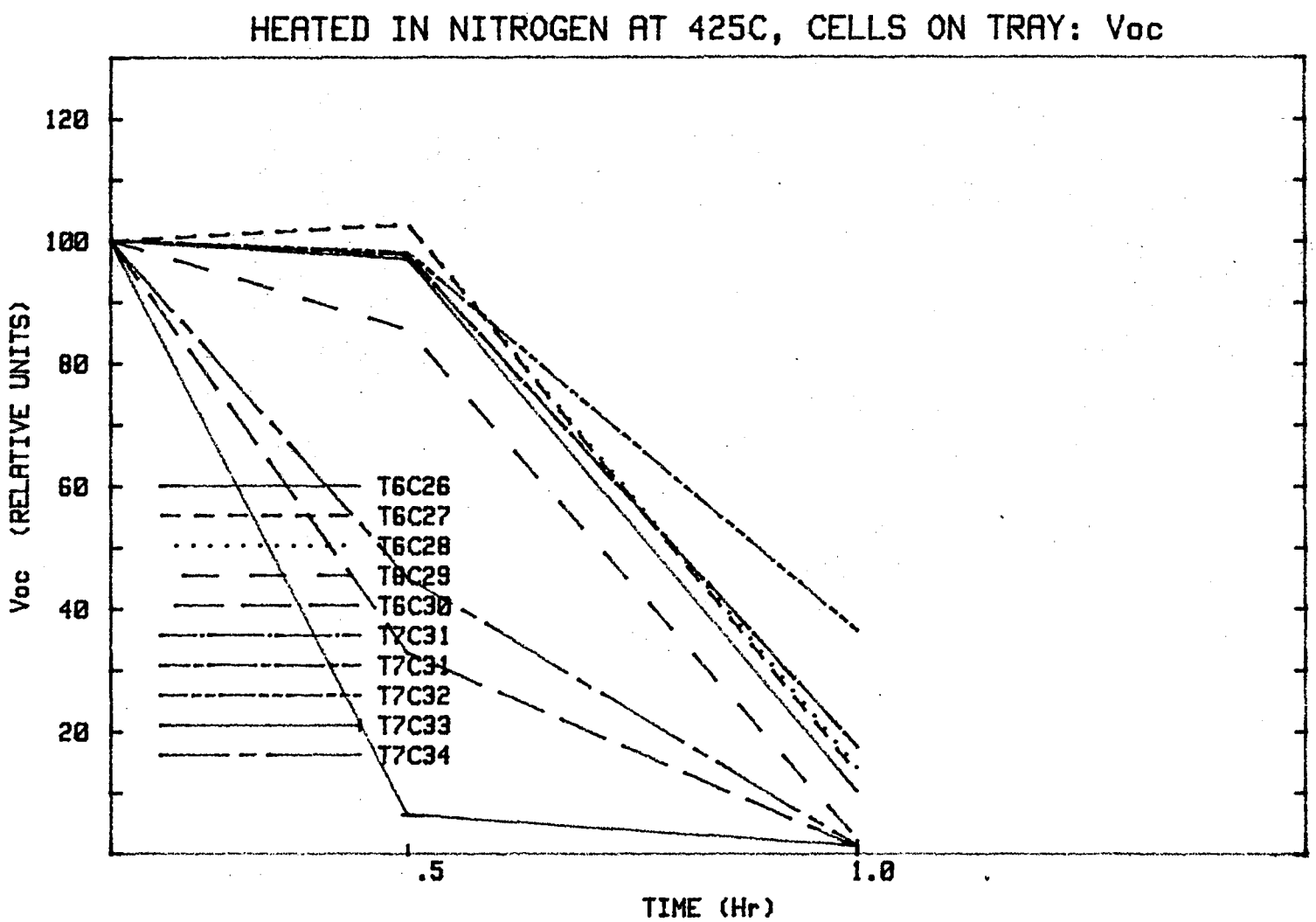

Fig. 2-14 Normalized open circuit voltage versus storage time for cells soldered to trays and stored at 425°C in nitrogen.

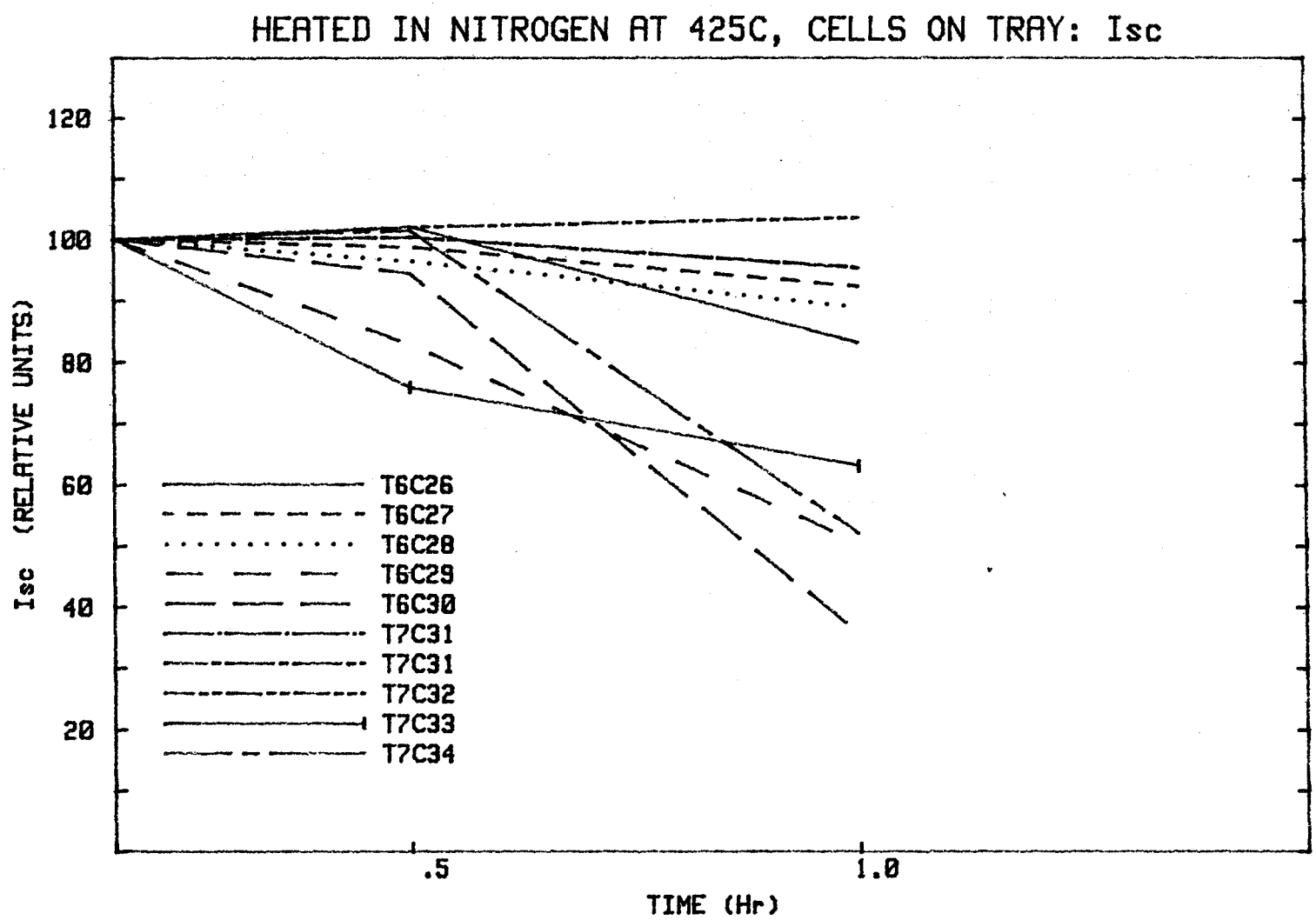

Fig. 2-15 Normalized short circuit current versus storage time for cells soldered to trays and stored at 425°C in nitrogen.

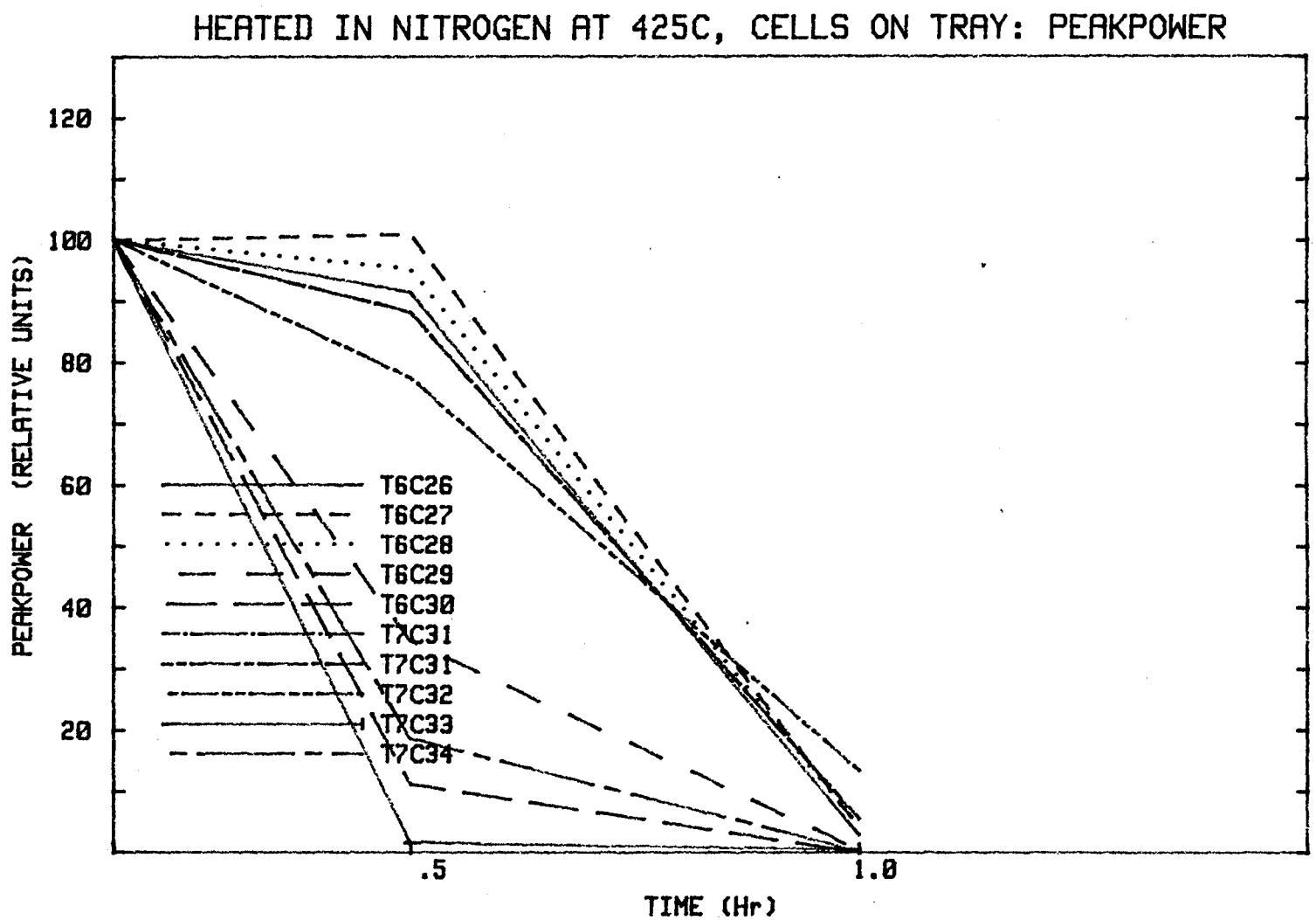

Fig. 2-16 Normalized peak power output versus storage time for cells soldered to trays and stored at 425°C in nitrogen.

Figures 2-17 through 2-22 show the normalized data measured for this group of cells, and Figs. 2-23 through 2-26 show the actual values of V_{oc}, I_{sc}, V_{pk-pwr}, and Peak Power.

As Figs. 2-17 through 2-22 show, there was little degradation for this group of cells until after 30-100 hours of storage; by 267 hours, all had failed. The fact that the loose cells survived much longer than the cells soldered to trays is strong evidence that the solder is the cause of the early failure of the soldered cells.

To see if the solder had simply shorted out the cells by flowing up the cell edge and bridging the p-n junction, the edges of one shorted cell were sanded to remove any possible solder, but the sanding produced no change in the cell I-V characteristic. Furthermore, there was no visible evidence of solder on the cell edge, so solder flow can be ruled our as a failure mechanism. As a further test, the cell was cleaved into several pieces. Some of the pieces remained shorted, some exhibited a good I-V characteristic, and some had a soft I-V intermediate between a shorted and a good characteristic. Thus the failure mechanism affected a broad area of the cell, but not the whole cell.

The above observations point to diffusion of a component or impurity from the solder as the source of the cell failure. Gold is known to react with GaAs, even at room temperature.(2) The Au-GaAs eutectic is ~450°C, and annealing of Au-GaAs near this temperature has been found to produce significant Au diffusion into the GaAs.(3) Furthermore, films of Au-Ge eutectic have been shown to diffuse into GaAs at lower temperatures than for pure Au films, and both Au and Au-Ge films produce pits in the GaAs upon annealing at ~400°C.(4) Therefore, it seems reasonable that the cell failures were caused by the Au-Ge diffusing into and attacking the GaAs cell.

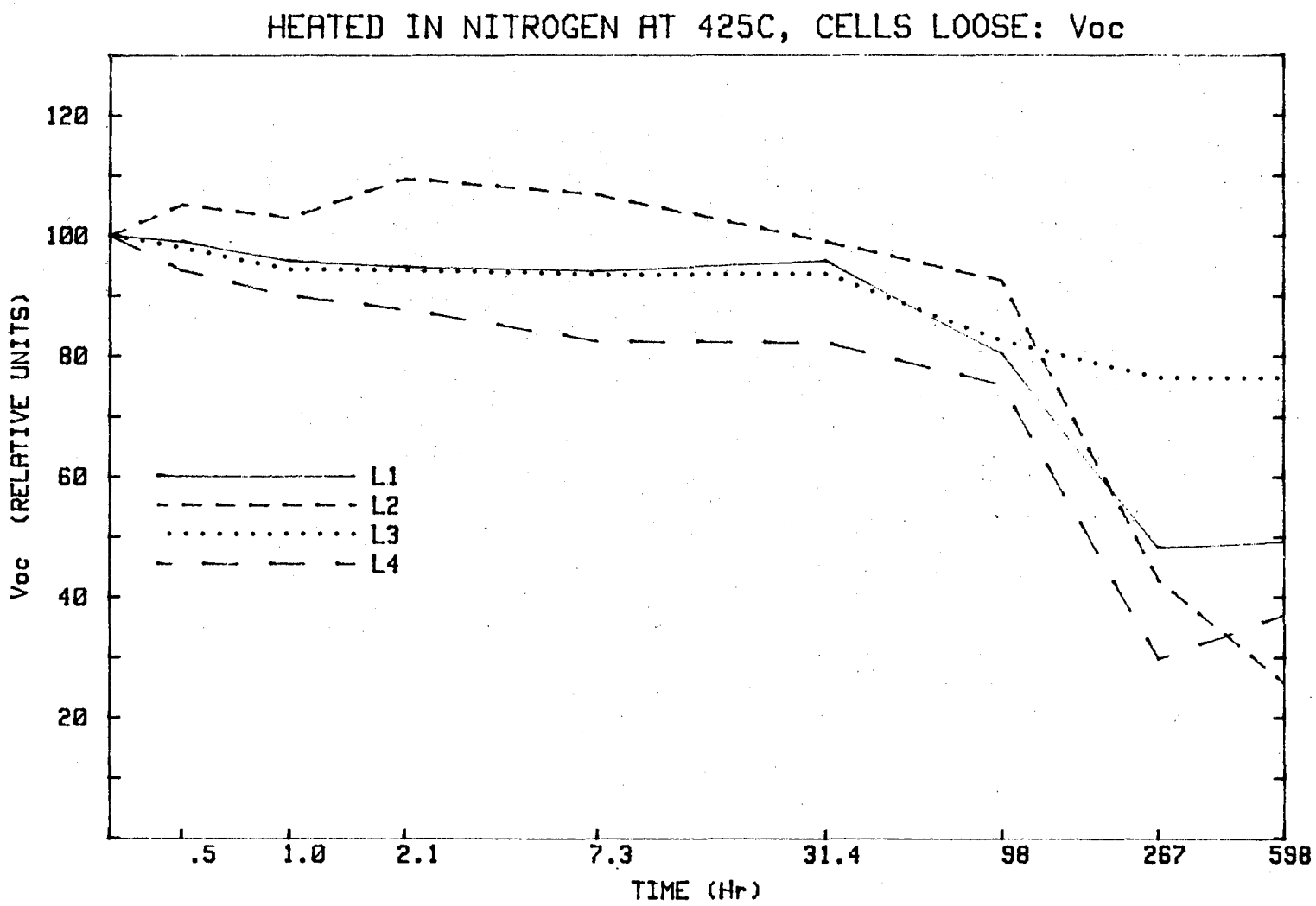

Fig. 2-17 Normalized open circuit voltage versus thermal storage time for cells stored at 425°C in nitrogen, not soldered.

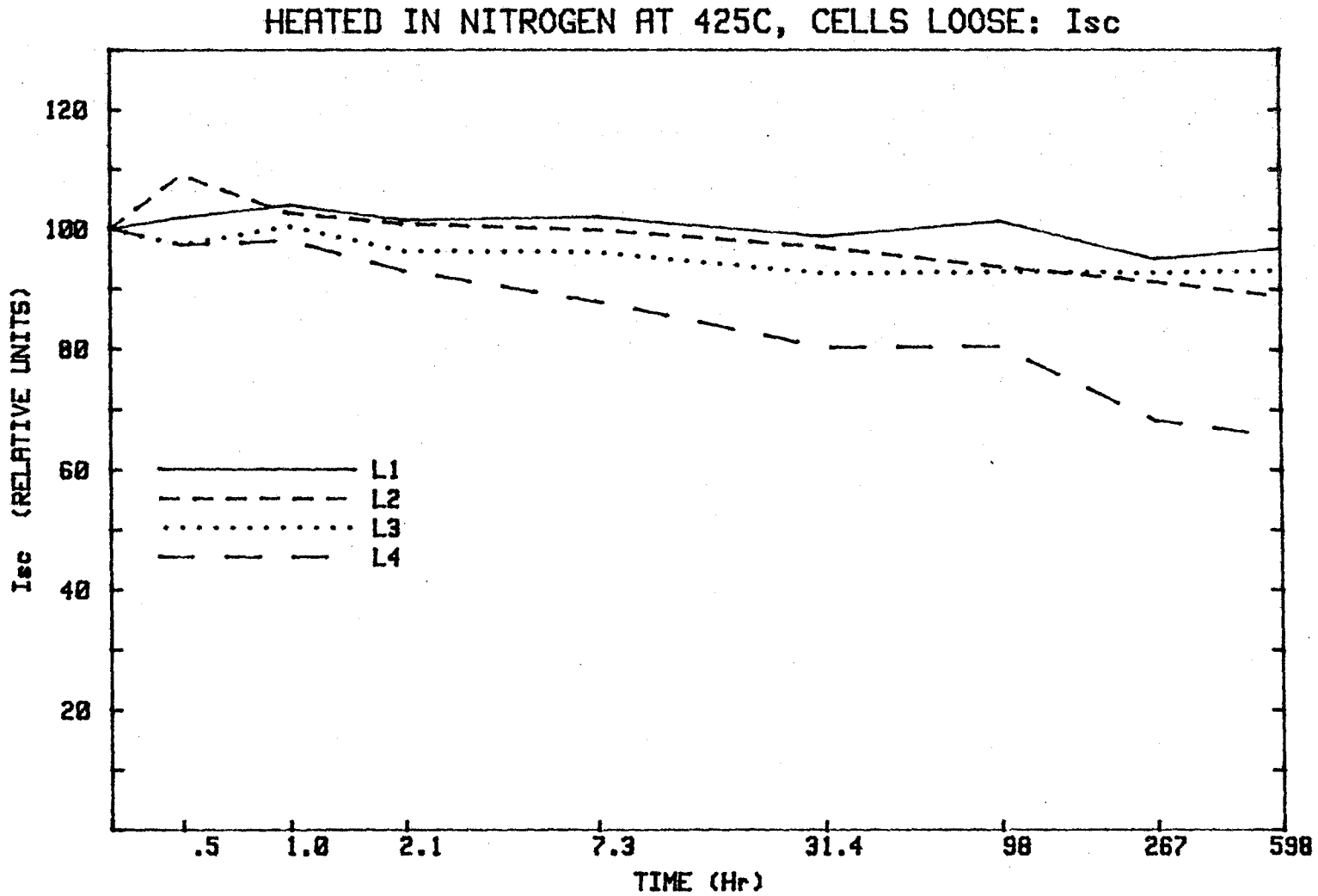

Fig. 2-18 Normalized short circuit current versus thermal storage time for cells stored at 425°C in nitrogen, not soldered.

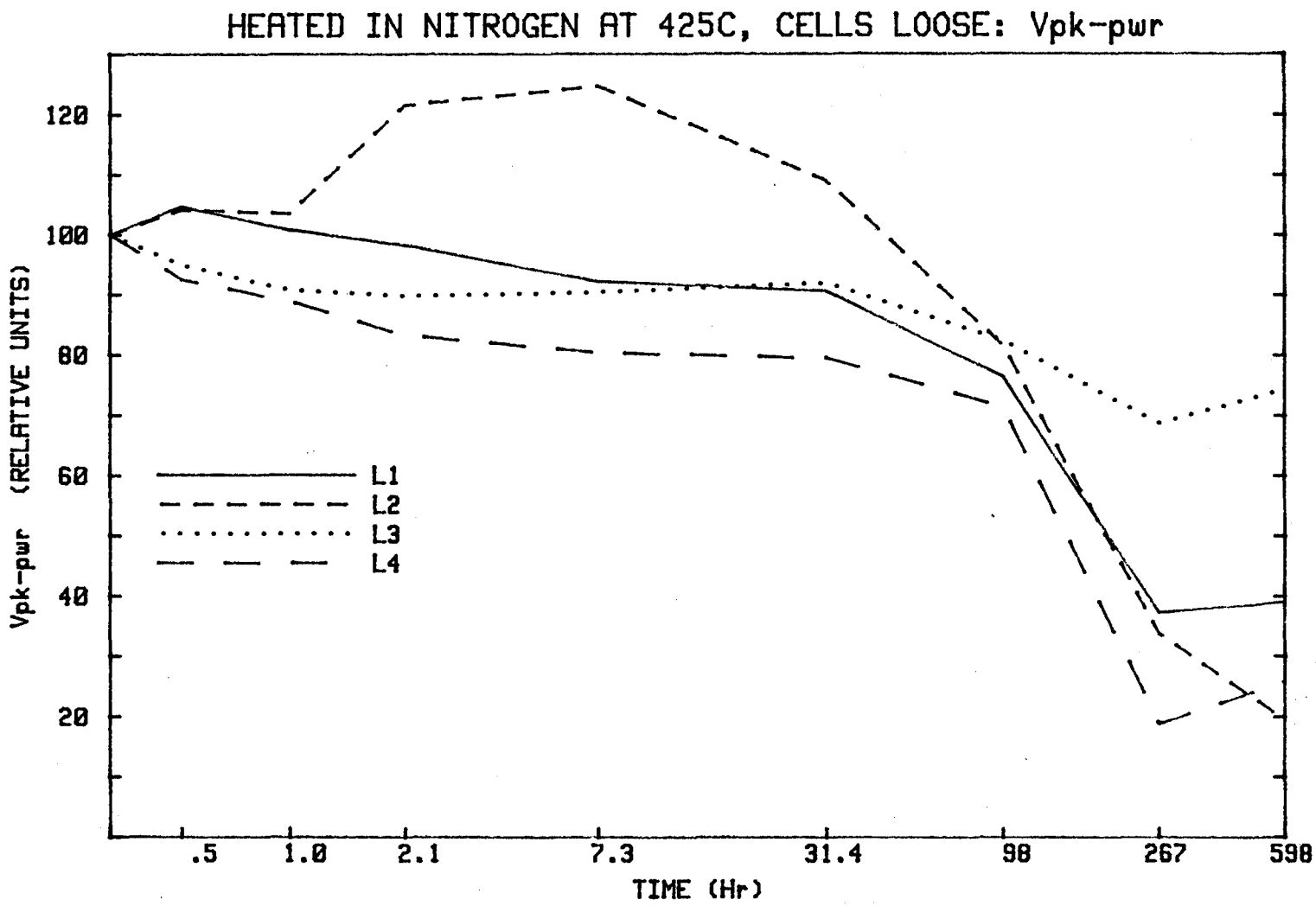

Fig. 2-19 Normalized voltage at peak power point versus thermal storage time for cells stored at 425°C in nitrogen, not soldered.

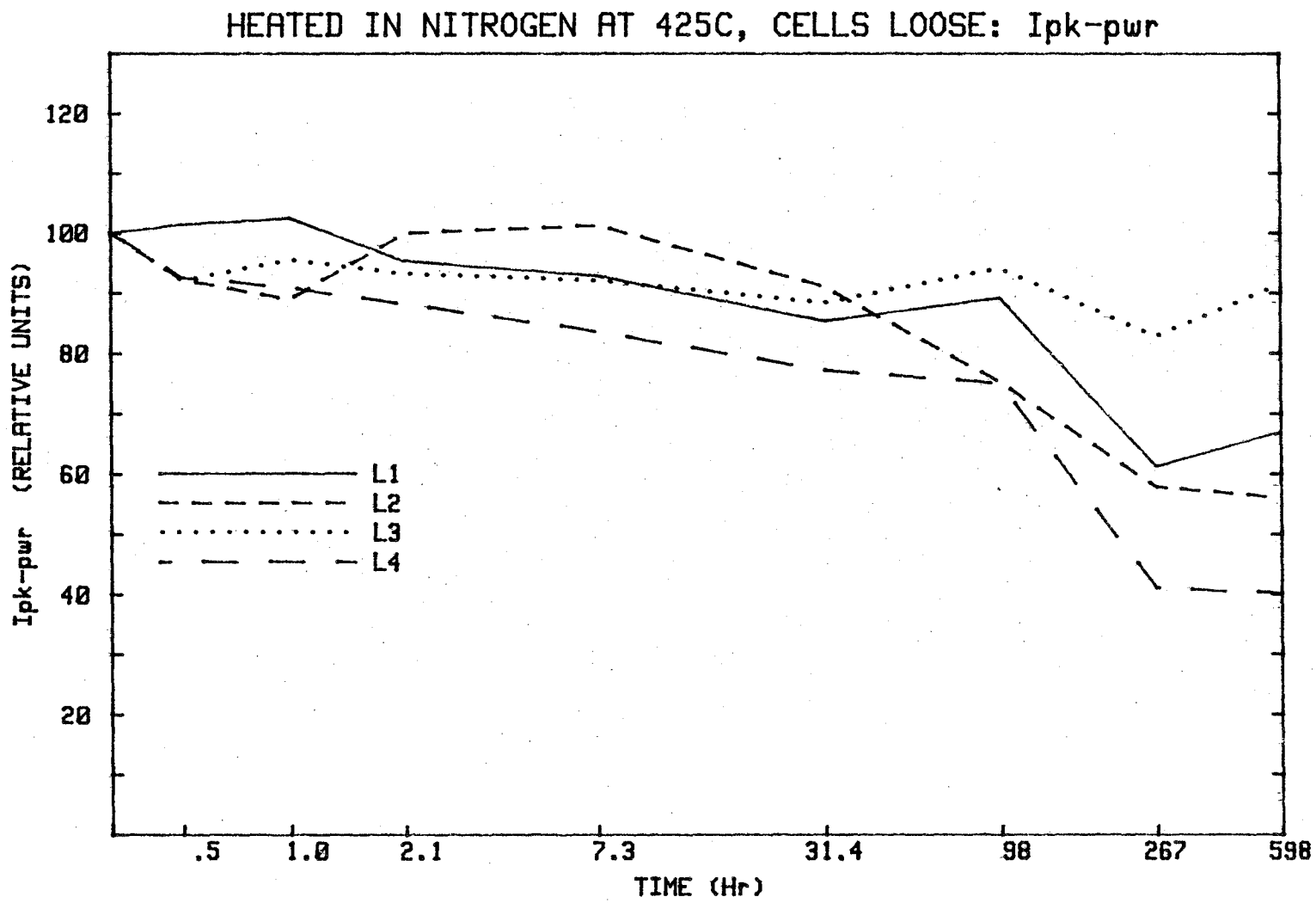

Fig. 2-20 Normalized current at peak power point versus thermal storage time for cells stored at 425°C in nitrogen, not soldered.

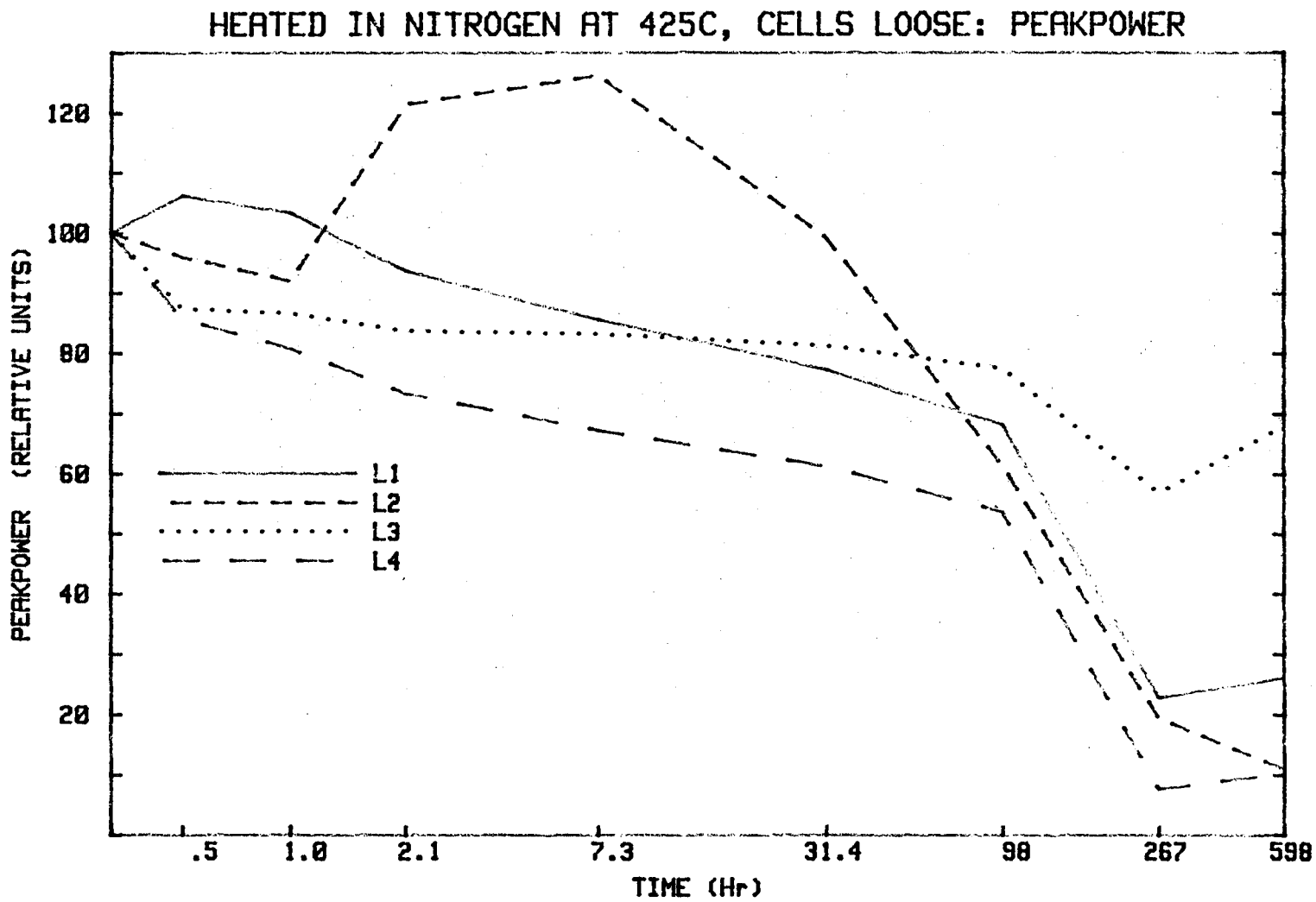

Fig. 2-21 Normalized peak power output versus thermal storage time for cells stored at 425°C in nitrogen, not soldered.

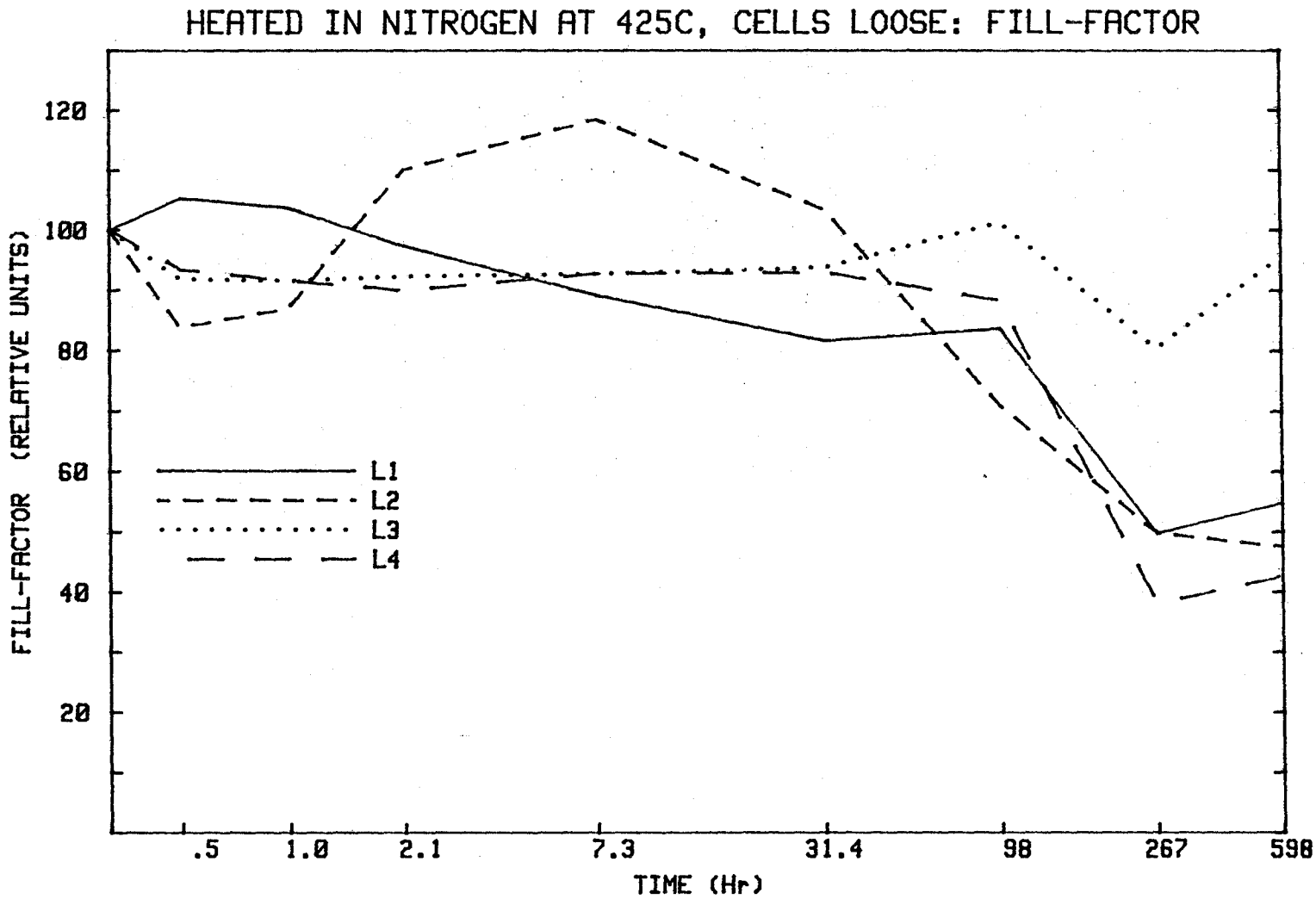

Fig. 2-22 Normalized fill-factor versus thermal storage time for cells stored at 425°C in nitrogen, not soldered.

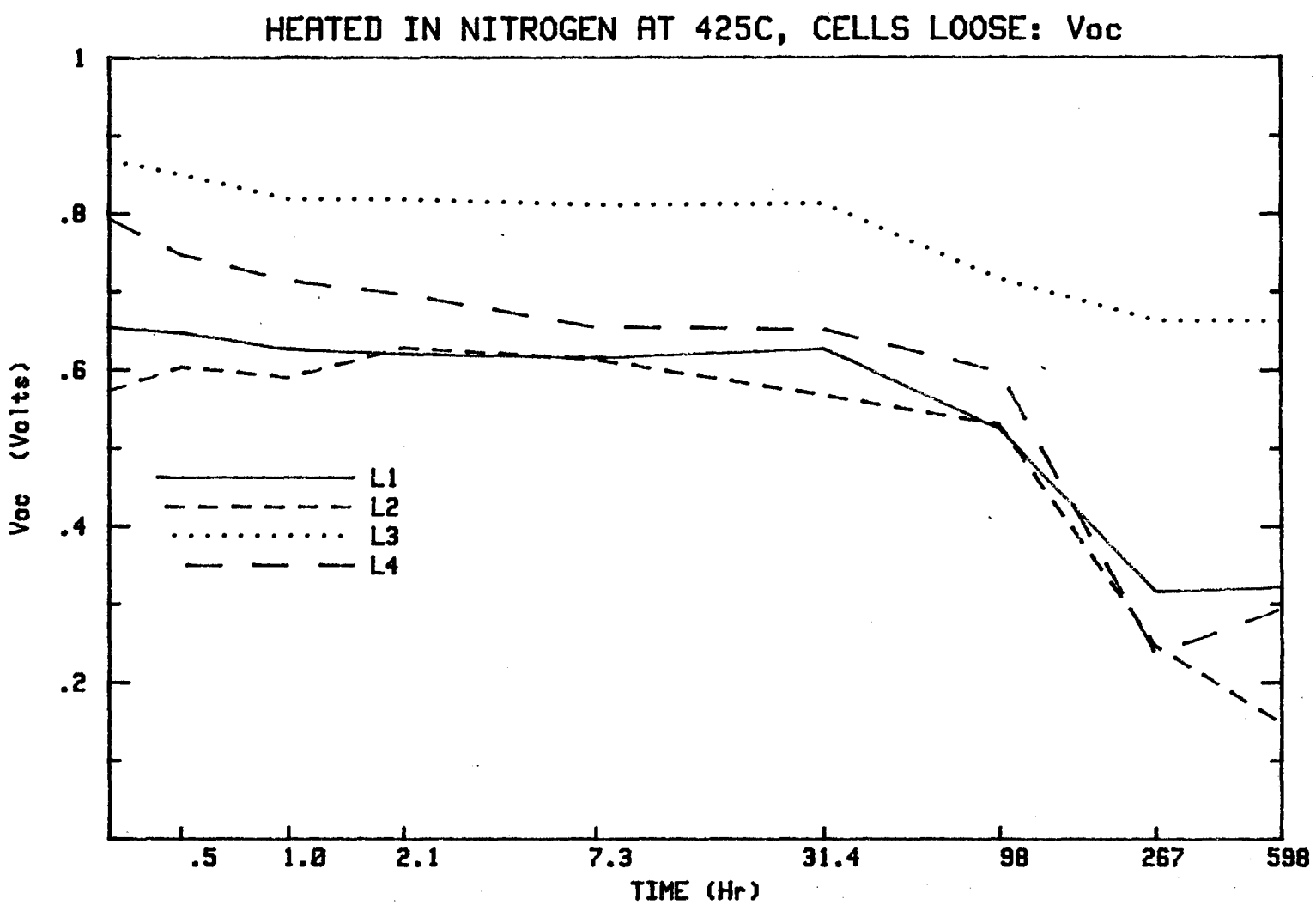

Fig. 2-23 Open circuit voltage versus thermal storage time for cells stored at 425°C in nitrogen, not soldered.

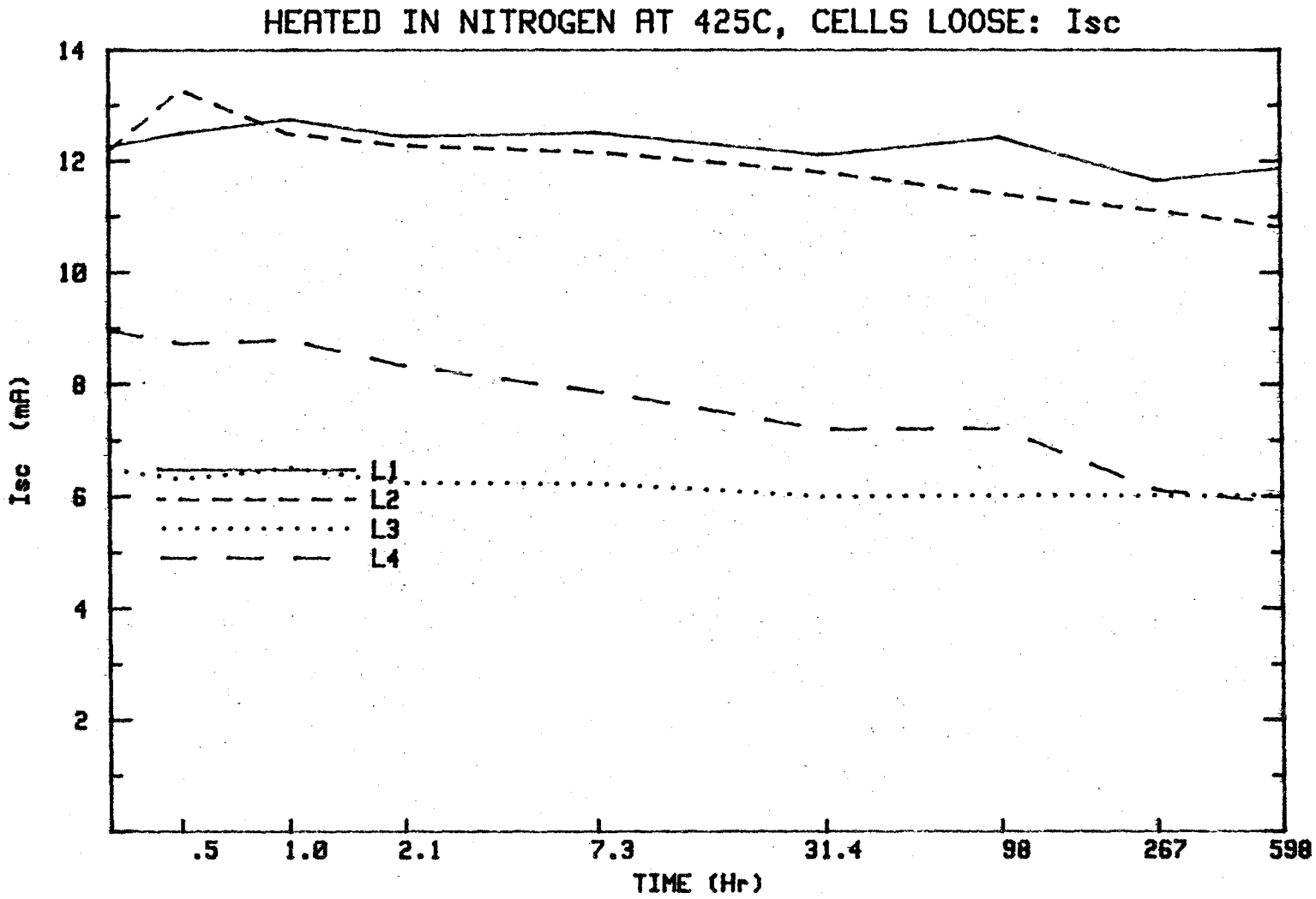

Fig. 2-24 Short circuit current versus thermal storage time for cells stored at 425°C in nitrogen, not soldered.

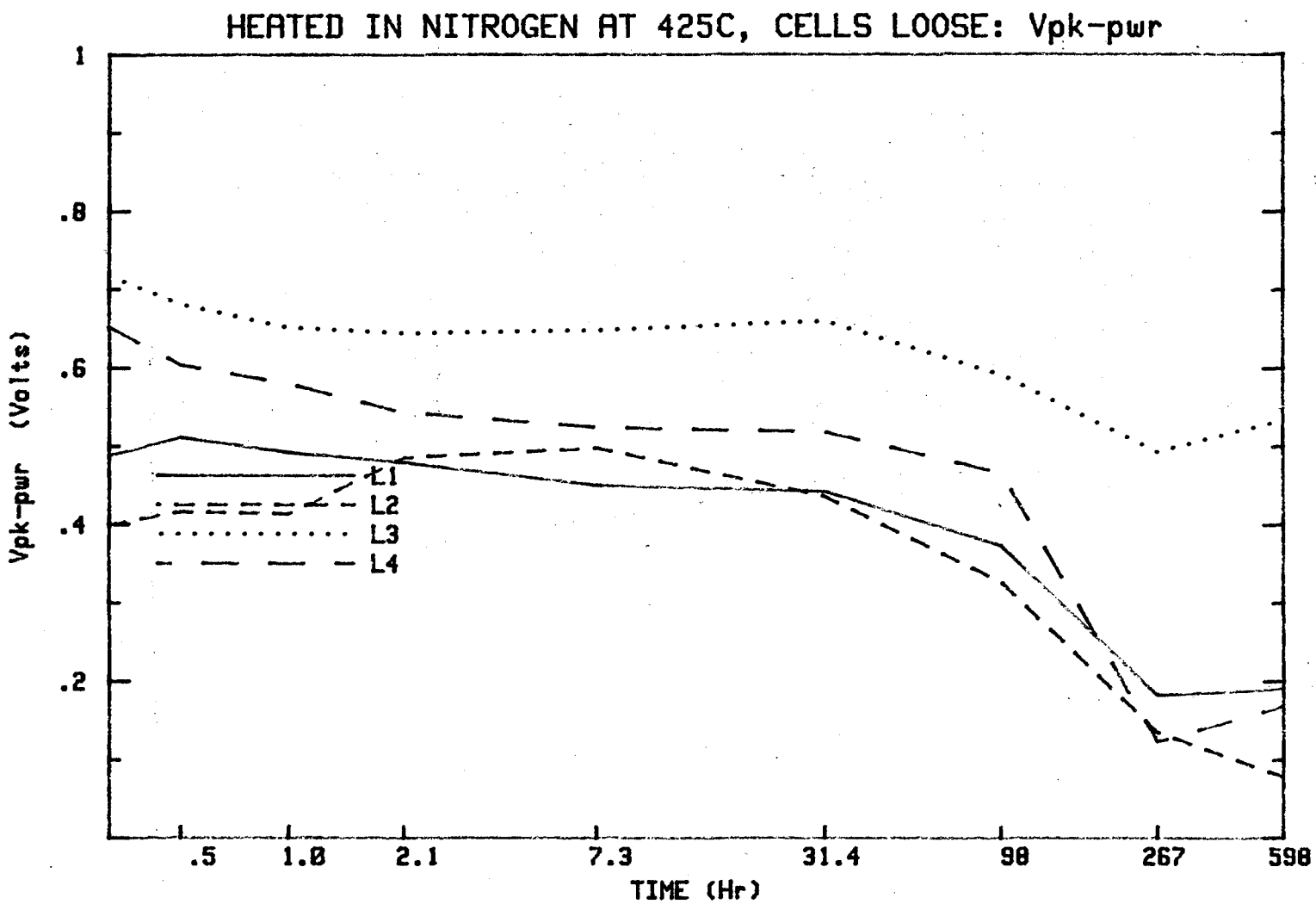

Fig. 2-25 Voltage at peak power point versus thermal storage time for cells stored at 425°C in nitrogen, not soldered.

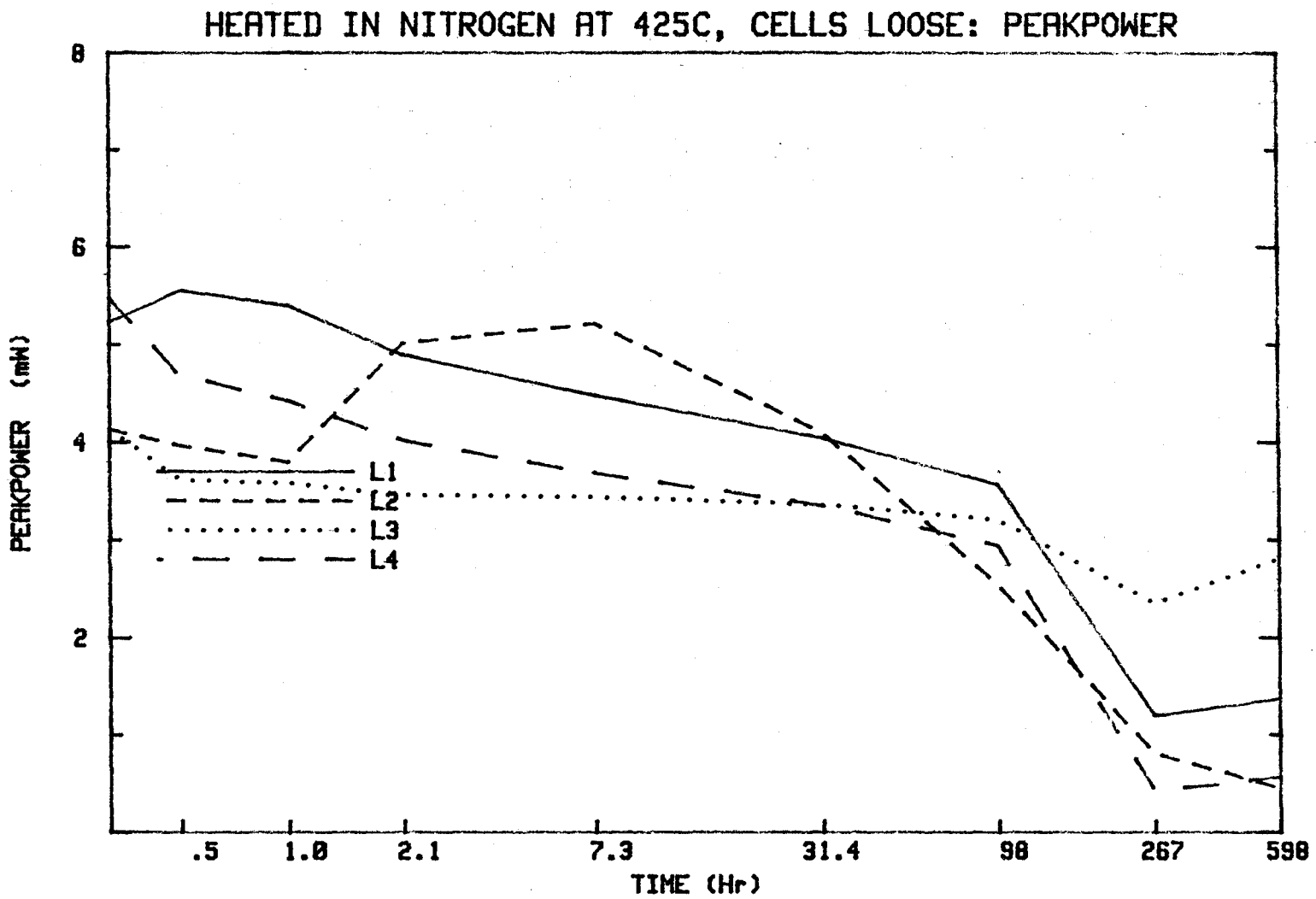

Fig. 2-26 Peak power output versus thermal storage time for cells stored at 425°C in nitrogen, not soldered.

Since the cells are cycled back to room temperature to measure their I-V characteristics, there is a possibility that the degradation seen in the testing was caused by the temperature cycling rather than by the static thermal storage. To examine this possibility, one OM and nine LPE cells soldered to two trays were cycled between 25°C and 400°C in nitrogen ambient (cell T4C20 is the OM cell). As discussed in Sec. A-2, the temperature cycle had a period of about 1/2 hour and had the profile shown in Fig. 2-3. Figures 2-27 through 2-32 show the normalized one-sun data for these cells. As the figures show, the short circuit current held fairly constant throughout the tests, while the other parameters showed a gradual decline for 8 of the 10 cells. Two of the 10 cells, cells T4C16 and T5C25, failed rapidly, their peak power falling below 80% of their initial values by the first measurement after 21 cycles. After 800 cycles, all ten cells had failed. As will be discussed in Sec. B-2, below, an analysis of the thermal cycling results shows that the 50% failure point for this group of cells is 300 cycles. Since the cells in the static thermal storage tests were cycled back to room temperature at most eleven times, we can conclude that returning the cells to room temperature for measurements had a negligible effect on cell failures.

b. High Temperature Storage in Air

Two groups of cells were stored at 250°C and 320°C in air ambient. The air ambient allows oxidation to take place, so these tests are expected to be more severe than storage in nitrogen ambient.

Ten cells, soldered to two trays, were held at 250°C in air ambient. Cell T3C15 was OM; the others were LPE. Figures 2-33 through 2-38 show the normalized one-sun data for these cells, and Figs. 2-39 through 2-42 plot the actual values for V_{oc}, I_{sc}, V_{pk-pwr}, and Peak Power. As these figures show, the cell performance was quite constant during the tests. The consistency of the short circuit current is

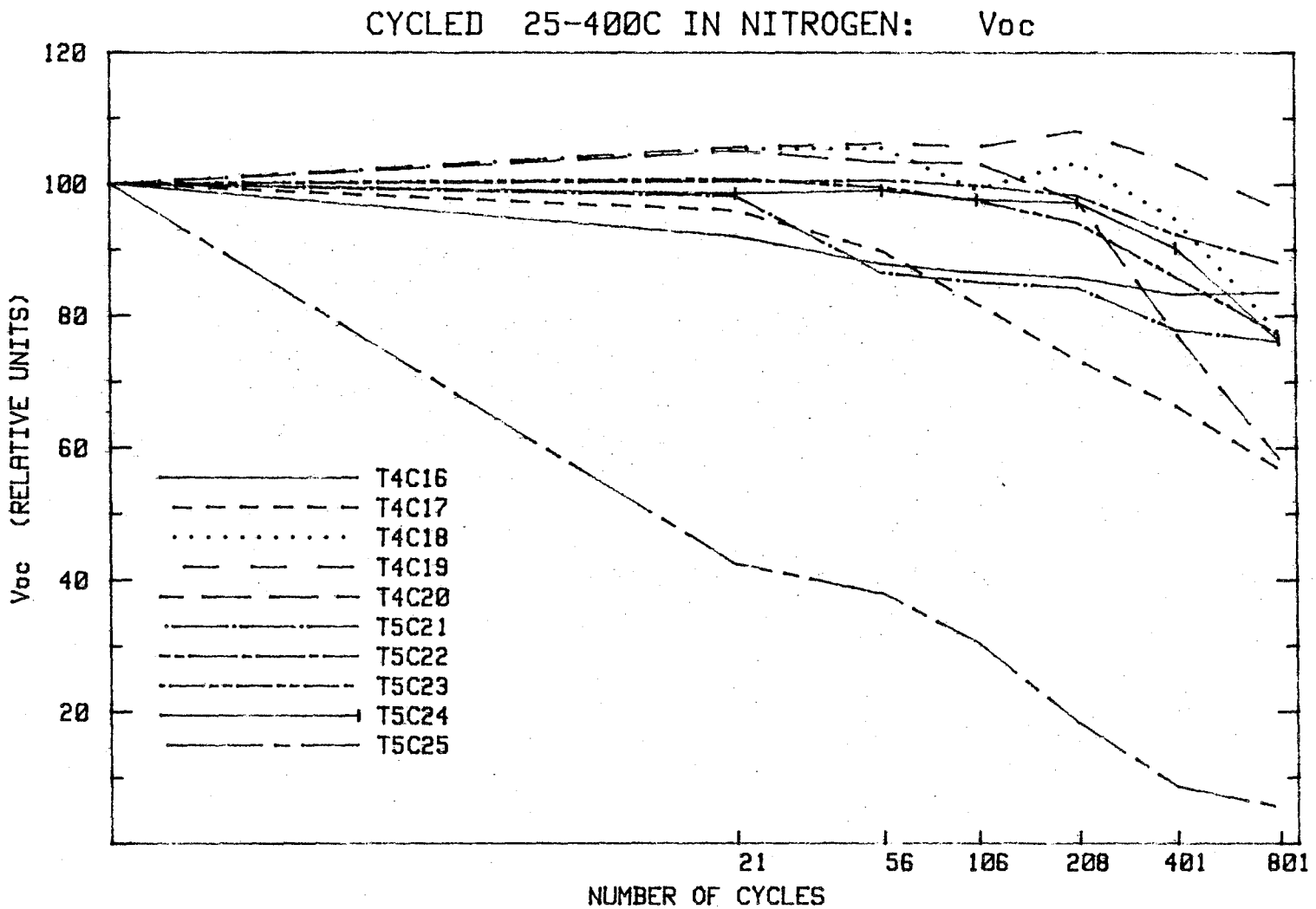

Fig. 2-27 Normalized open circuit voltage versus number of cycles for cells cycled 25-400°C in nitrogen.

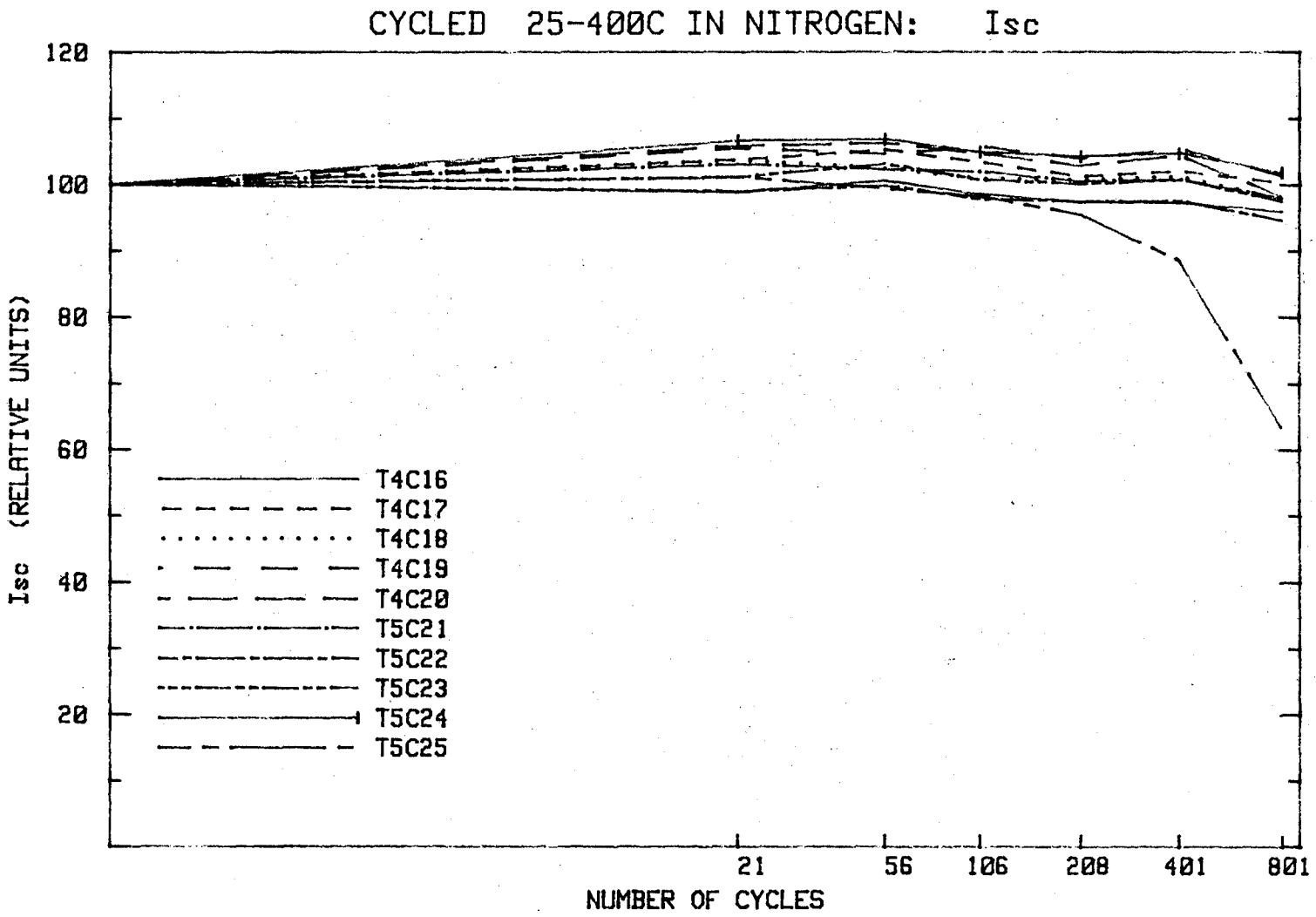

Fig. 2-28 Normalized short circuit current versus number of cycles for cells cycled 25-400°C in nitrogen.

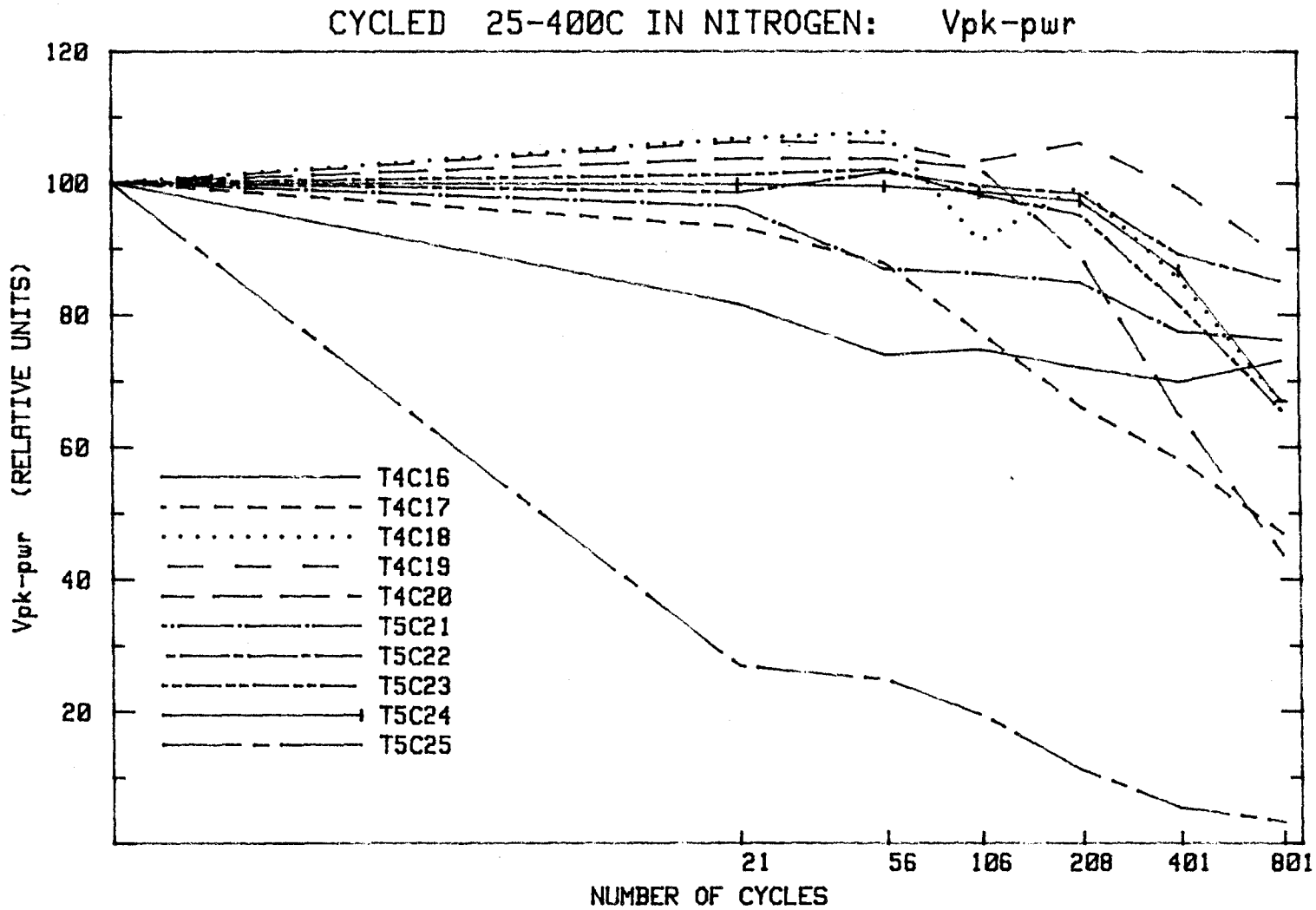

Fig. 2-29 Normalized voltage at peak power point versus number of cycles for cells cycled 25-400°C in nitrogen.

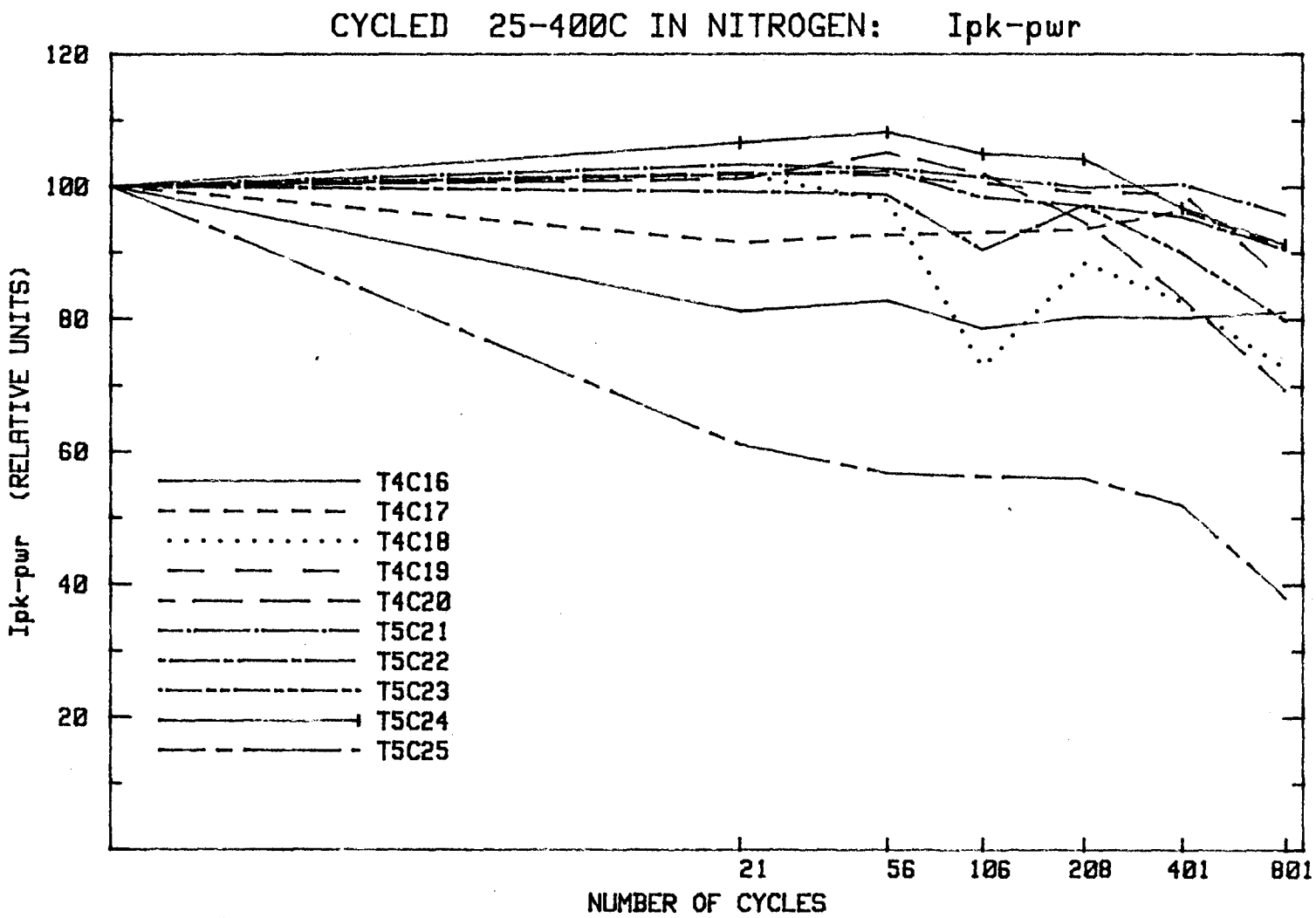

Fig. 2-30 Normalized current at peak power point versus number of cycles for cells cycled 25-400°C in nitrogen.

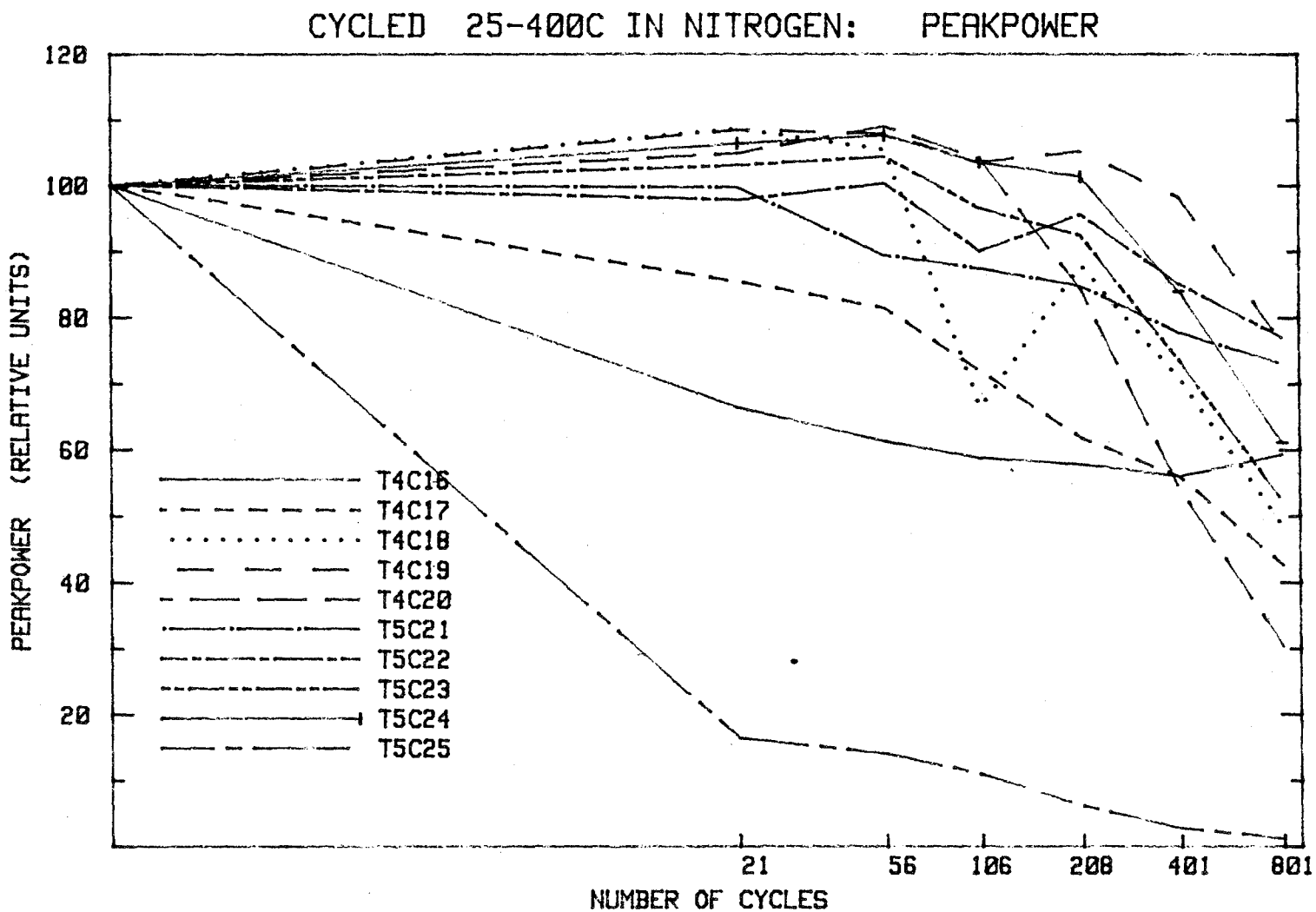

Fig. 2-31 Normalized peak power output versus number of cycles for cells cycled 25-400°C in nitrogen.

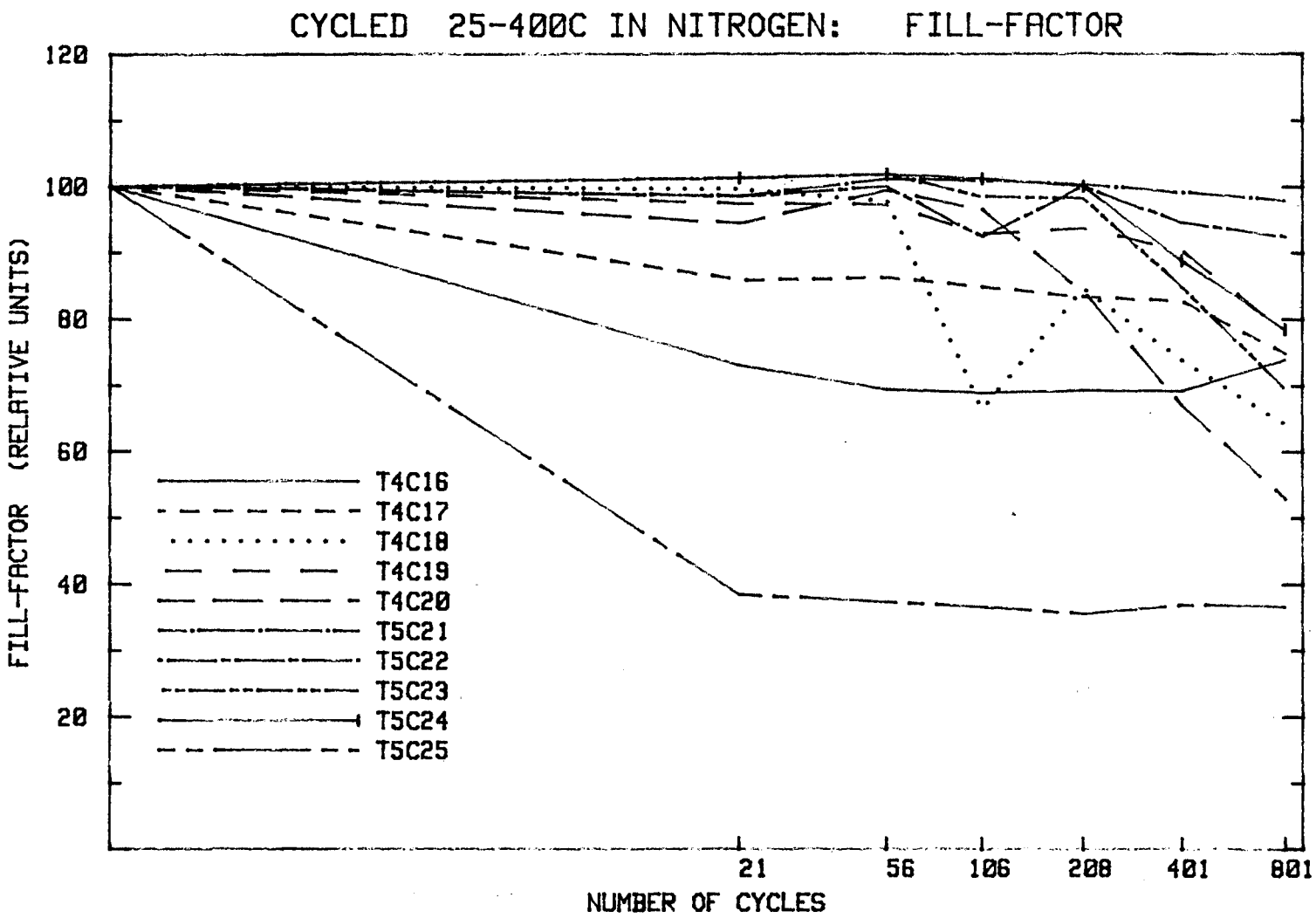

Fig. 2-32 Normalized fill-factor versus number of cycles for cells cycled 25-400°C in nitrogen.

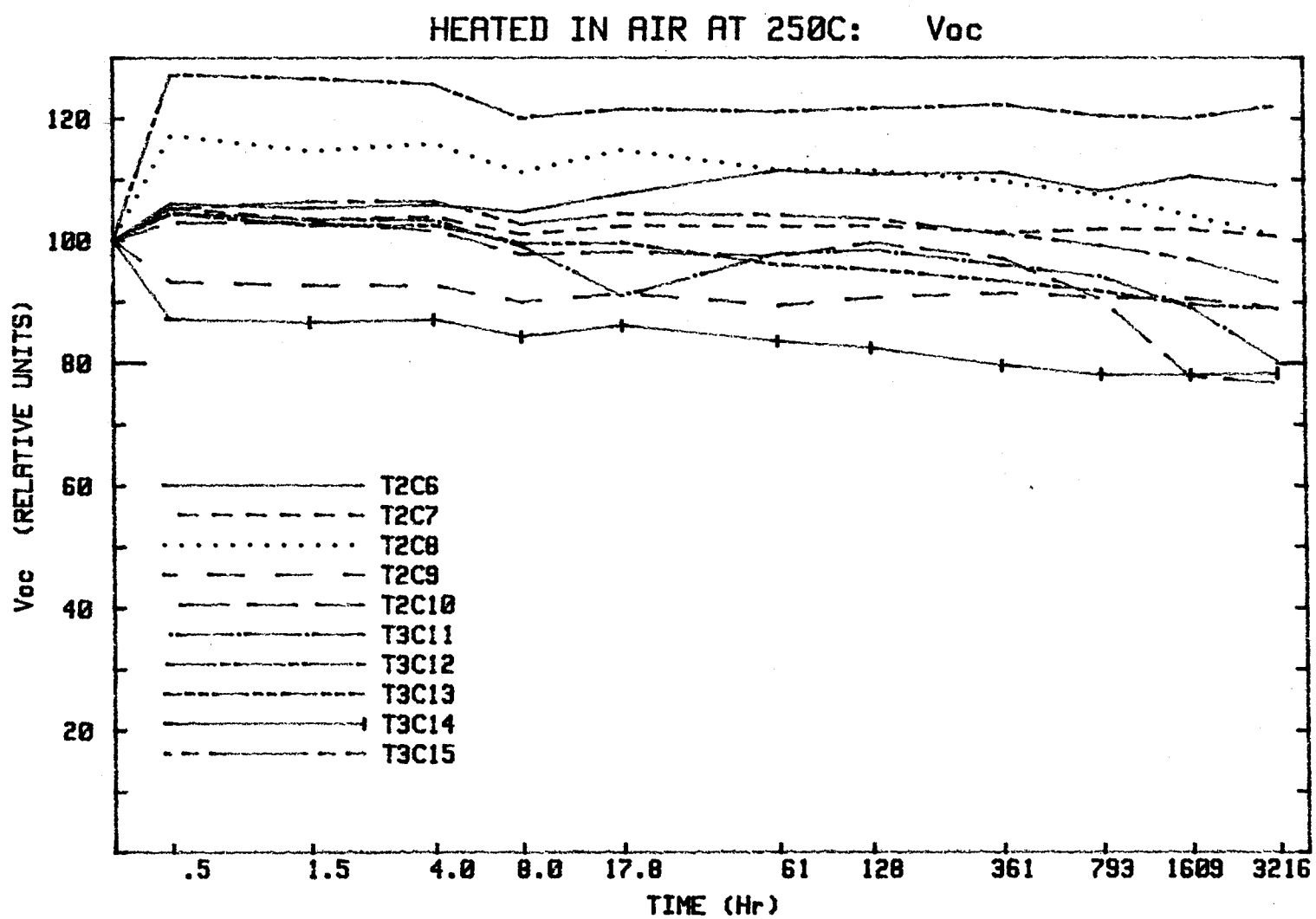

Fig. 2-33 Normalized open circuit voltage versus thermal storage time for cells stored at 250°C in air.

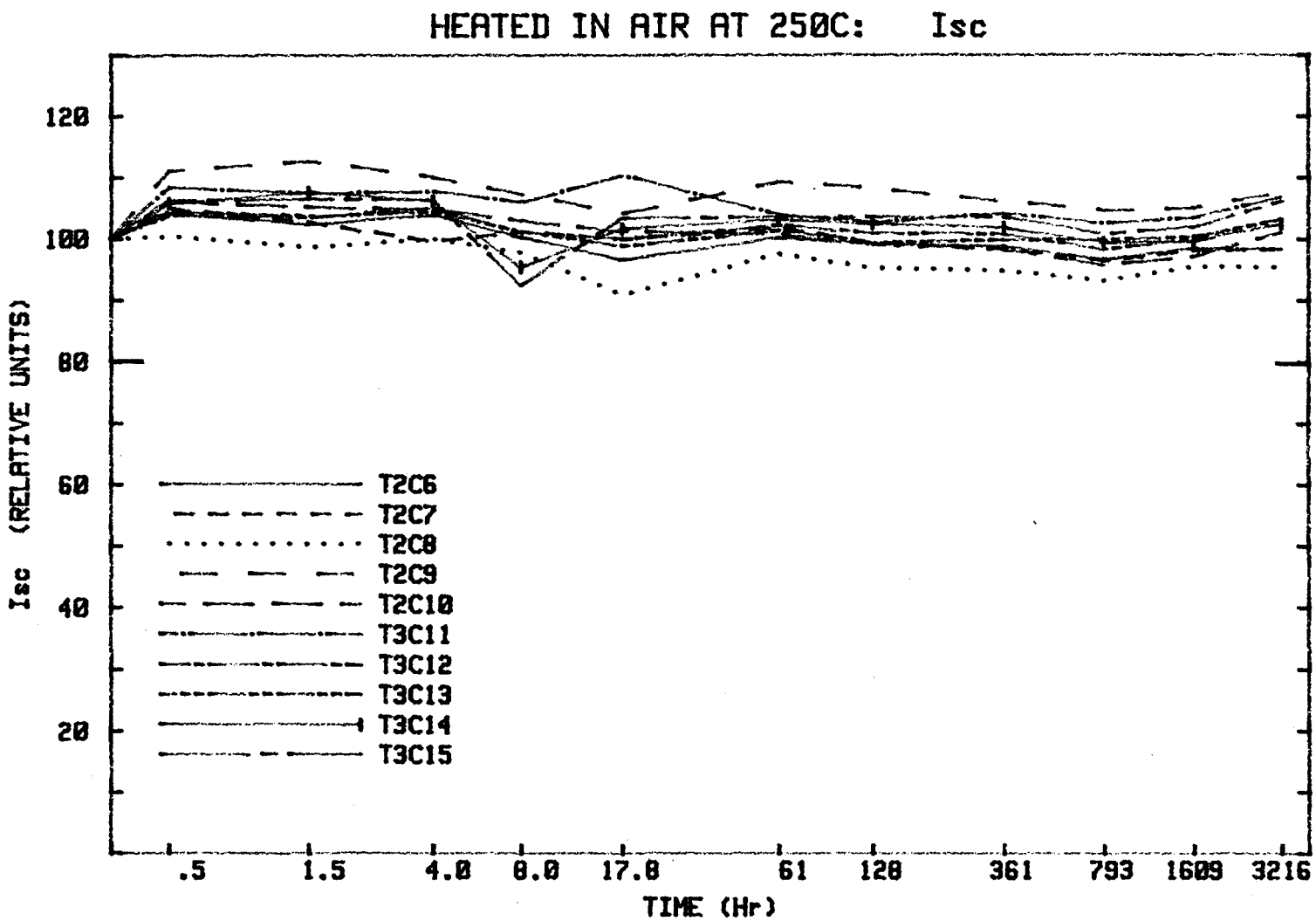

Fig. 2-34 Normalized short circuit current versus thermal storage time for cells stored at 250°C in air.

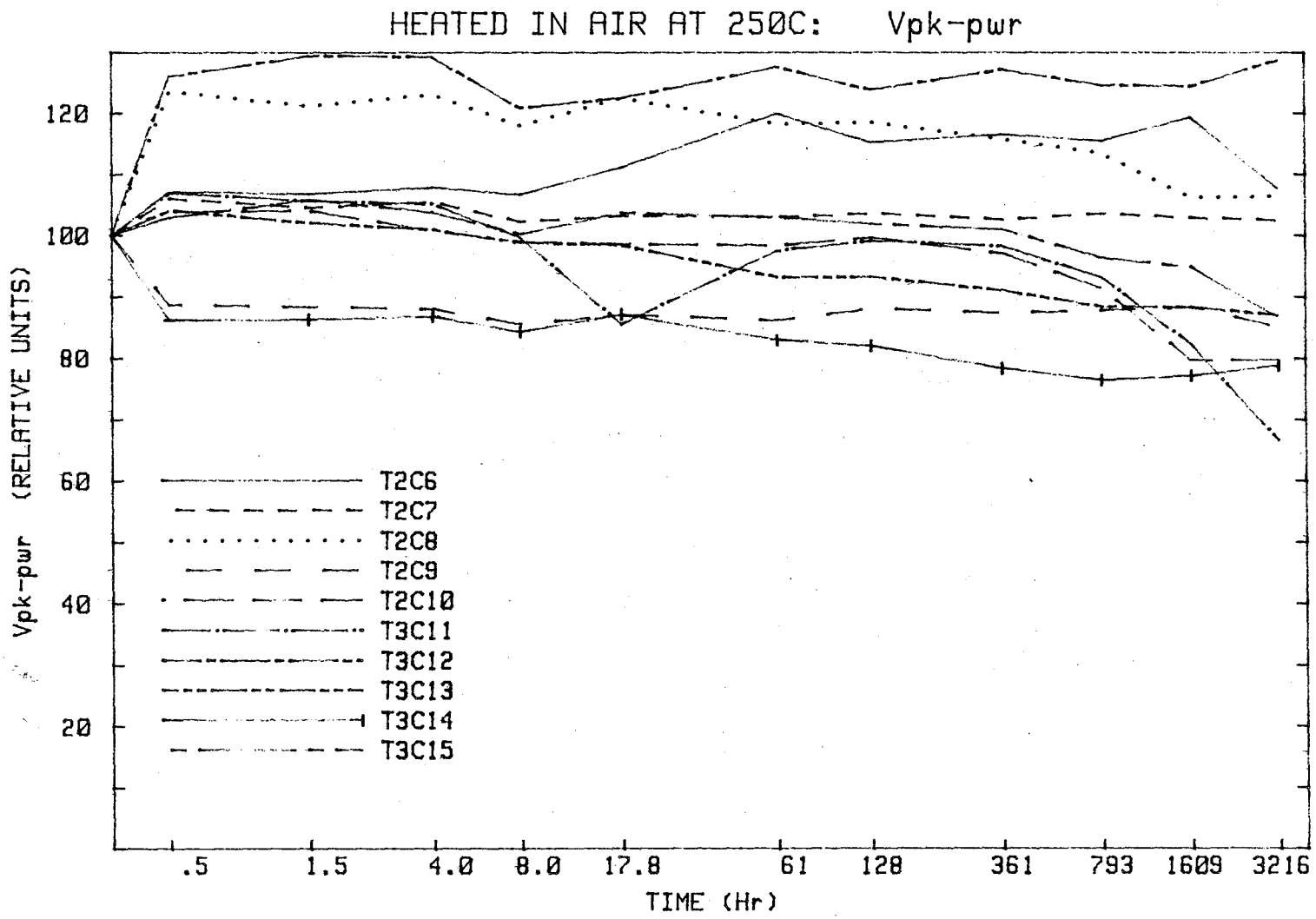

Fig. 2-35 Normalized voltage at peak power point versus thermal storage time for cells stored at 250°C in air.

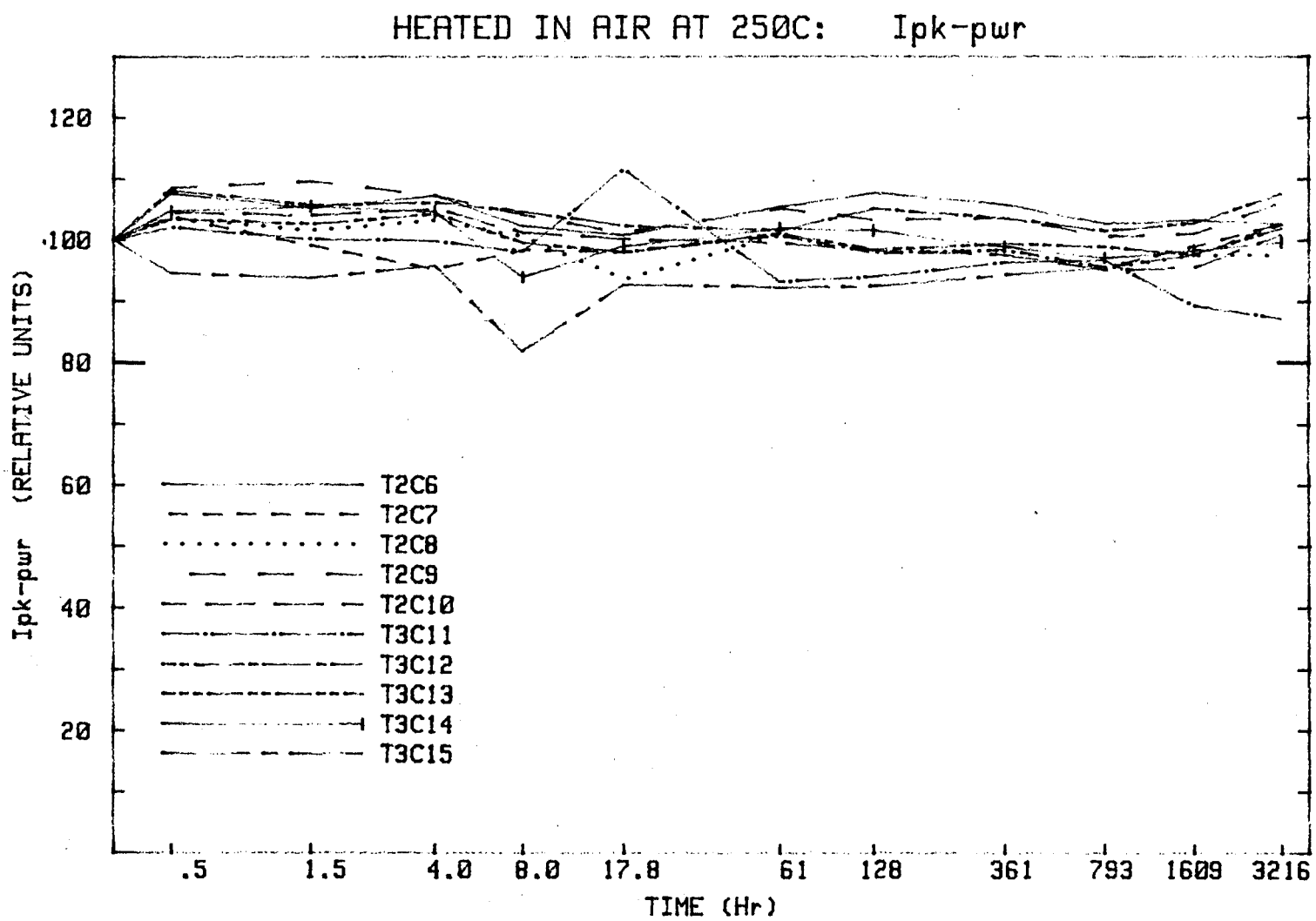

Fig. 2-36 Normalized current at peak power point versus thermal storage time for cells stored at 250°C in air.

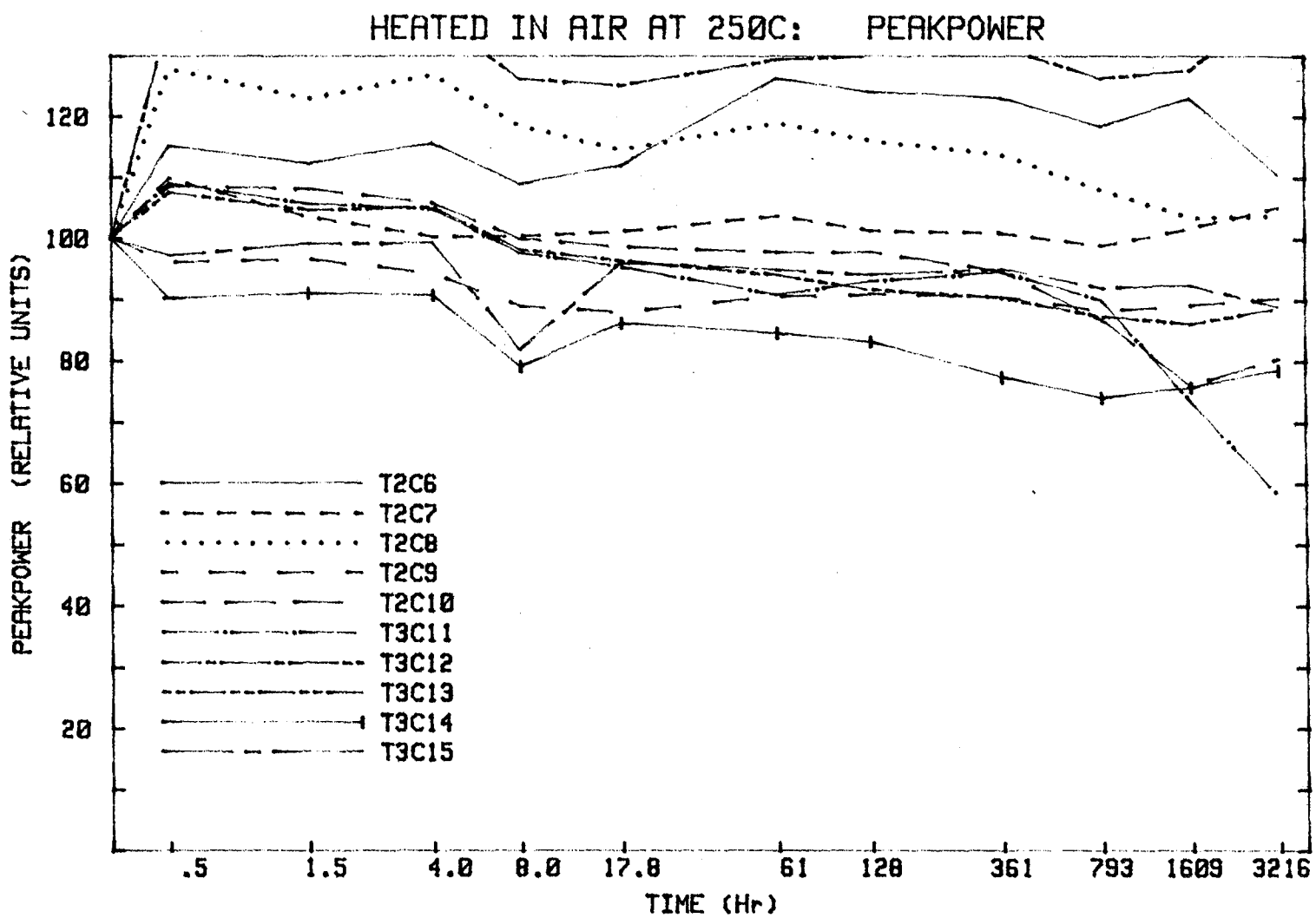

Fig. 2-37 Normalized peak power output versus thermal storage time for cells stored at 250°C in air.

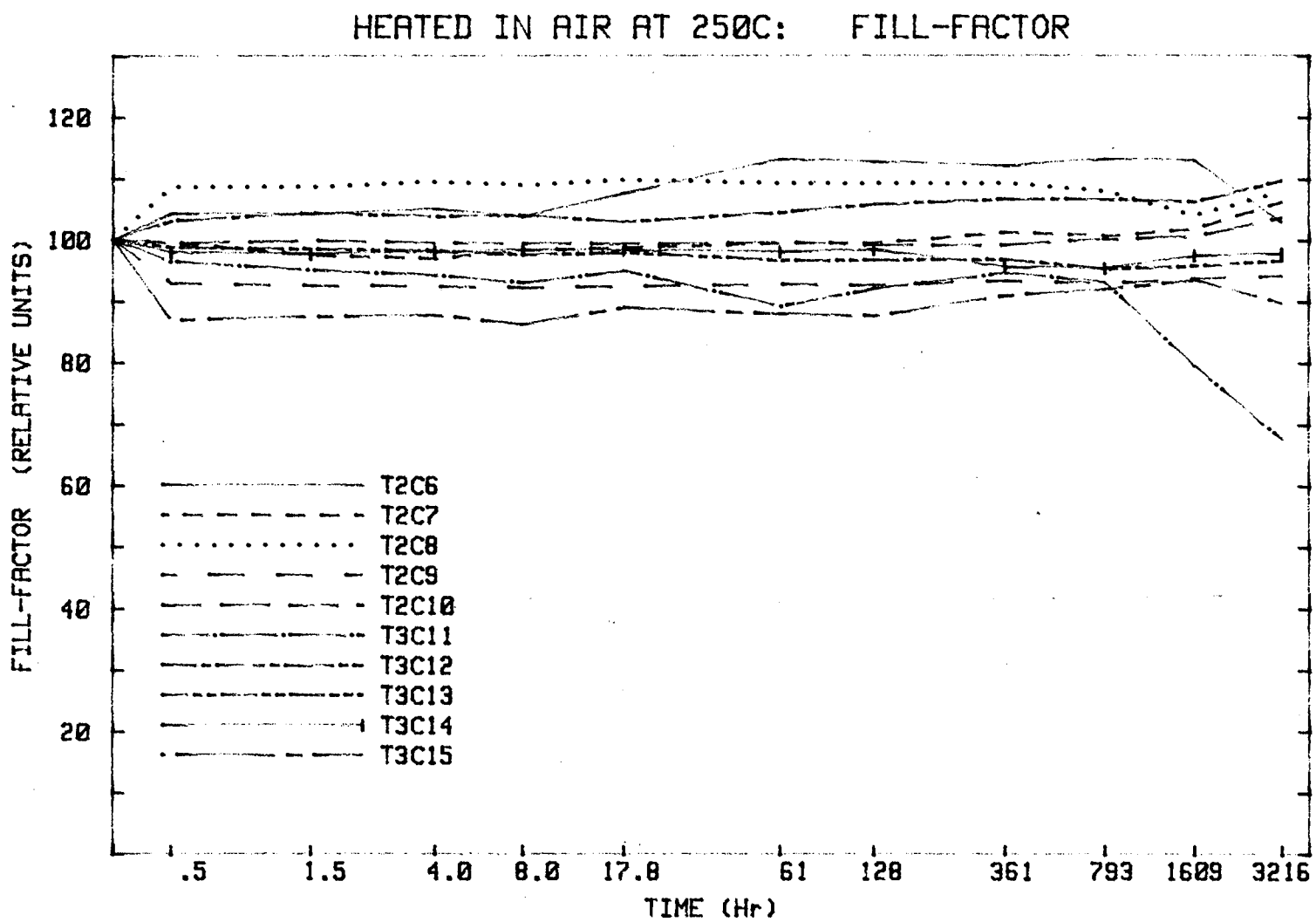

Fig. 2-38 Normalized fill-factor versus thermal storage time for cells stored at 250°C in air.

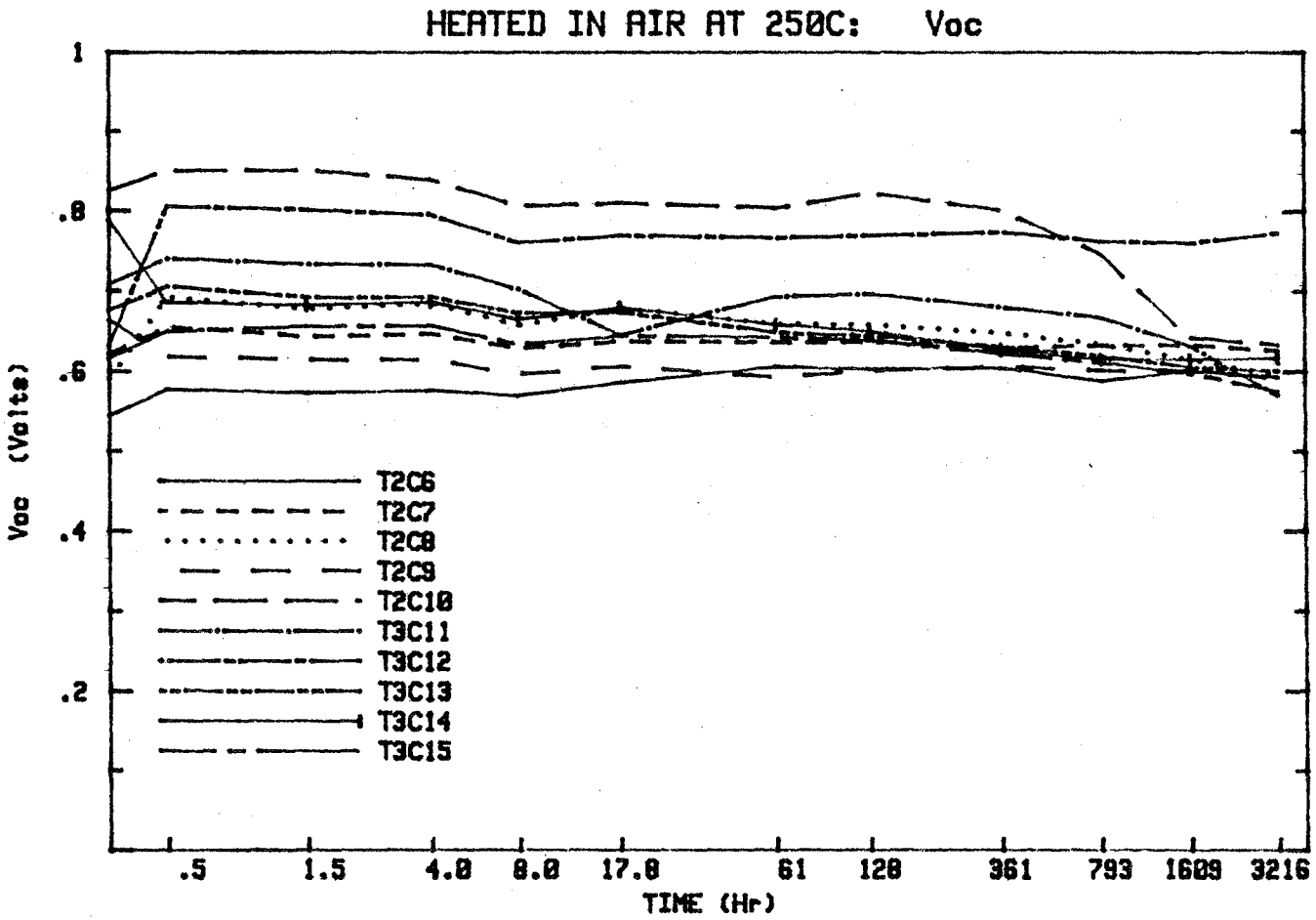

Fig. 2-39 Open circuit voltage versus thermal storage time for cells stored at 250°C in air.

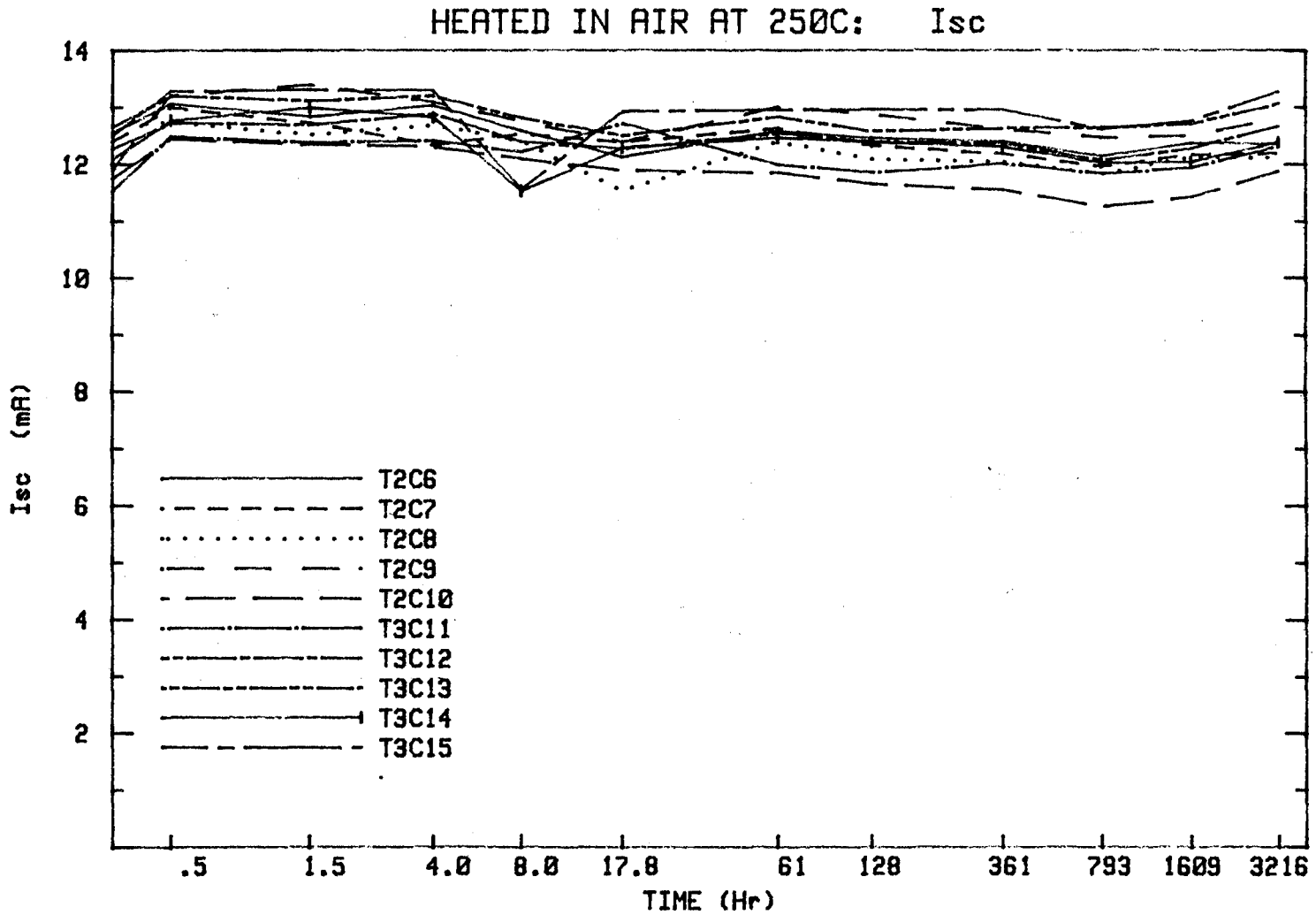

Fig. 2-40 Short circuit current versus thermal storage time for cells stored at 250°C in air.

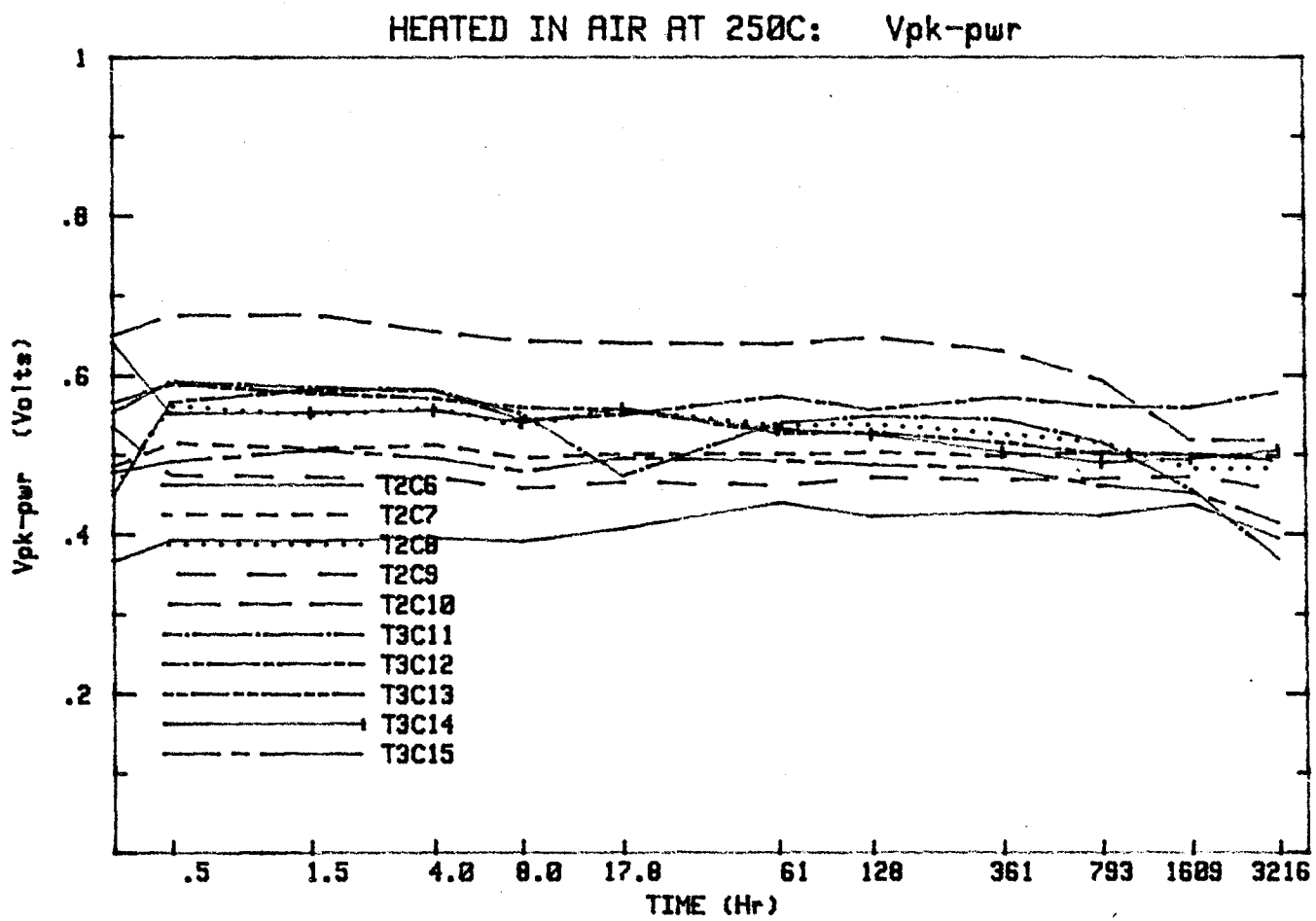

Fig. 2-41 Voltage at peak power point versus thermal storage time for cells stored at 250°C in air.

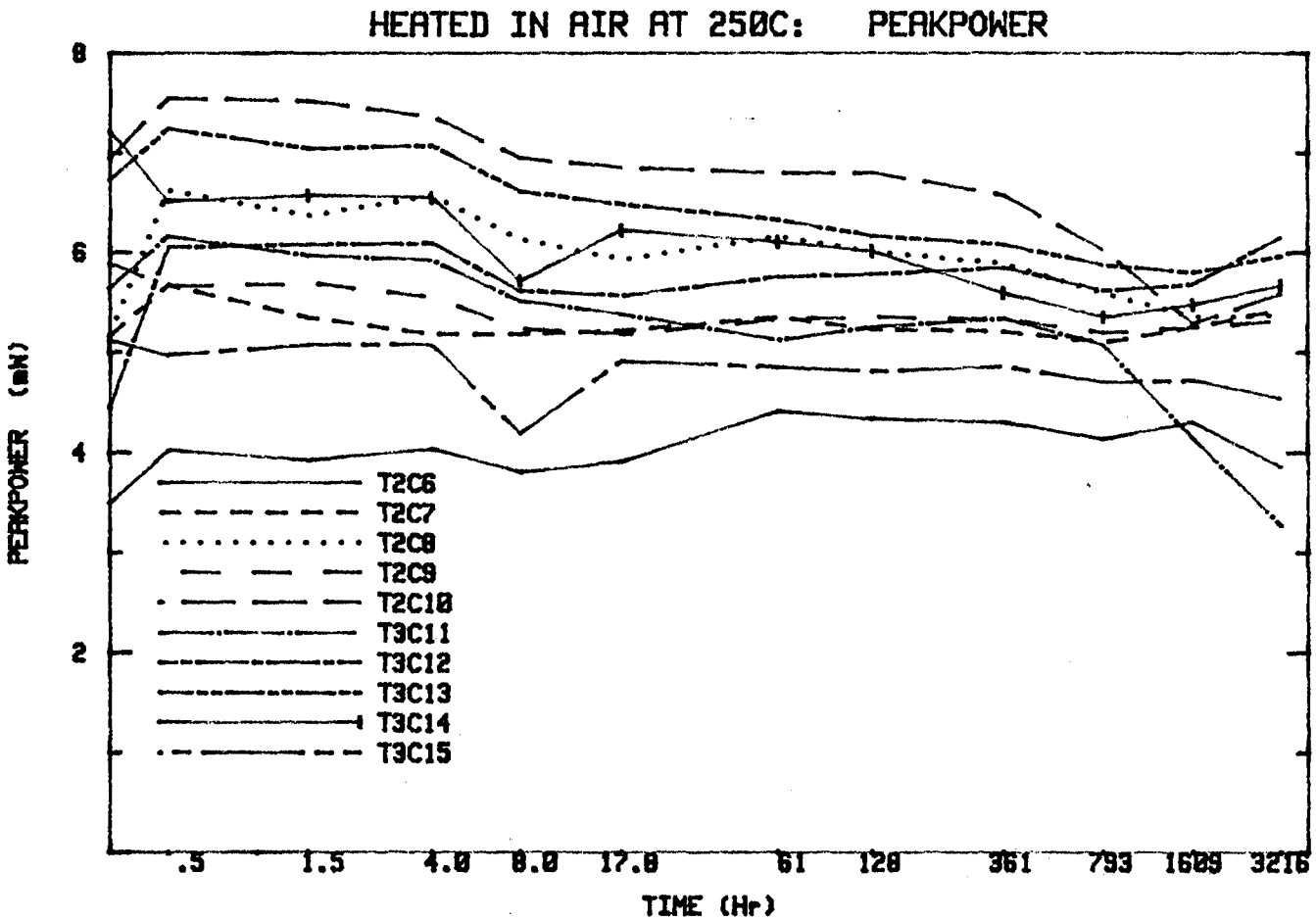

Fig. 2-42 Peak power output versus thermal storage time for cells stored at 250°C in air.

especially striking. Only 3 of the 10 cells failed in over 3000 hours at 250°C, and none failed catastrophically (for example, by shorting out). The performance of the OM cell does not appear to be different than that of the LPE cells.

Ten LPE cells were stored in air at 320°C. These cells were stored loose in the aluminum holders. After 250 hours of storage, three of the ten cells had failed. As with the cells stored at 250°C in air, none of the failures were catastrophic. Figures 2-43 through 2-48 show the normalized one-sun data for these cells, while Figs. 2-49 through 2-52 show the actual values of V_{oc}, I_{sc}, V_{pk-pwr}, and peak power for this group of cells.

2. Analysis of Test Results for Cell Lifetime

In this section, we will analyze the test results of the previous section in order to estimate the cell lifetime at normal operating temperatures. The analysis will be of a standard type commonly used for accelerated life testing.[5-7] The analysis proceeds as follows: the cumulative percentage of cell failures versus test time is found and plotted on log-normal probability paper, for each test temperature. Straight lines are fitted to the plotted points for each temperature, with the lines for each temperature being parallel to each other. The lines are used to interpolate, or extrapolate, to the 50% failure time, or median life time for each temperature. The median lifetimes are then fitted to an Arrhenius equation of the form

$$t_{50} = R_o \, e^{E_A/kT}$$

where t_{50} is the median lifetime, R_o is a constant, E_A is the activation energy, K is Boltzmann's constant, and T is the absolute temperature. The fit to the Arrhenius equation can be done by plotting t_{50} versus 1/T on semilog paper. The cumulative percentage of cell failures for a

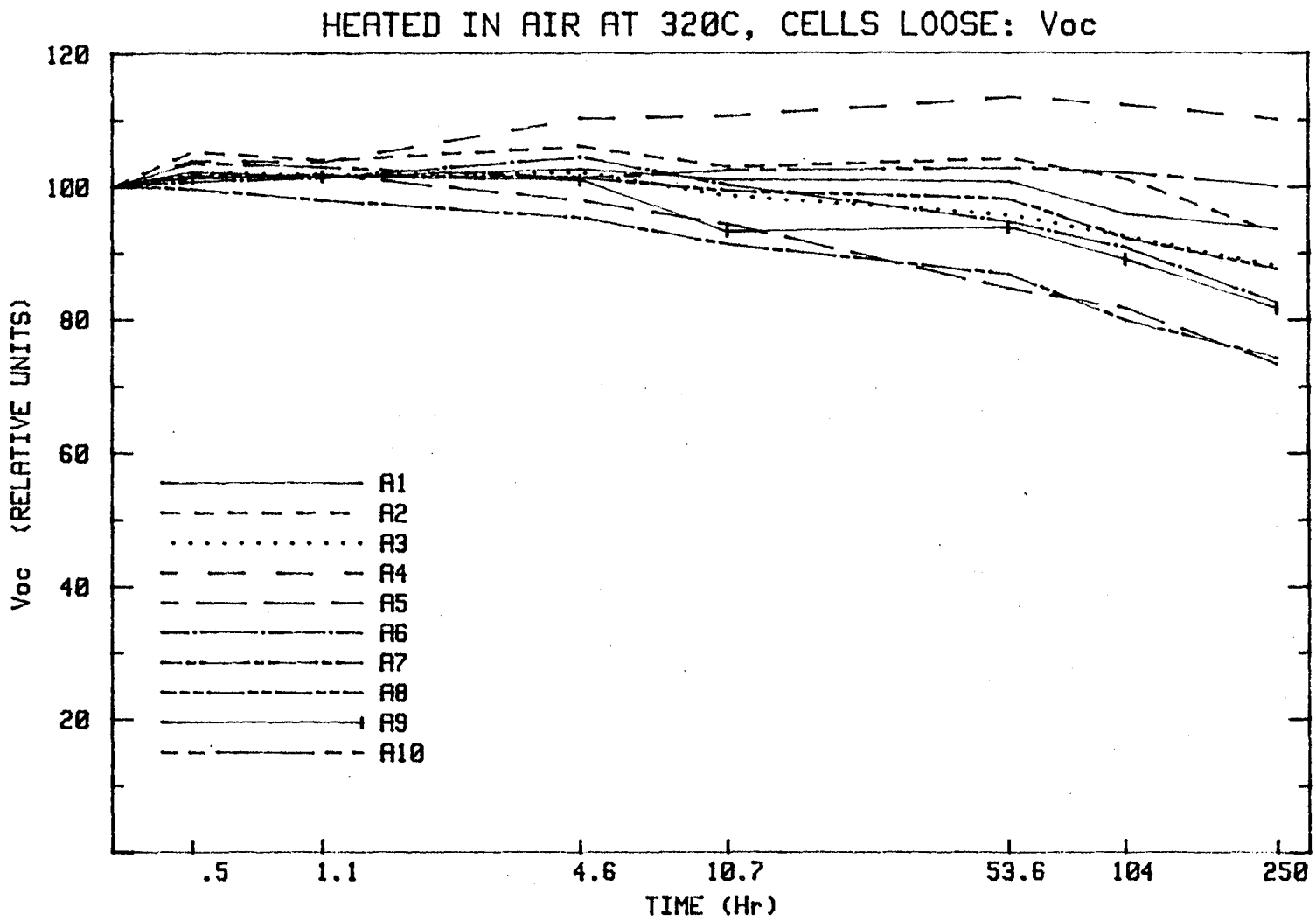

Fig. 2-43 Normalized open circuit voltage versus thermal storage time for cells stored at 320°C in air.

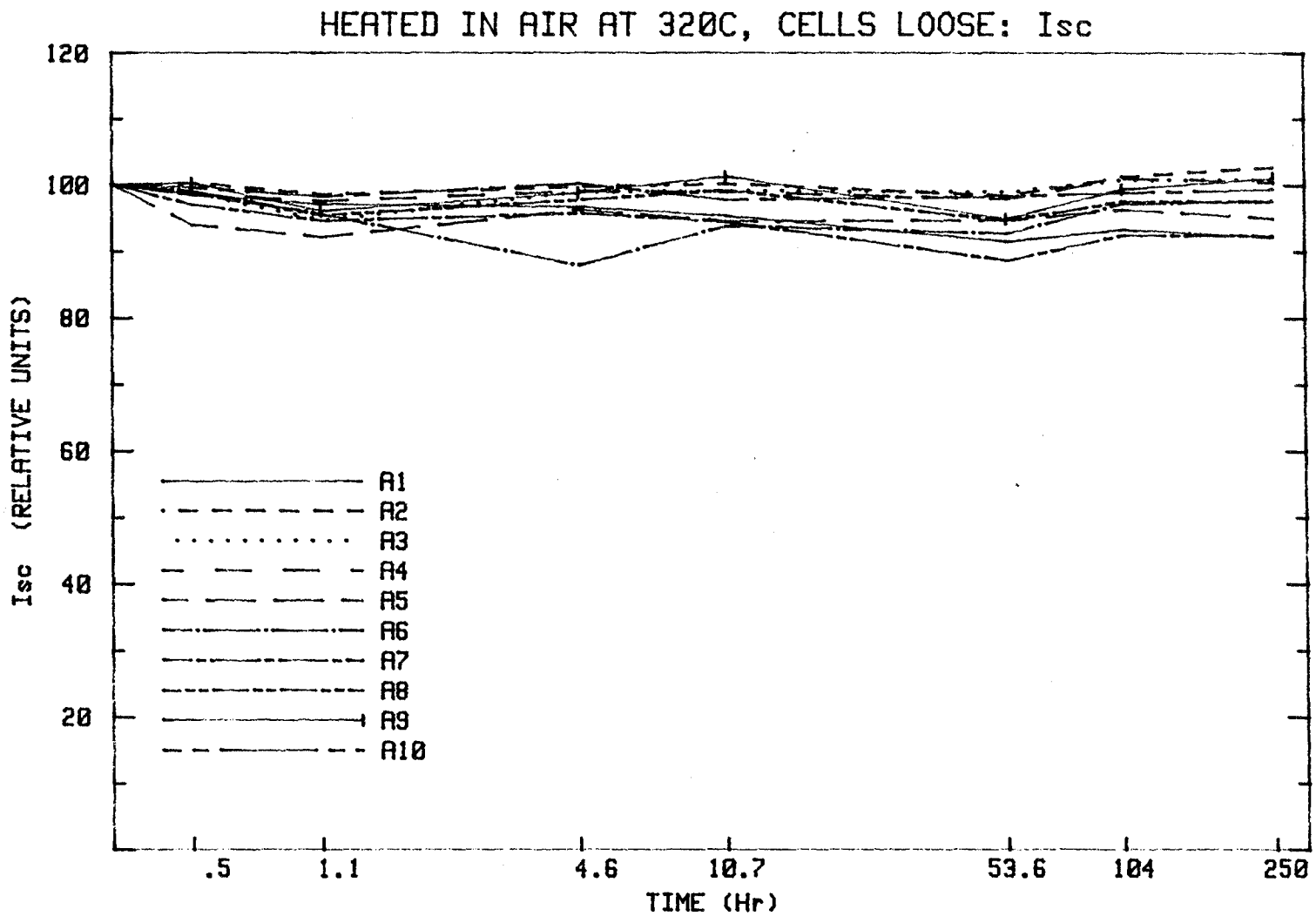

Fig. 2-44 Normalized short circuit current versus thermal storage time for cells stored at 320°C in air.

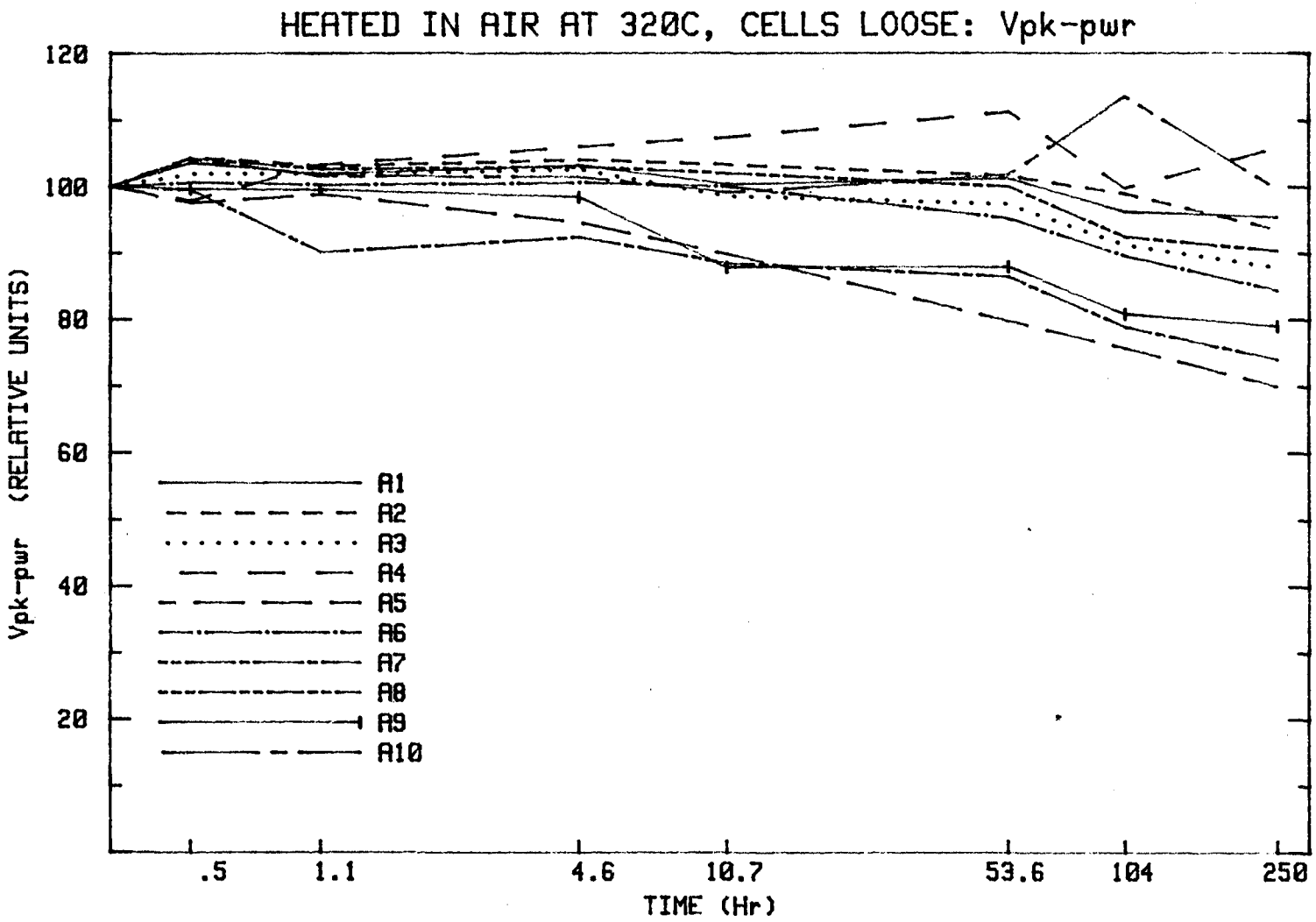

Fig. 2-45 Normalized voltage at peak power point versus thermal storage time for cells stored at 320°C in air.

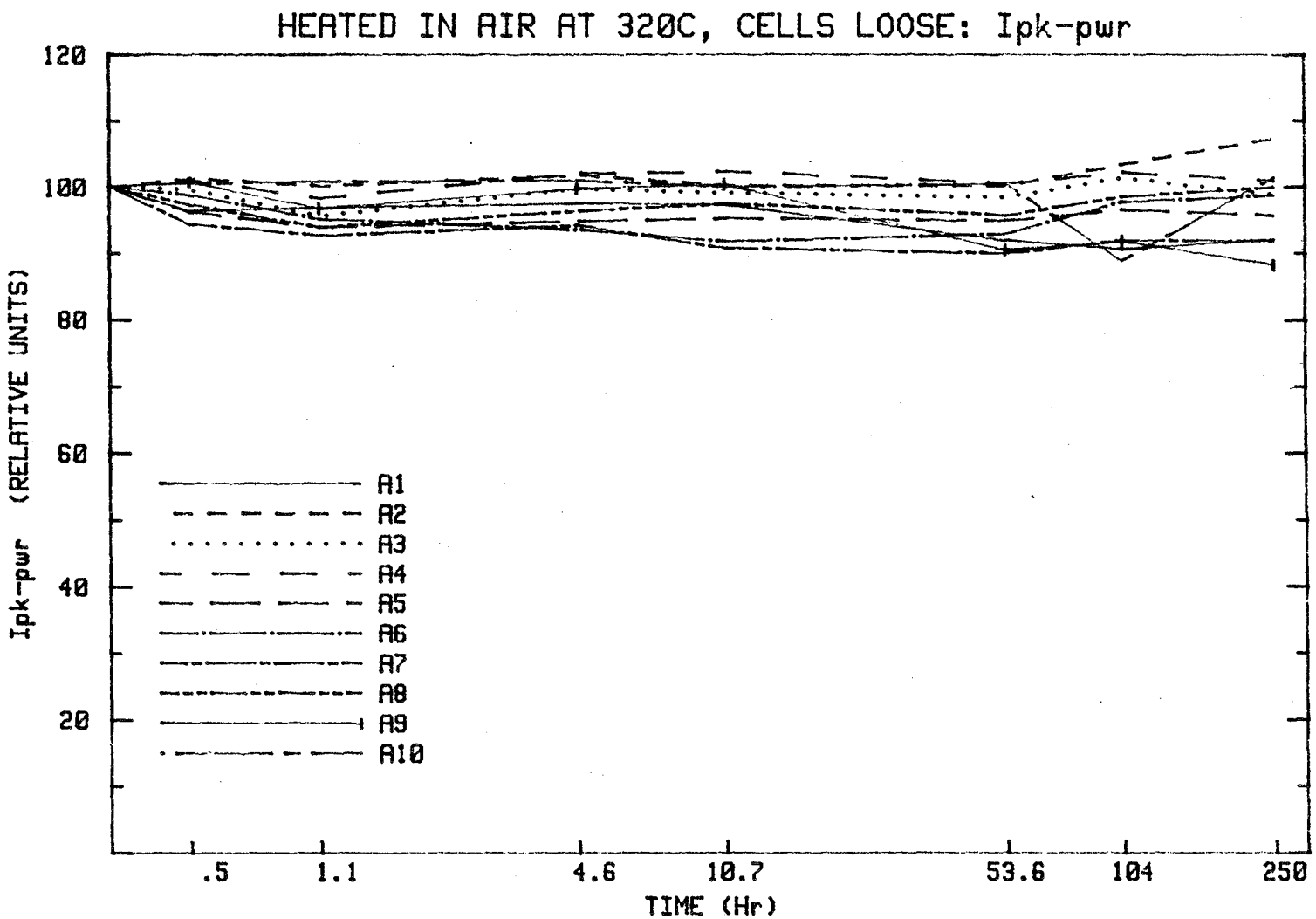

Fig. 2-46 Normalized current at peak power point versus thermal storage time for cells stored at 320°C in air.

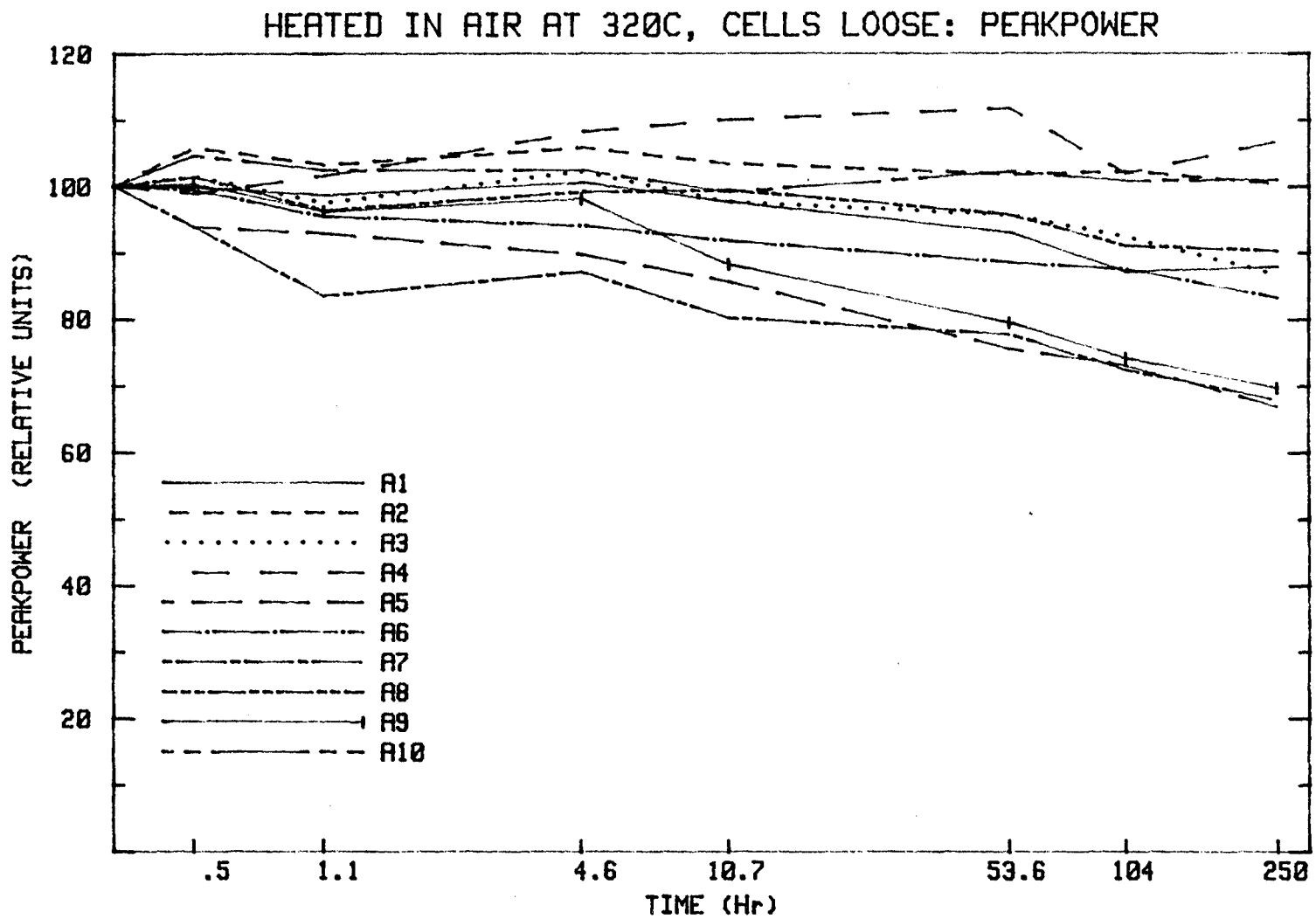

Fig. 2-47 Normalized peak power output versus thermal storage time for cells stored at 320°C in air.

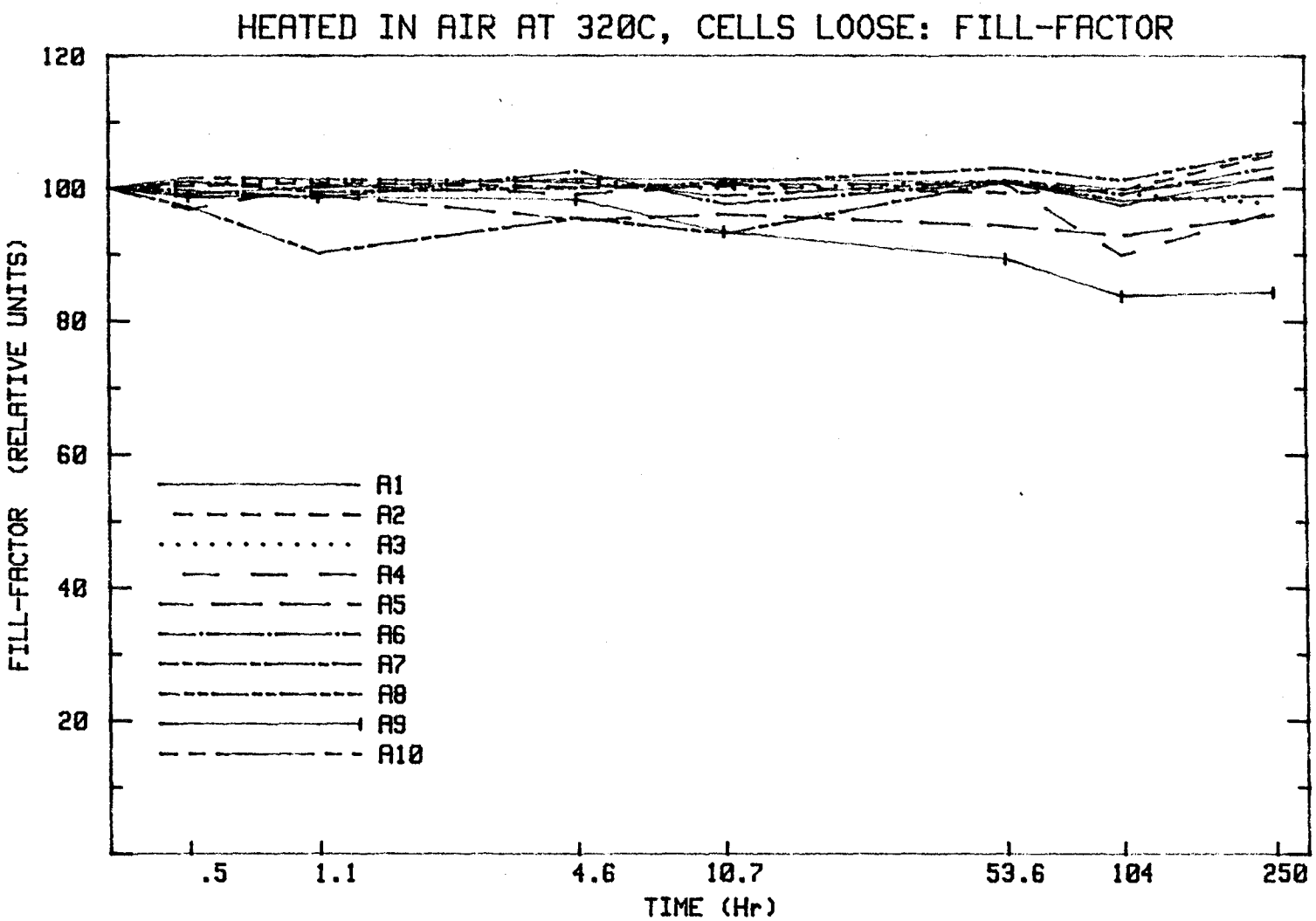

Fig. 2-48 Normalized fill-factor versus thermal storage time for cells stored at 320°C in air.

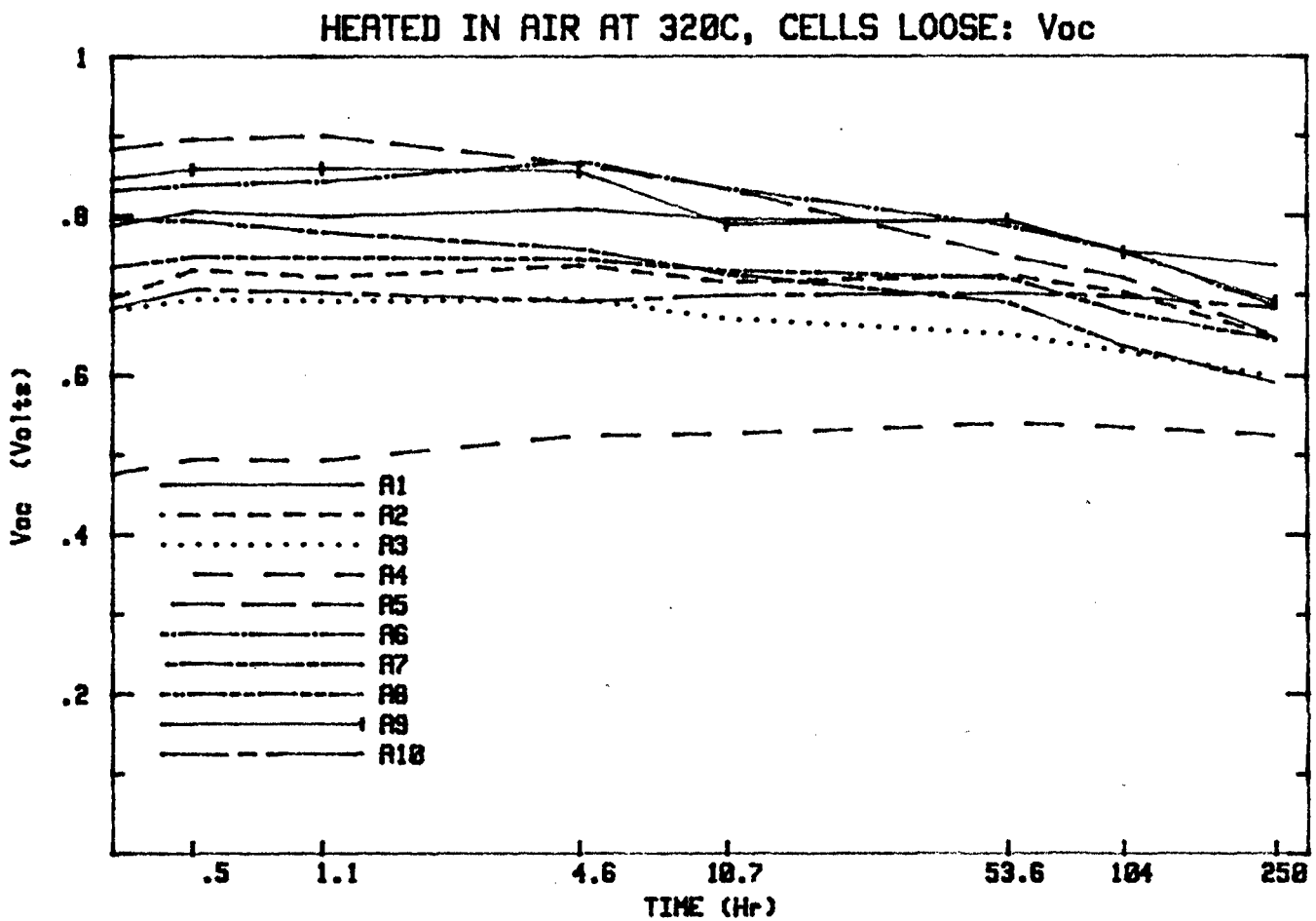

Fig. 2-49 Open circuit voltage versus thermal storage time for cells stored at 320°C in air.

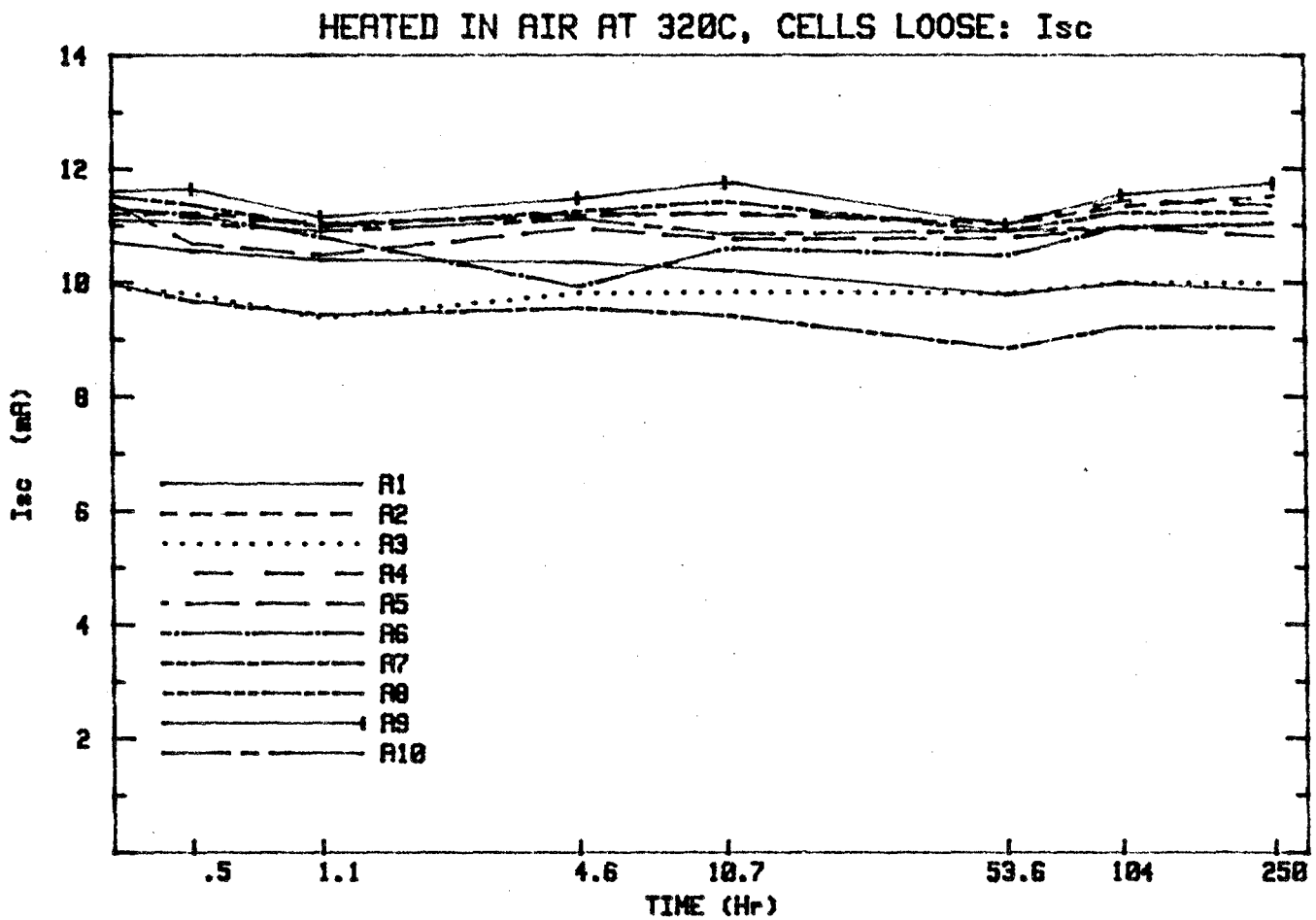

Fig. 2-50 Short circuit current versus thermal storage time for cells stored at 320°C in air.

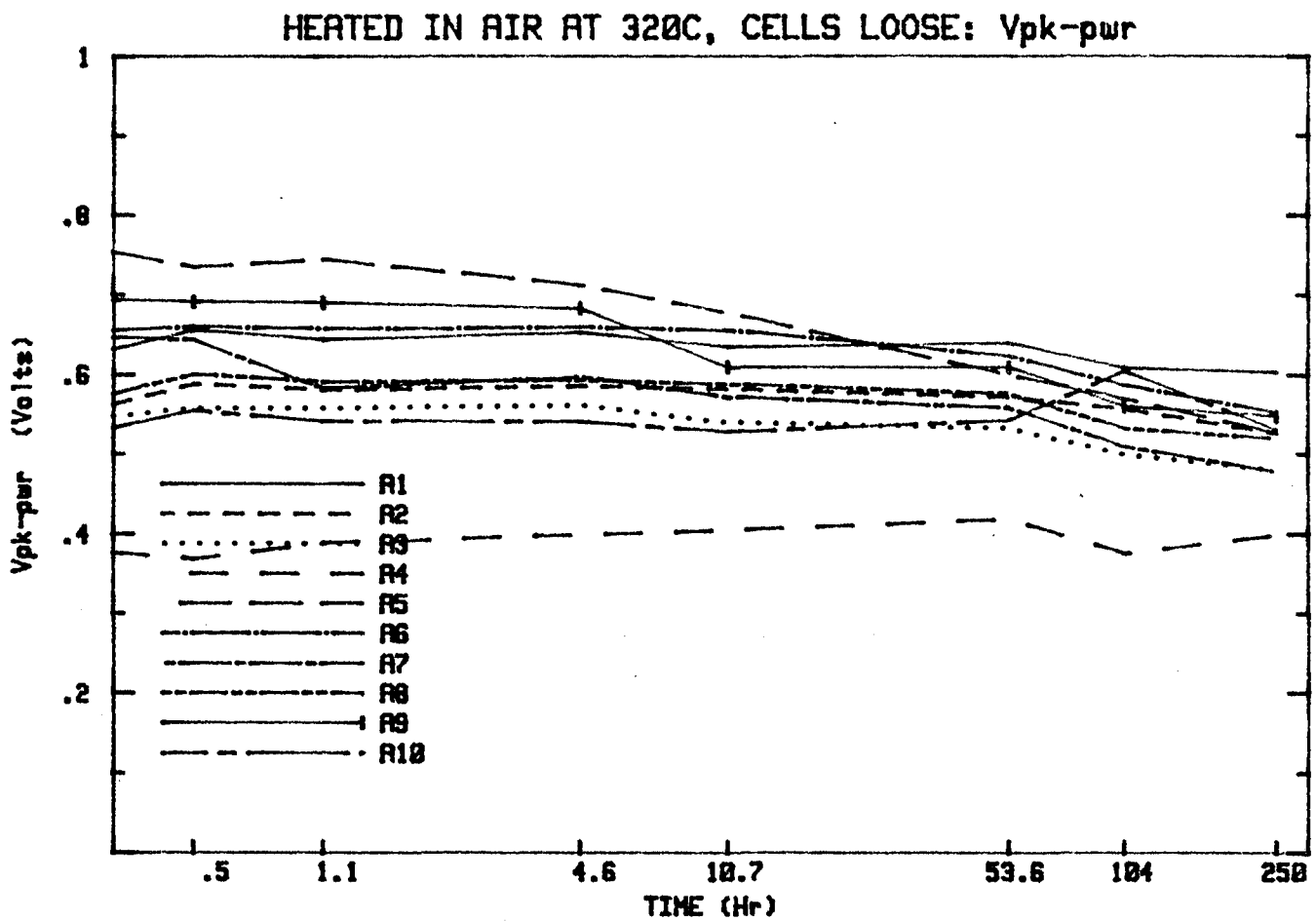

Fig. 2-51 Voltage at peak power point versus thermal storage time for cells stored at 320°C in air.

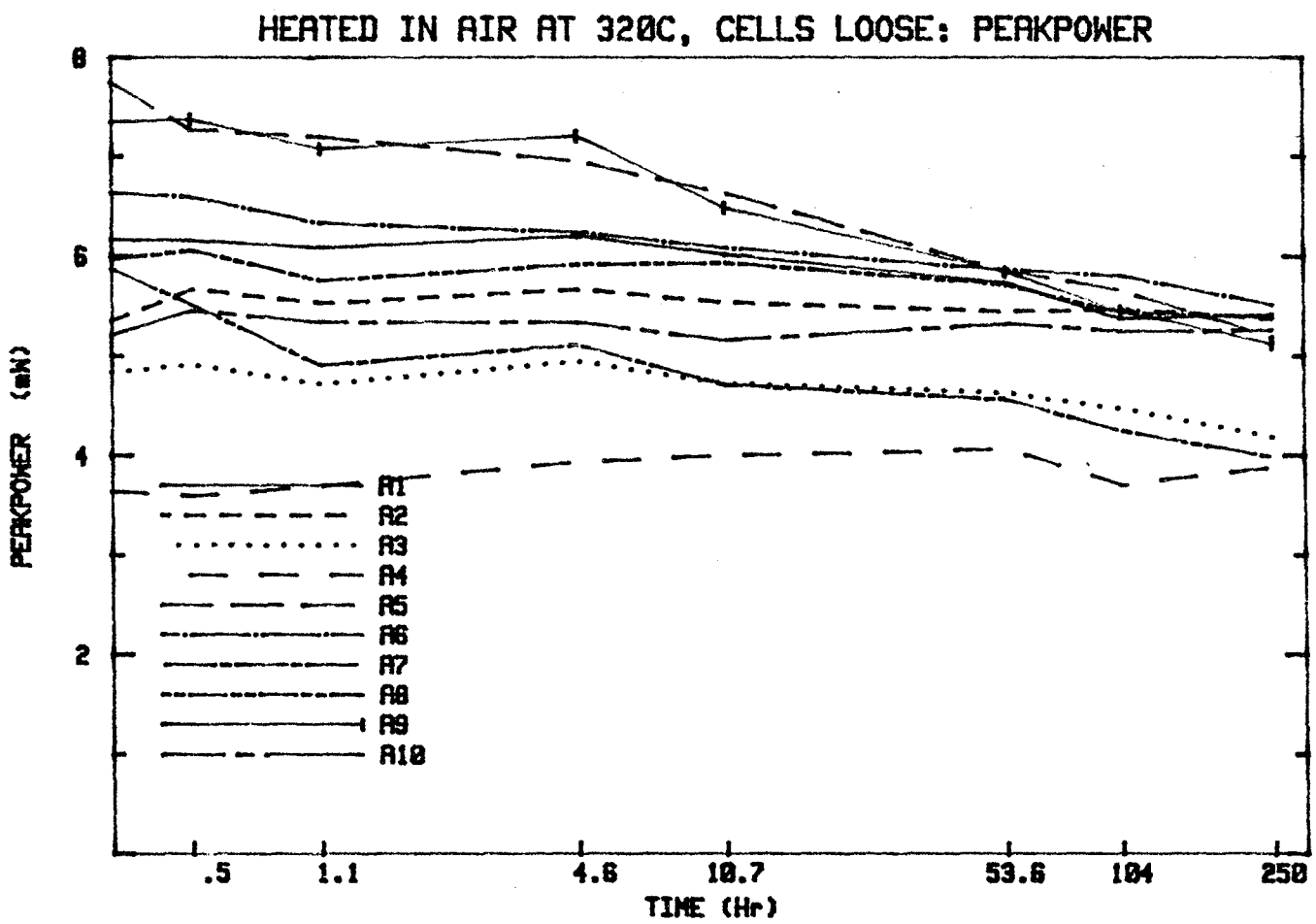

Fig. 2-52 Peak power output versus thermal storage time for cells stored at 320°C in air.

particular time of test is calculated from $100 \cdot N_f/(N + 1)$, where N_f is the total number of failed cells at that time and N is the total number of cells in the test.[5] For this work, we have defined a failed cell to be one for which a given parameter (V_{oc}, I_{sc}, etc.) has fallen below 80% of its initial value. We will analyze failure data from the peak power, open circuit voltage, and short circuit current measurements from the tests at 400 and 425°C in N_2 and 250 and 320°C in air.

Figure 2-53 is a lognormal plot of the cell failures derived from the one-sun peak power measurements, along with the lines fit to the points by eye. The median lifetime points determined by the line are indicated by a + sign. The test at 320°C only had three failures, which occurred relatively early in the test at about 50 hours. There were no more failures until 250 hours, the last point for which data is available. The three early failures appear to represent cases of infant mortality, and would be disregarded if more failures from longer testing were available; thus, it is not possible to estimate a median lifetime for the 320°C test.

The median lifetimes from Fig. 2-53 are shown on an Arrhenius plot in Fig. 2-54. (We have plotted the 400°C data at 386° because a failed thermocouple compensator was found at the end of the test. An accurate temperature measurement showed that the temperature had been 386° rather than 400°.)

Since there are only three points in Fig. 2-55, and they do not lie on a single line, it is not immediately obvious what is the best straight line fit to the points. The point from the 400°C test is the most certain; it represents 8 failures out of 9 cells. There were only 3 failures at 250°C, and the sample size was only 4 for the 425°C test. The best fit line should be weighted towards the 400° point.

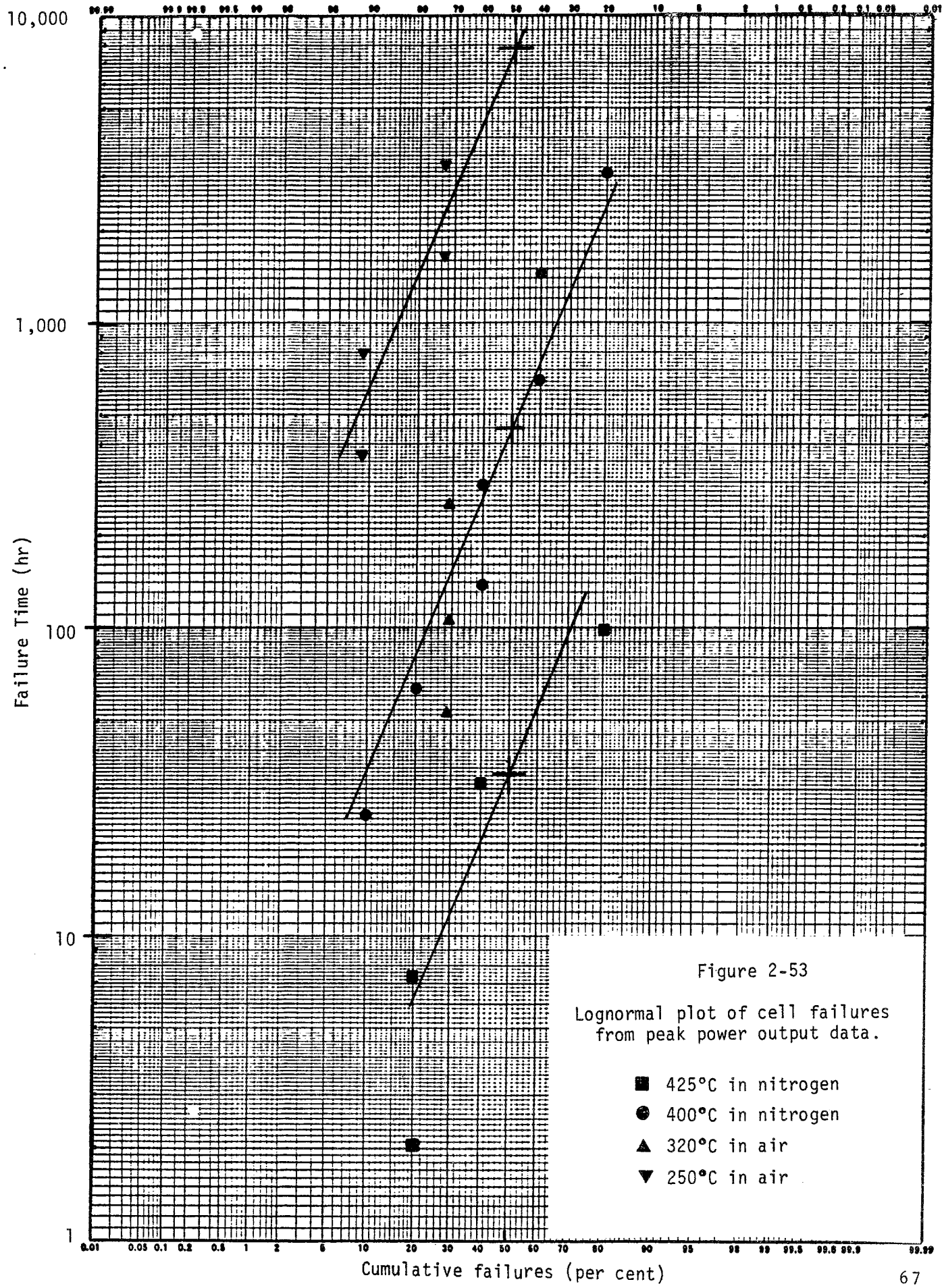

Figure 2-53

Lognormal plot of cell failures from peak power output data.

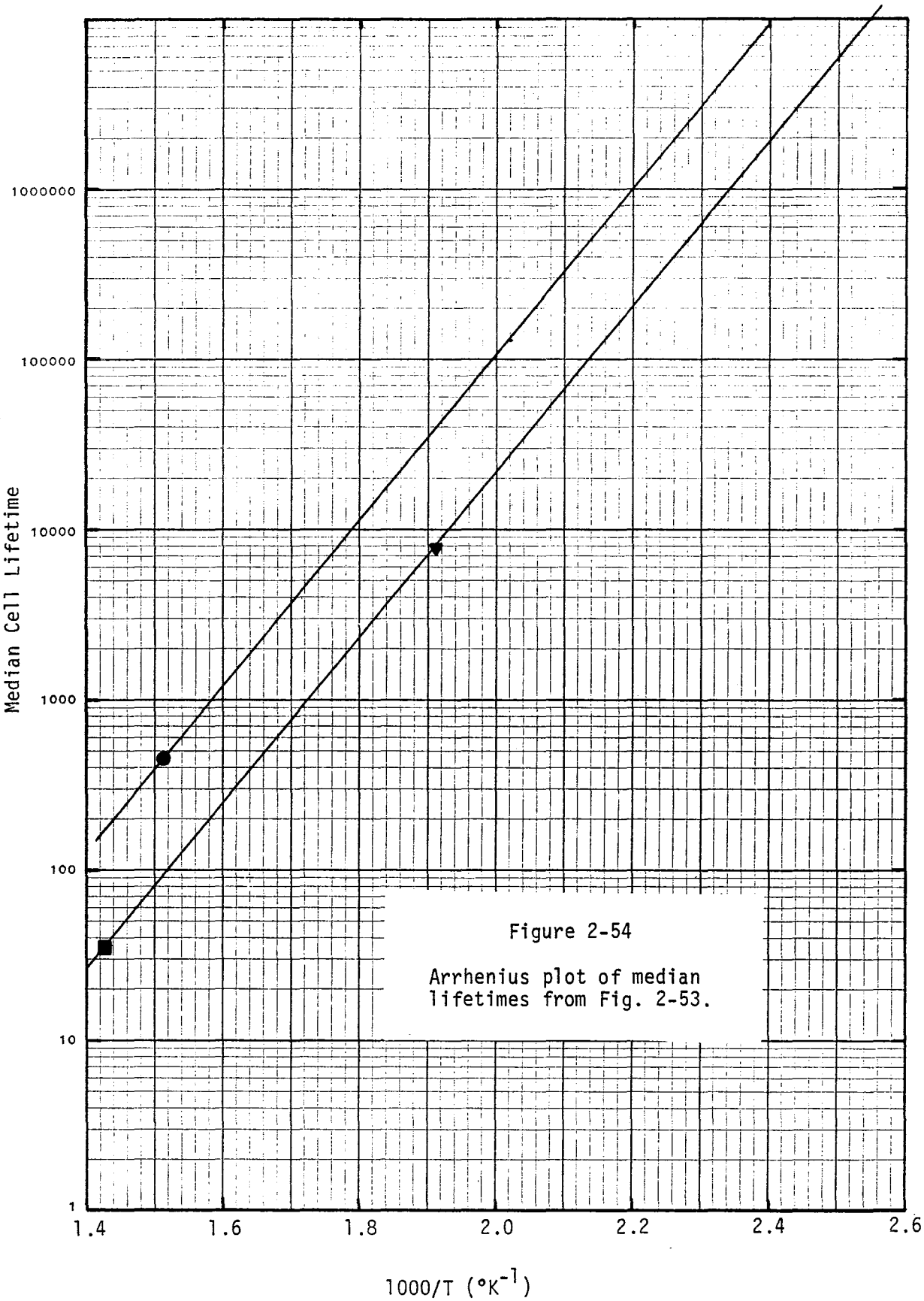

Figure 2-54

Arrhenius plot of median lifetimes from Fig. 2-53.

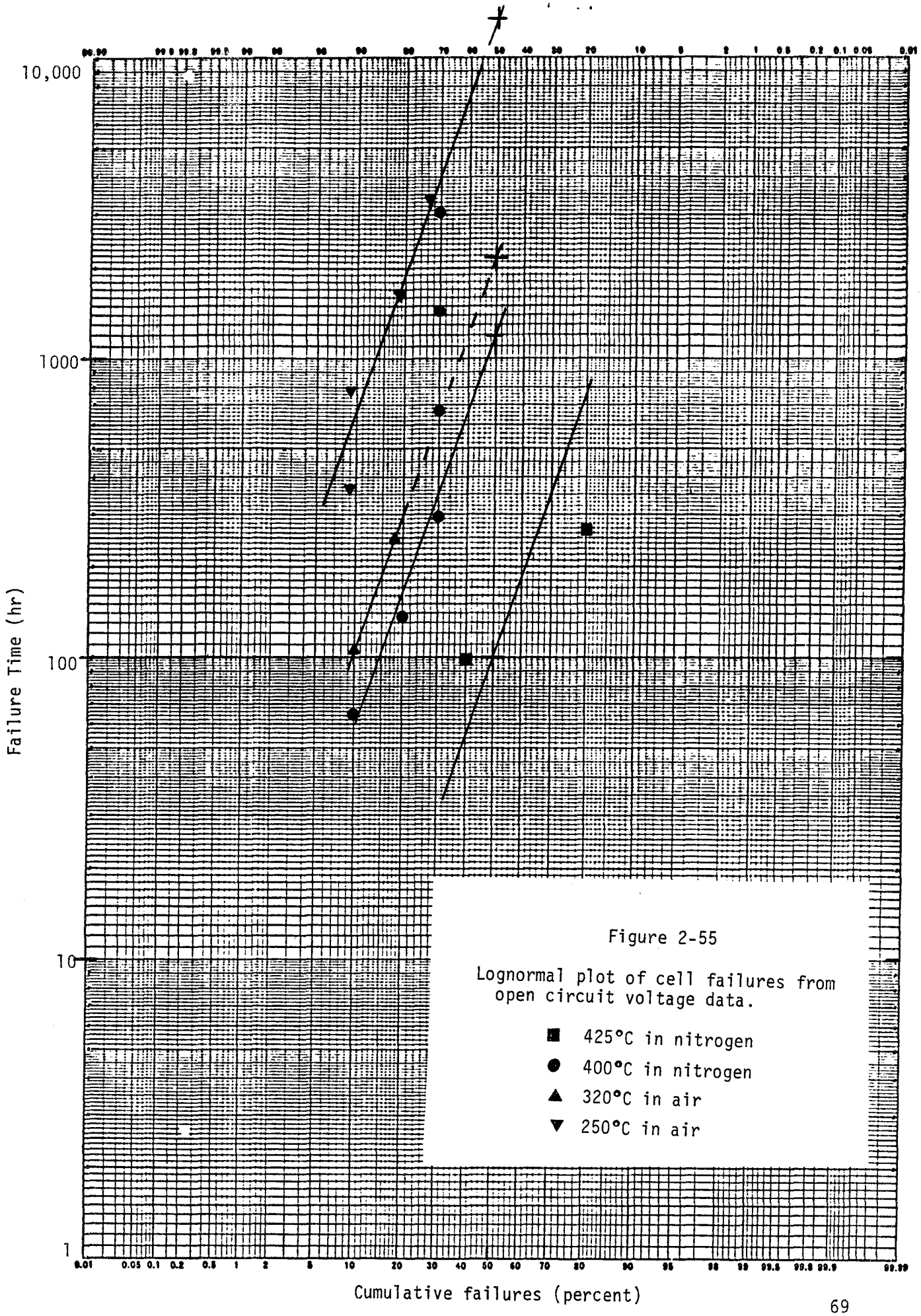

Figure 2-55

Lognormal plot of cell failures from open circuit voltage data.

Ideally, the air and nitrogen tests should be considered separately, but there is not enough data to do that. Furthermore, if we concentrate on only the nitrogen tests and draw the line through the 400 and 425° points, an activation energy of 2.7 eV results, which is unreasonably large. Even worse, if we extrapolate this line to 50°C, we get a median lifetime of $\sim 10^{20}$ years, which seems very unrealistic, especially considering that the estimated age of the universe is $\sim 10^{10}$ years.

A more reasonable estimate is given by connecting the 425 and 250° points. This line gives $E_A = 0.98$ eV, a reasonable number, and an estimated median life at 50°C of 6.5×10^5 years. If we draw a line through the 400° point that is parallel to the line through the 425 and 250°C points, and use the line through the 400° point for an upper limit estimate and the line through the 425 and 250°C points to get a lower limit estimate, we get the estimates in Table I.

TABLE I

Cell Median Lifetime Estimates from Peak Power Data

Cell Temperature (°C)	Estimated Median Lifetime (years)
150	150 - 800
100	5700 - 30,000
50	650,000 - 3,400,000

Figure 2-55 is a lognormal plot of cell failure times taken from the open circuit voltage data. The median lifetimes from Fig. 2-55 are plotted in Fig. 2-56. Again, the 400° point does not lie on a line with the other three points. Drawing two lines, as was done for the peak power data, we get the lifetime estimates in Table II.

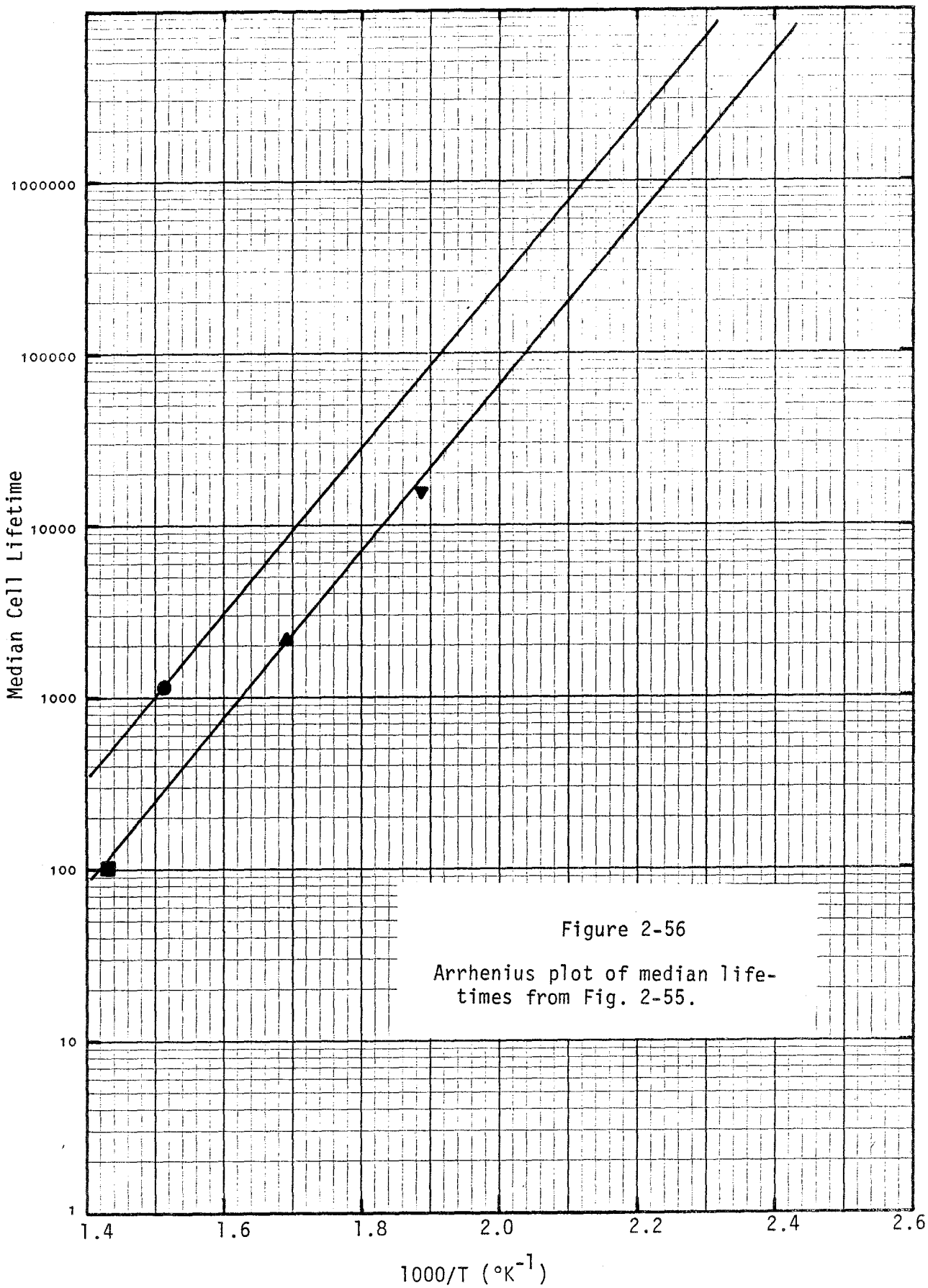

Figure 2-56

Arrhenius plot of median lifetimes from Fig. 2-55.

TABLE II

Estimates of Cell Median Lifetime from Open Circuit Voltage Data

Cell Temperature (°C)	Estimated Median Lifetime (years)
150	420 - 1700
100	14,000 - 58,000
50	1,500,000 - 6,000,000

The activation energy derived from the open circuit voltage data is 0.96 eV, essentially the same as from the peak power data.

Figure 2-57 is a lognormal plot of cell failures from the short circuit current data. The short circuit current was the cell parameter least affected during the life tests; there were no short circuit current failures in either the 250 or 320° tests in air, and only one failure in the cells held at 425°. The number of short circuit current failures is so small that it is not possible to make a meaningful prediction of cell lifetime on the basis of that data.

Figure 2-58 shows a lognormal plot from the peak power measurements from the cells cycled between 25 and 400°C. Discounting the one early failure, we get a median lifetime of ~300 cycles. Since the cells stored at a constant temperature were cycled back to room temperature at most 12 times, the failures seen in those tests were unlikely to have been caused by the thermal cycling.

Although the estimates of cell lifetime presented above are based on a limited amount of data, they strongly indicate that the cell is quite rugged. Even the lowest estimate above of a median cell lifetime of 150 years at 150°C is far beyond expected solar array system lifetimes.

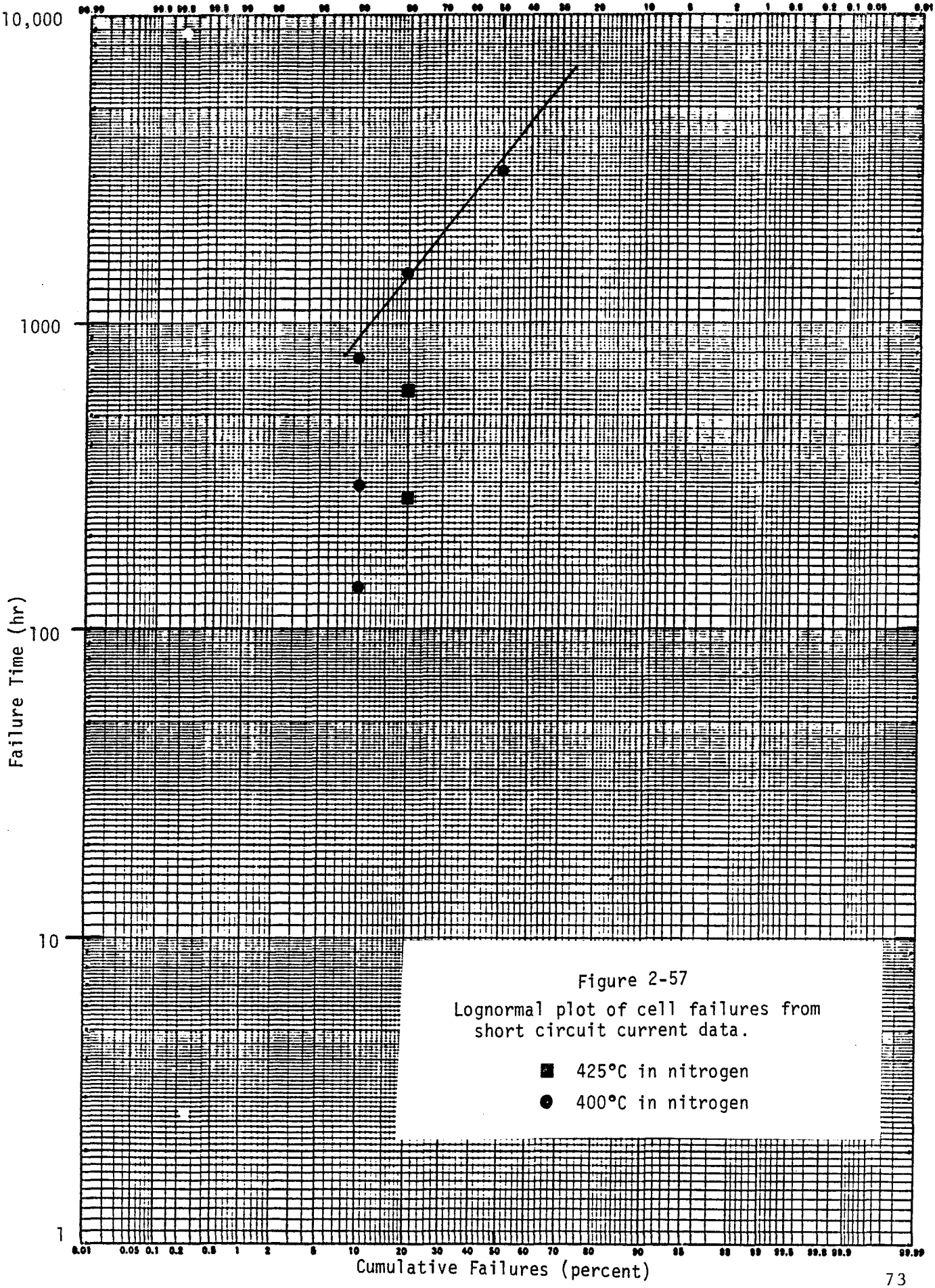

Figure 2-57

Lognormal plot of cell failures from short circuit current data.

■ 425°C in nitrogen

● 400°C in nitrogen

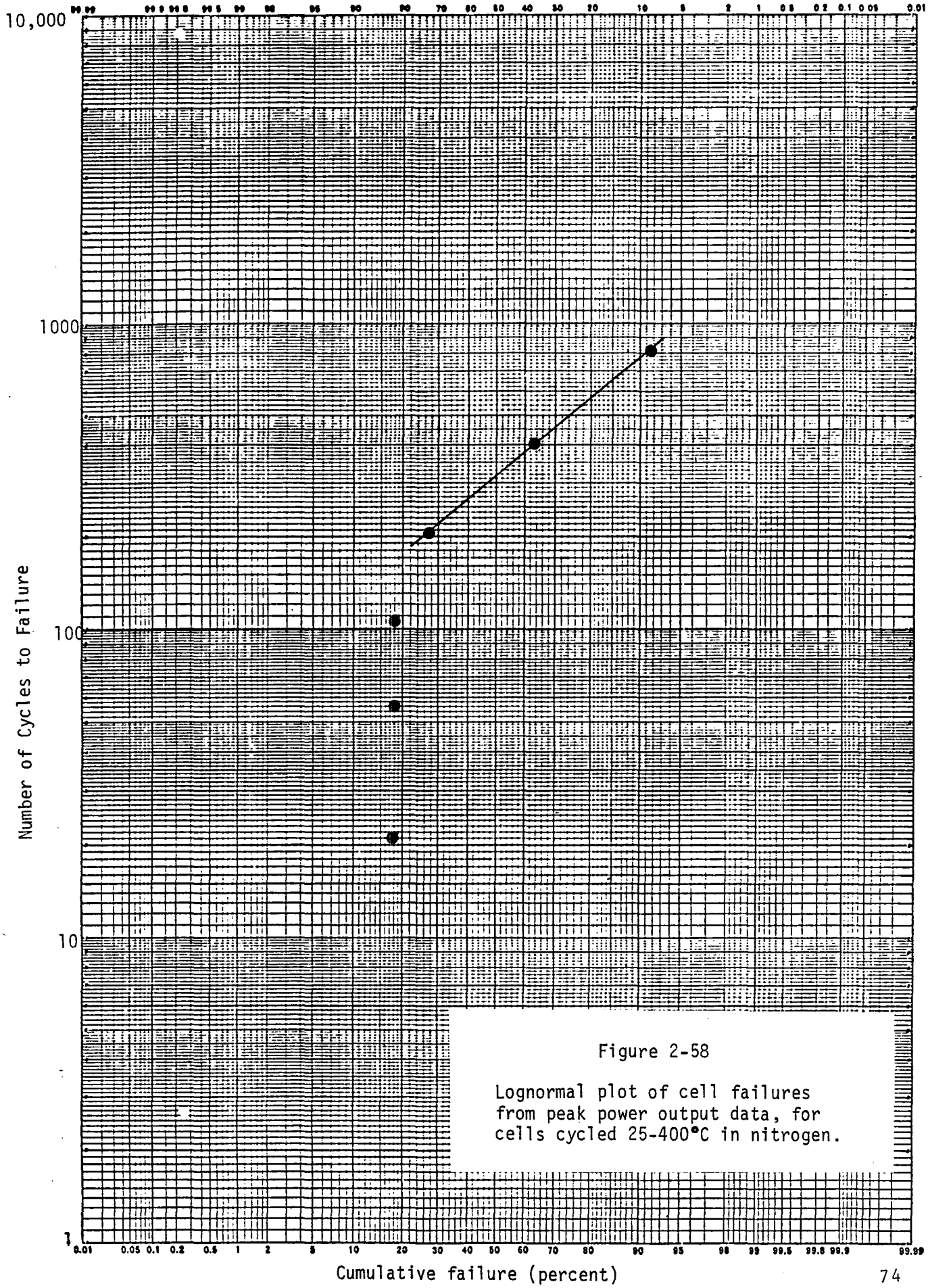

Figure 2-58

Lognormal plot of cell failures from peak power output data, for cells cycled 25-400°C in nitrogen.

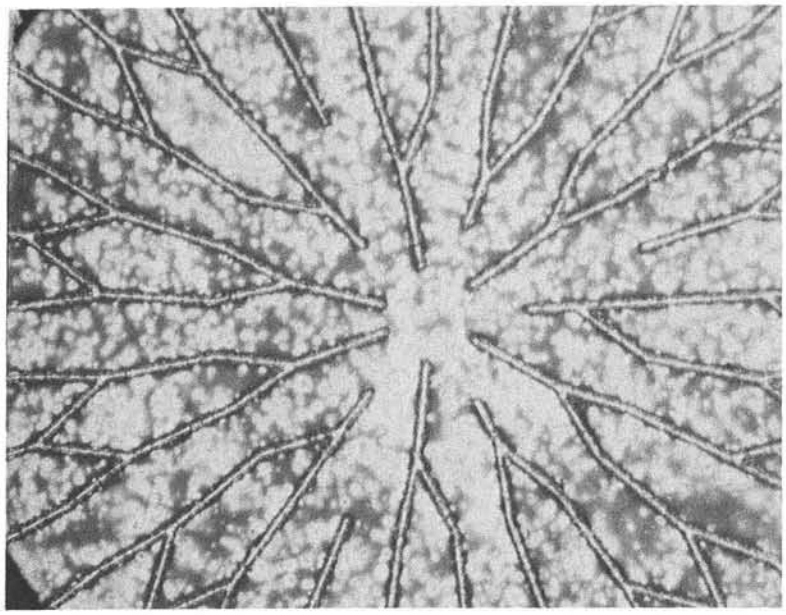

(a) 136 hours

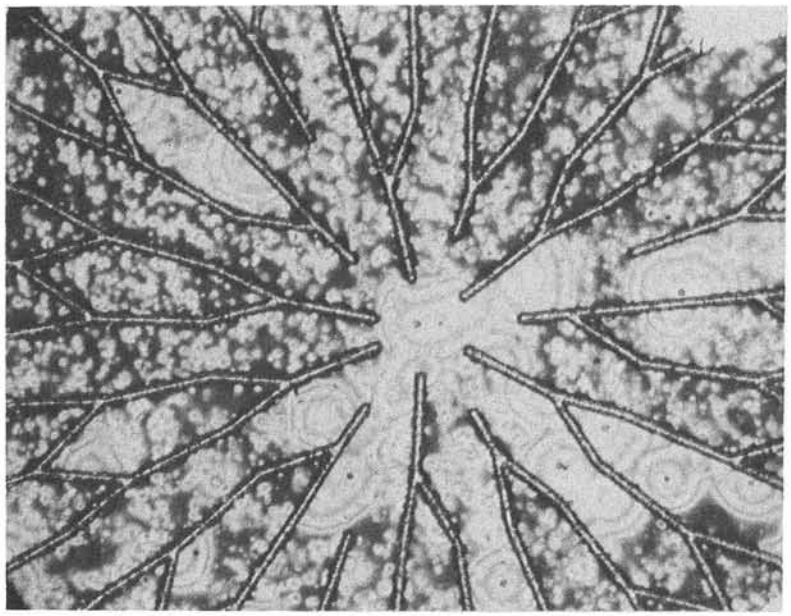

(b) 295 hours

Fig. 2-59 Photomicrograph of center of cell Tray 3 for storage times from 136 hours to 3046 hours at 400°C in nitrogen ambient.

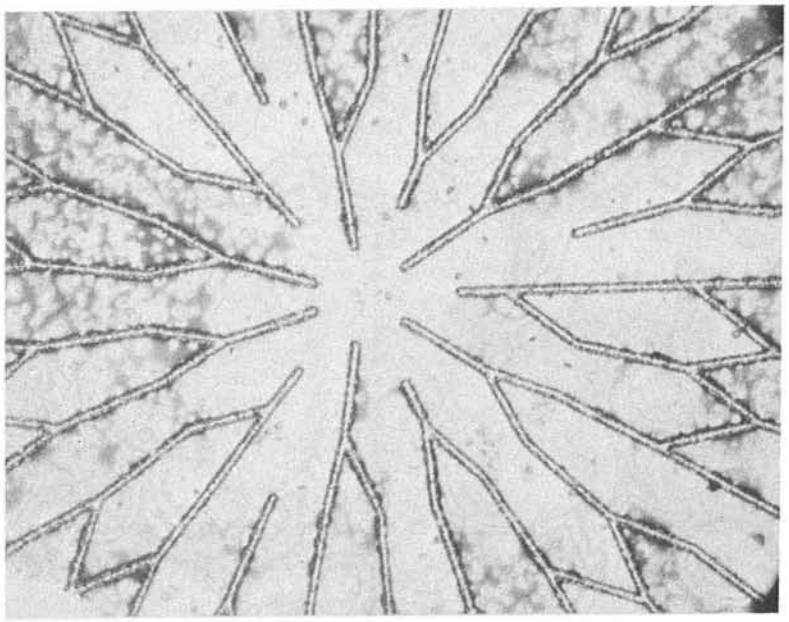

(c) 648 hours

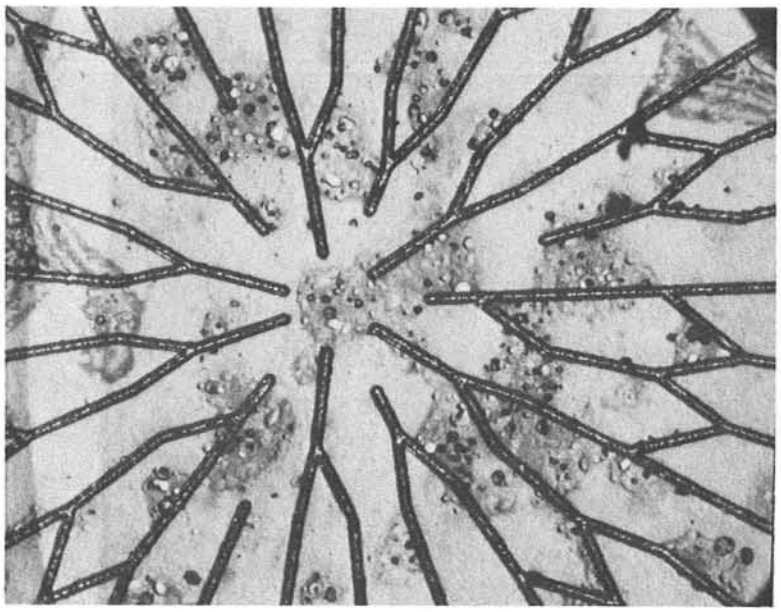

(d) 1440 hours

Fig. 2-59 (continued)

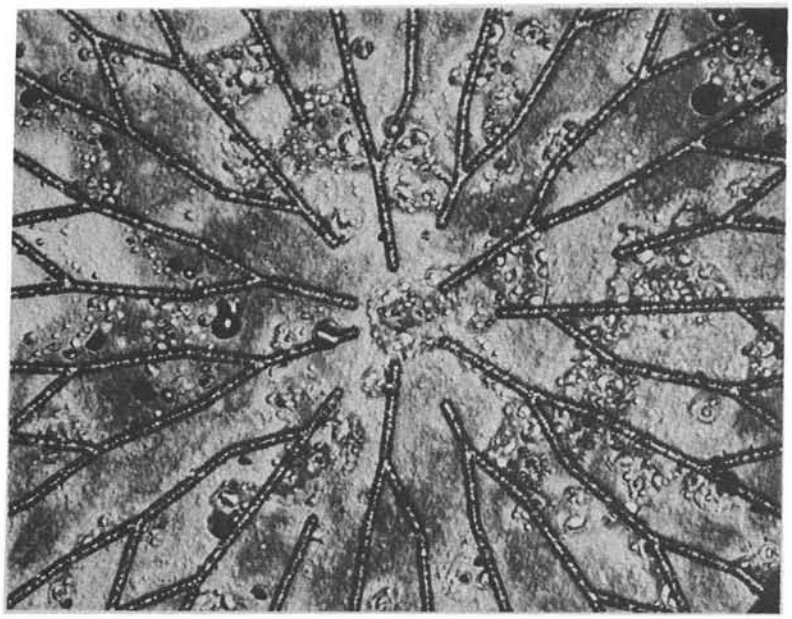

(e) 3046 hours

Fig. 2-59 (continued)

Of course, there may well be degradation mechanisms other than those which were activated in these tests which would place a more severe limit on cell lifetime. For example, effects of the cell package on the cell lifetime were not studied in these tests.

3. Solar Cell Surface Degradation

Surface degradation was observed on some of the cells in the thermal storage tests. It might be expected that the cells stored in air ambient would show the most severe degradation, but that is not what happened; the cells stored at 400°C in nitrogen showed the most severe degradation. The cells stored in air at 250°C showed a very small cosmetic degradation. Only two of the cells stored at 320°C in air showed any surface degradation, and it was found that those two cells had experienced an unusual surface preparation prior to Si_3N_4 deposition.

Figure 2-59 shows the surface degradation of the center of cell TRAY3 at times from 136 to 3046 hours at 400°C in nitrogen. Notice that the defects first appear as light-colored points which spread laterally and merge. By 3046 hours, the entire surface has decomposed.

Figure 2-60 shows the center of the surface of cell TRAY5 at the same times as are shown in Fig. 2-59. The surface of TRAY5 degraded at a much lower rate than cell TRAY3, but nevertheless, had severely degraded by the end of the test. The cell which showed the most severe surface degradation at the earliest time was cell JRF2, whose surface is shown in Fig. 2-61 at 136 hours. Most of the surface of JRF2 showed severe degradation by 136 hours of storage. Cell JRF2 also showed the earliest failure in one-sun performance (see Fig. 2-5). It is difficult to correlate the surface degradation with cell performance for the other cells because the changes exhibited by those cells were less severe, and because the photomicrographs show only a portion of the cell surface and the whole surface may show a different fraction of degraded area than

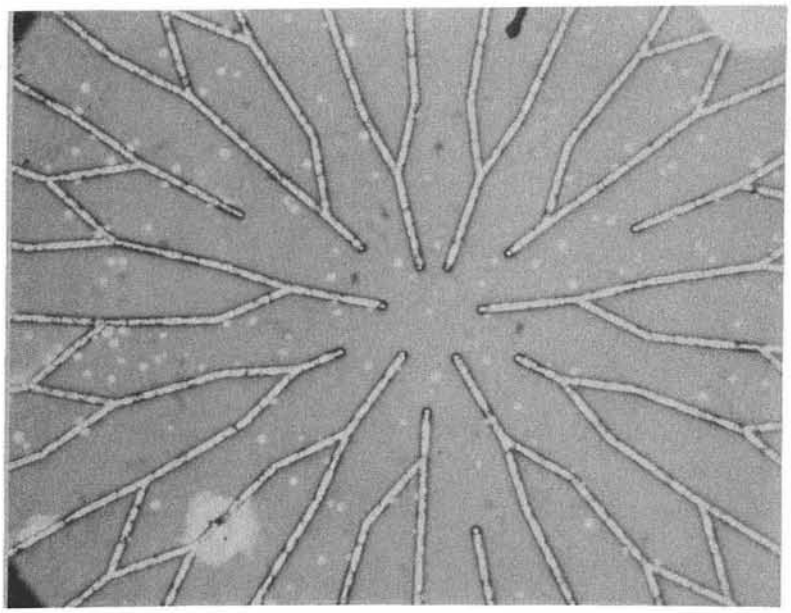

(a) 136 hours

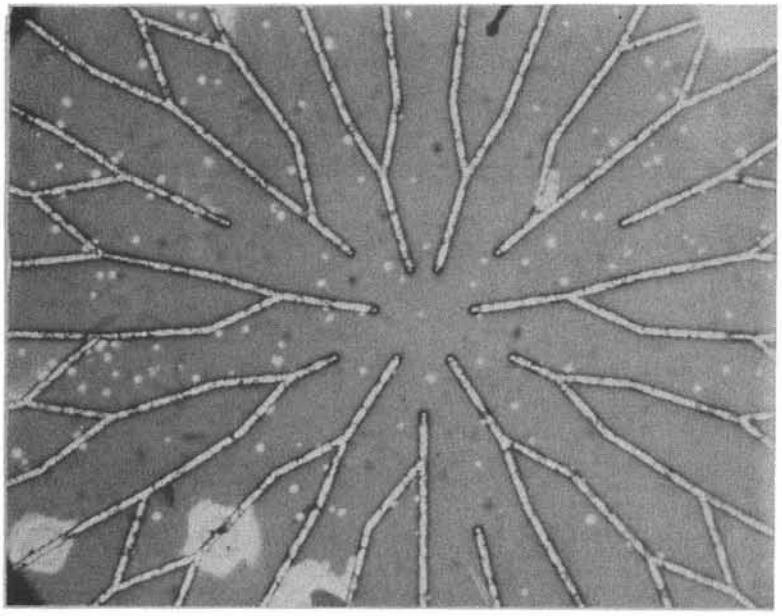

(b) 295 hours

Fig. 2-60 Photomicrograph of center of cell Tray 5 for storage times from 136 to 3046 hours at 400°C in nitrogen ambient.

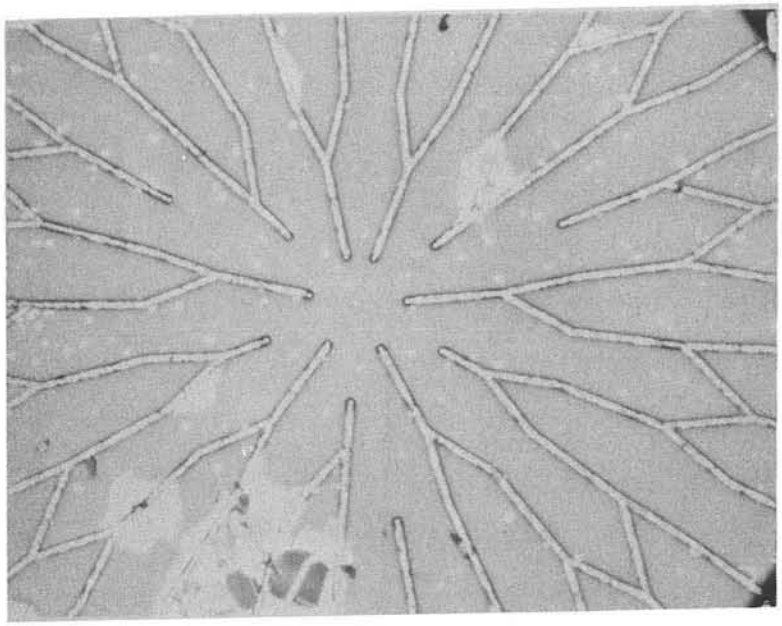

(c) 648 hours

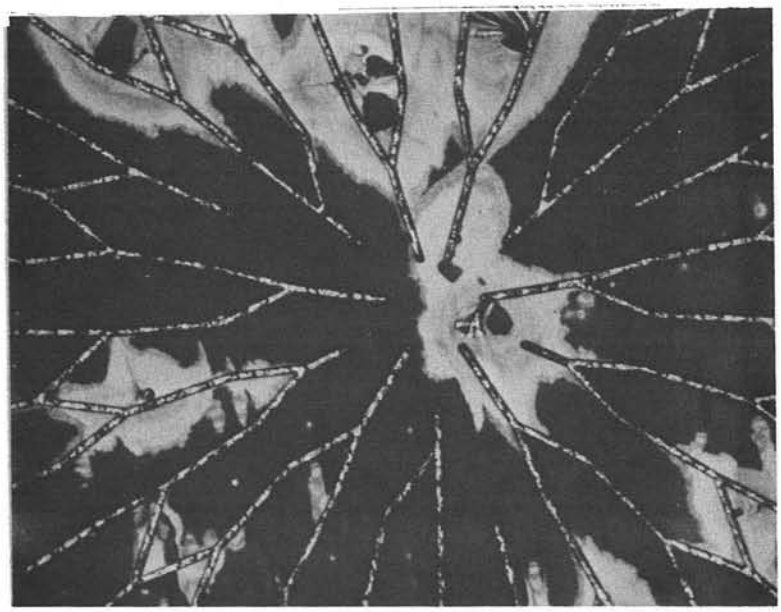

(d) 1440 hours

Fig. 2-60 (cont.) Cell Tray 5 after (c) 648 hrs and 1440 hours.

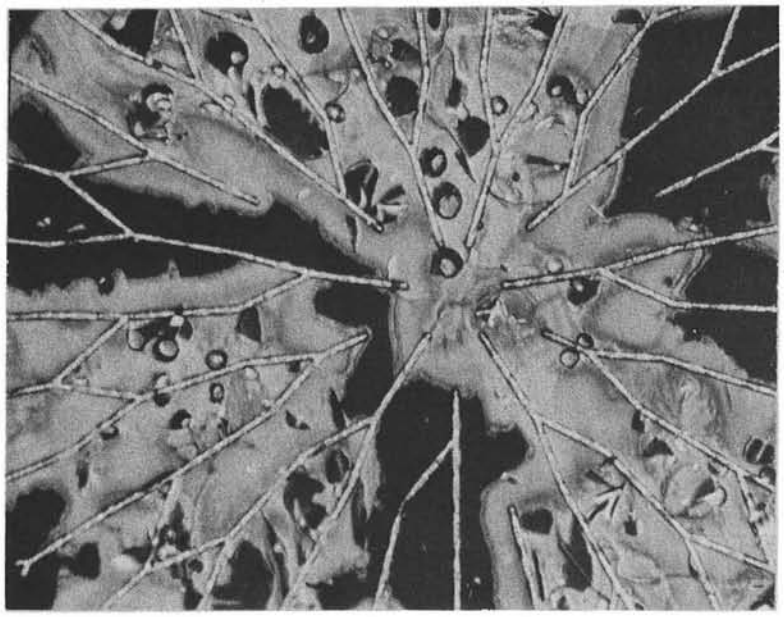

(e) 3046 hours

Fig. 2-60 (cont) Photomicrograph of center of cell Tray 5 after 3046 hours at 400°C in nitrogen ambient.

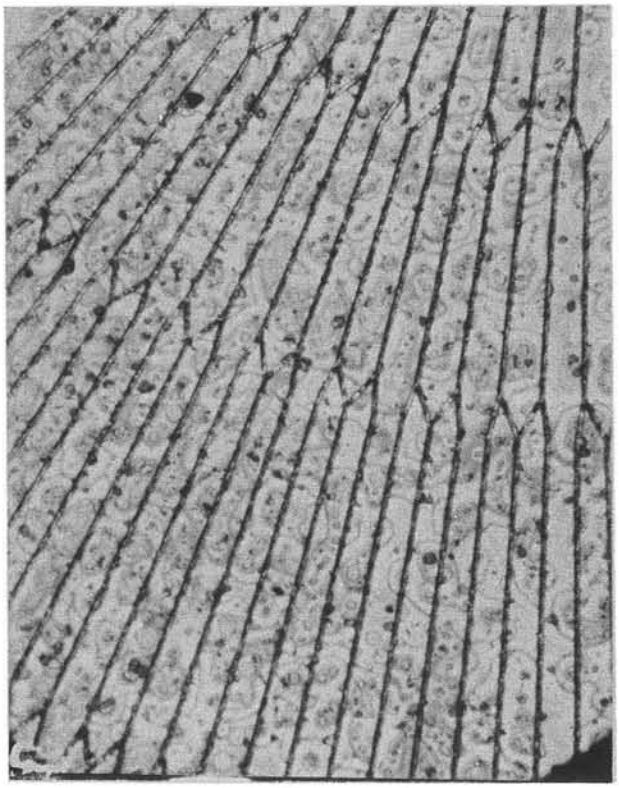

Fig. 2-61 Photomicrograph of surface of cell JRF2 after 136 hours at 400°C in nitrogen ambient.

does the portion shown in Figs. 2-59 through 2-61. Nevertheless, it is reasonable that a drop in short circuit current should accompany the surface degradation. The degraded areas have a higher reflectance than do the good areas and appear to be less transparent than the good areas, so less light probably reaches the cell beneath the regions of surface degradation. Also, if the AlGaAs layer is disrupted or destroyed down to the GaAs surface in the region of degradation, the surface recombination would be greatly increased there. This effect would also decrease the short circuit current.

The degraded areas appeared to start at surface defects and spread from there. Figure 2-62 shows an especially striking example of this. The figure is a composite of photomicrographs tracing a line of surface degradation from one edge of cell HRF1 to the other. The defect appears to follow a "drag line" generated during the LPE growth of the cell. The drag line could have trapped contaminants which caused poor adhesion of the Si_3N_4 in that area. Delamination of the Si_3N_4 layer would then have allowed corrosion of the AlGaAs layer.

All of the cells stored at 400°C in nitrogen showed extensive surface degradation. Similarly, all the cells cycled between 25 and 400°C in nitrogen showed some surface degradation after 800 cycles. Figures 2-63 and 2-64 show two of the cells in the cycling test after 400 and 800 cycles. The degradation appears to be very similar to that seen in the static tests at 400°C. Since 800 cycles took about 400 hours, with the cells at high temperature for only a part of this time, the surface degradation appears to have proceeded at about the same rate in the static and cycling tests.

The surface degradation appears to be oxidation of the AlGaAs layer, although no analysis has been made to verify this hypothesis.

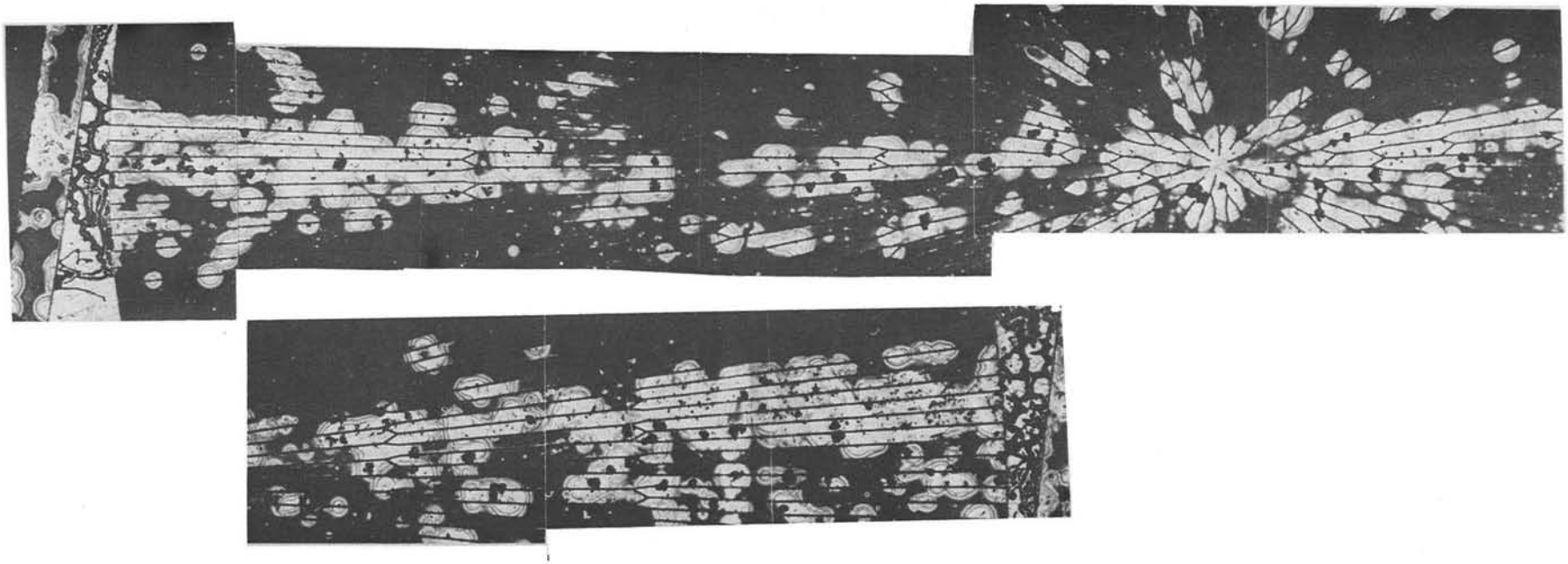

Fig. 2-62 Composite photomicrograph showing antireflection coating defect running across width of cell HRF 1 after 1440 hrs. at 400°C in N_2.

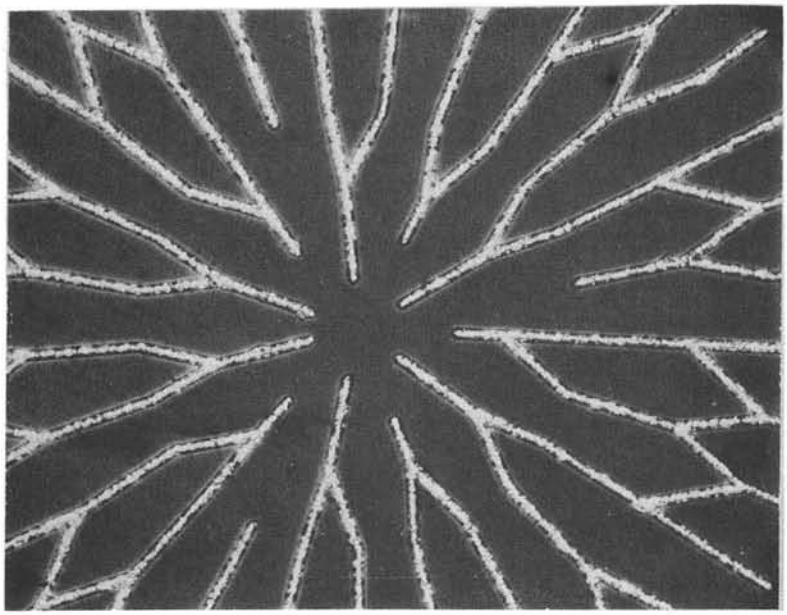

(a) 401 cycles

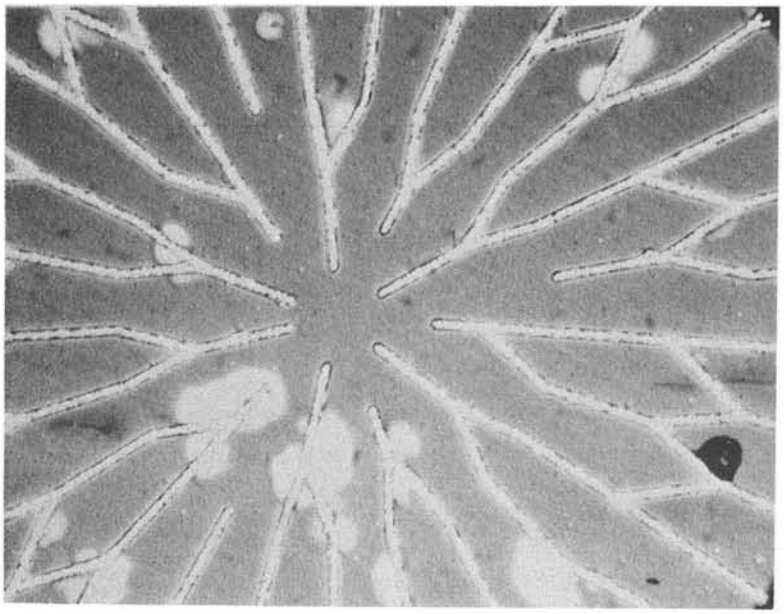

(b) 801 cycles

Fig. 2-63 Surface of cell T4C18 after cycling from 25-400°C in nitrogen.

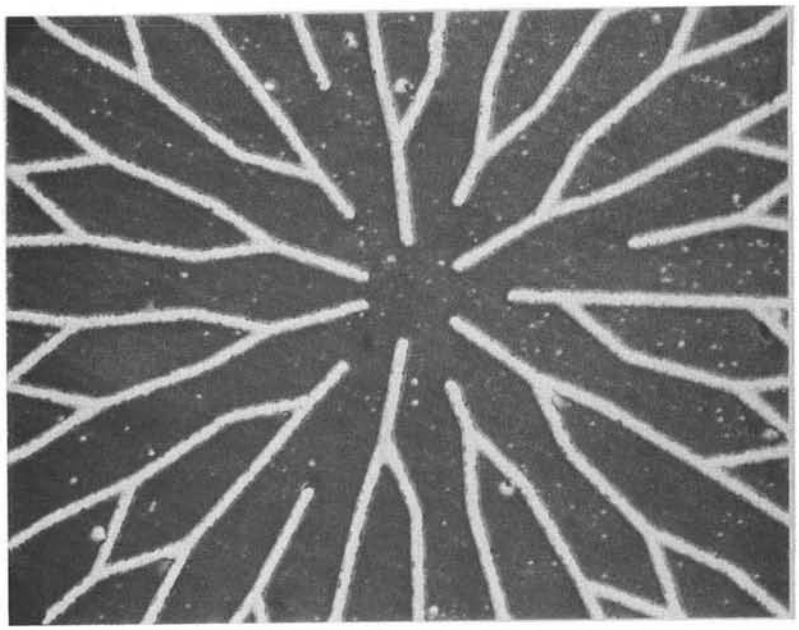

(a) 401 cycles

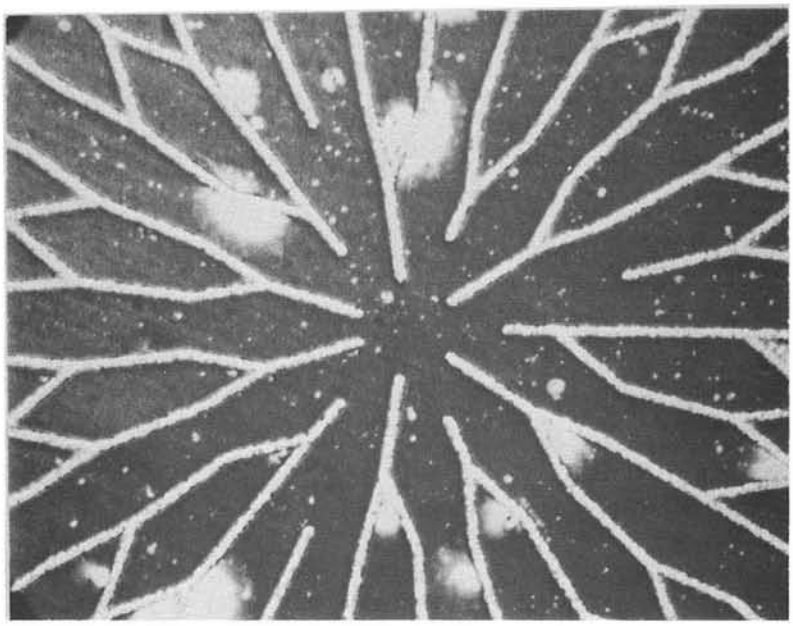

(b) 801 cycles

Fig. 2-64 Surface of cell T4C19 after cycling from 25-400°C in nitrogen.

Although the thermal storage was made in a nitrogen ambient, there could have been a significant oxygen impurity level in the nitrogen. At the conclusion of the cycling and static 400°C tests, the furnaces were helium leak checked. Several leaks were found and repaired, and a piece of tygon tubing used to connect the nitrogen to the furnaces was replaced with copper tubing.

After the leaks had been repaired, the temperature in the 400°C oven was increased to 425°C, and the thermal storage tests at 425°C were conducted. Even after 600 hours, no surface degradation was seen in the cells stored at 425°C. This fact lends support to the possibility of the surface degradation having been caused by an air leak. Further support comes from the fact that cell T5C25 in the cycling experiment and cell L1 in the 425°C test were cut from the same wafer and were Si_3N_4 coated in the same batch; the surface of T5C25 degraded, while that of L1 did not.

Six of the cells stored in air at 250°C showed a slight surface degradation, while four showed no surface degradation. Figure 2-65 is typical of the degradation seen in these cells. Between 61 and 361 hours, the cell developed a mottled appearance. The surface showed practically no further change to 3216 hours, the last point for which we have data. Figure 2-65 was made with a phase contrast microscope (as were all the other photomicrographs in this section), so the mottled appearance is exaggerated. There is no correlation between the cell surface appearance and the cell performance for this group of cells. Also, there is no correlation between the index of refraction and thickness of the Si_3N_4 on the cells and the cell surface appearance.

Figure 2-66 is a high magnification view of mottled areas on the surface of two of the cells. The mottling appears to be small areas of AlGaAs corrosion at pinholes in the Si_3N_4 coating. It is not obvious why these areas did not spread.

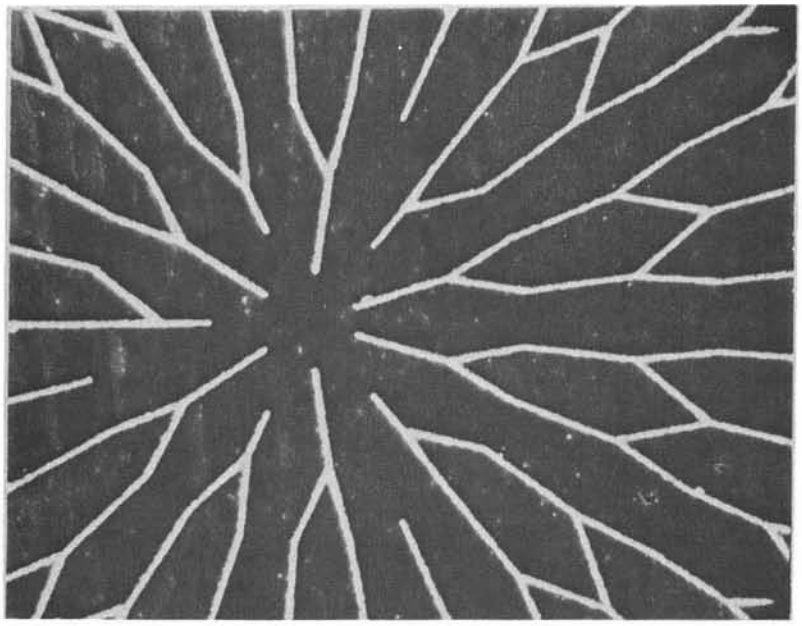

(a) 61 hours

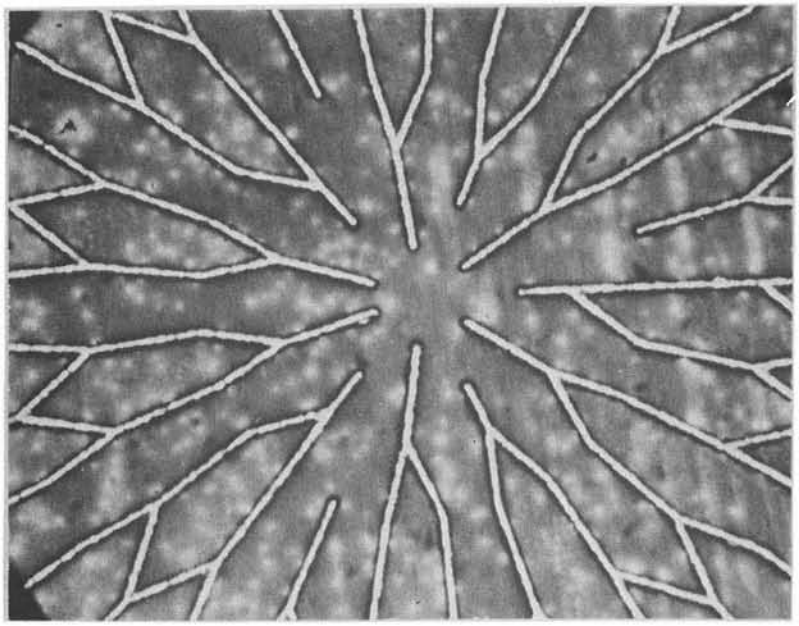

(b) 361 hours

Fig. 2-65 Photomicrographs of center of cell T2C7 for storage times from 61 to 3216 hrs. at 250°C in air.

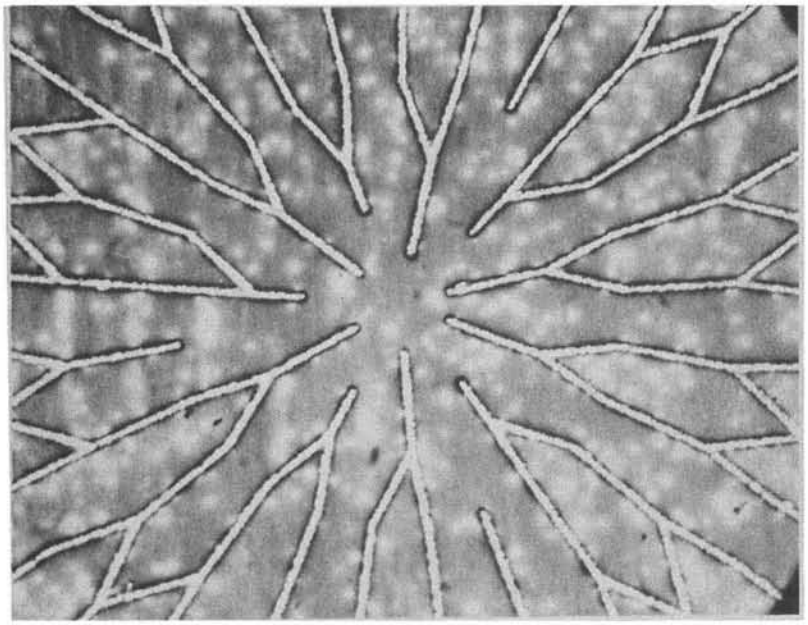

(c) 793 hours

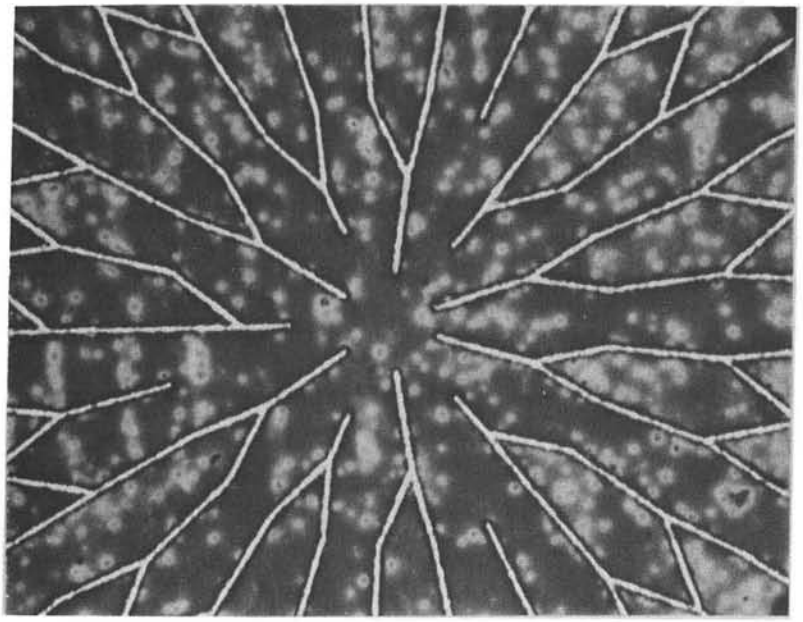

(d) 3216 hours

Fig. 2-65 (cont.) Photomicrographs for storage times of 793 and 3216 hours in air.

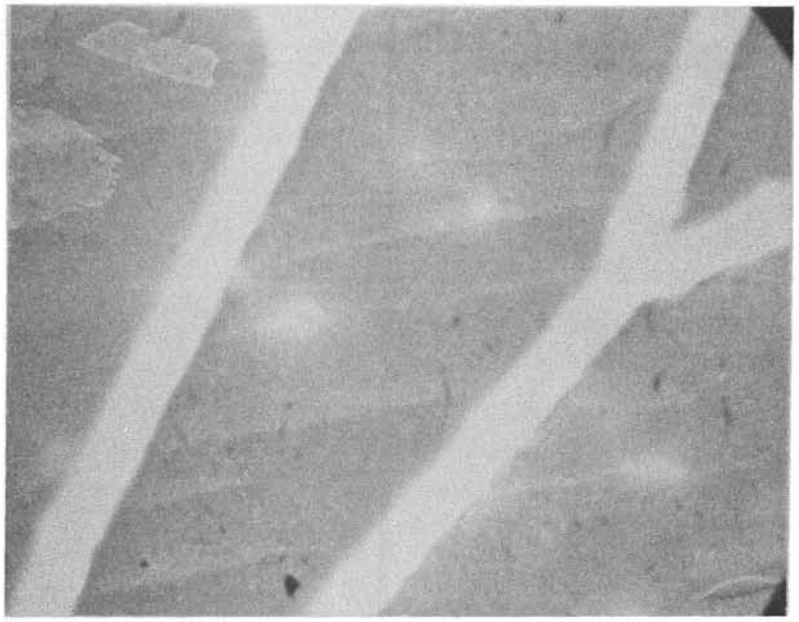

(a) Cell T2C6

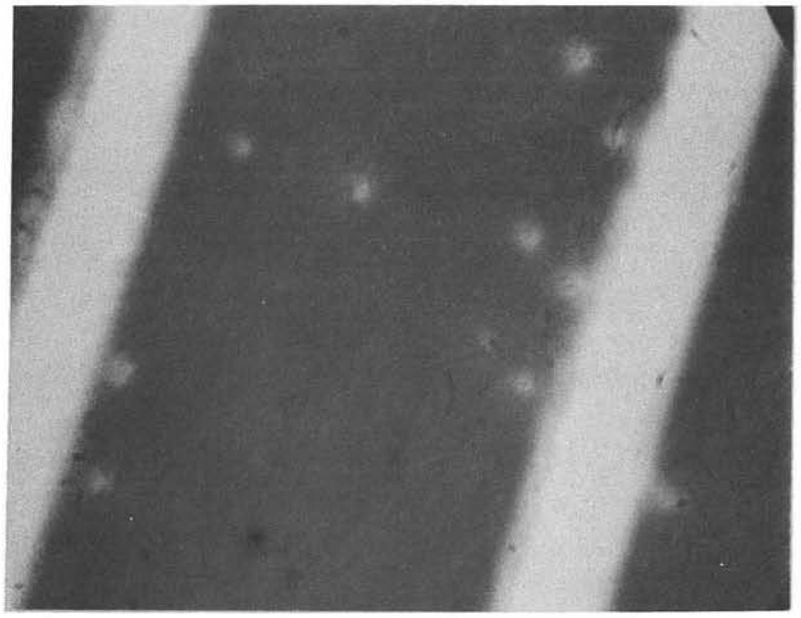

(b) Cell T2C10

0 10 20 30
microns

Fig. 2-66 Mottled areas on cell surface at high magnification.

One would assume that the surface degradation would be worse for cells stored at a higher temperature in air, but that is not what was observed. Only two of the cells stored at 320°C in air showed any surface degradation, and that turned out to be somewhat spurious. Figure 2-67 shows the surface of one cell which showed degradation; the surface of the other cell which degraded was very similar. Round blistered areas appeared after only 1/2 hour at 320°C. There were regular rings around the blisters, which may have been interference fringes formed by the Si_3N_4 lifting off the cell surface. The blisters did not grow with subsequent thermal testing, although some of them developed a roughened appearance. The blisters were explained when it was noticed that prior to Si_3N_4 deposition the two cells with blisters were subjected to an unusual surface treatment that has not been used on any other cells. The Si_3N_4 deposition has a freon cleaning gas supply that is periodically used to plasma etch Si_3N_4 deposits from the deposition chamber. The freon cleaning gas was used to plasma etch the surface of the two cells that later developed blisters prior to depositing the Si_3N_4. Apparently, this treatment left a residue in spots on the cell surface.

The fact that the cells stored at 320°C showed less surface degradation than those stored at 250°C may indicate that the quality of the Si_3N_4 was better for the cells stored at 320°C. The Si_3N_4 deposition system was modified after the cells stored at 250°C had been coated. Mass flow controllers and an accurate pressure gauge were added to give better control over the deposition parameters. Perhaps of more importance, the deposition system baseplate was redesigned and rebuilt to eliminate several air leaks. The average index of refraction measured for the cells held at 250°C was 1.965 with a standard deviation of .037, while it was 2.054 with a standard deviation of .022 for those stored at 320°C. The slightly higher index of refraction for the cells held at 320°C may indicate that the Si_3N_4 was somewhat more dense on those cells.

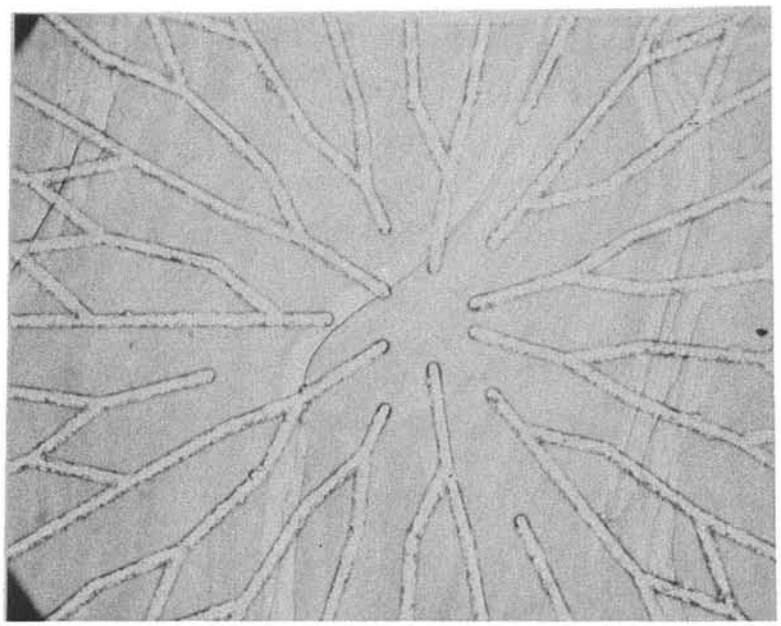

(a) before thermal storage

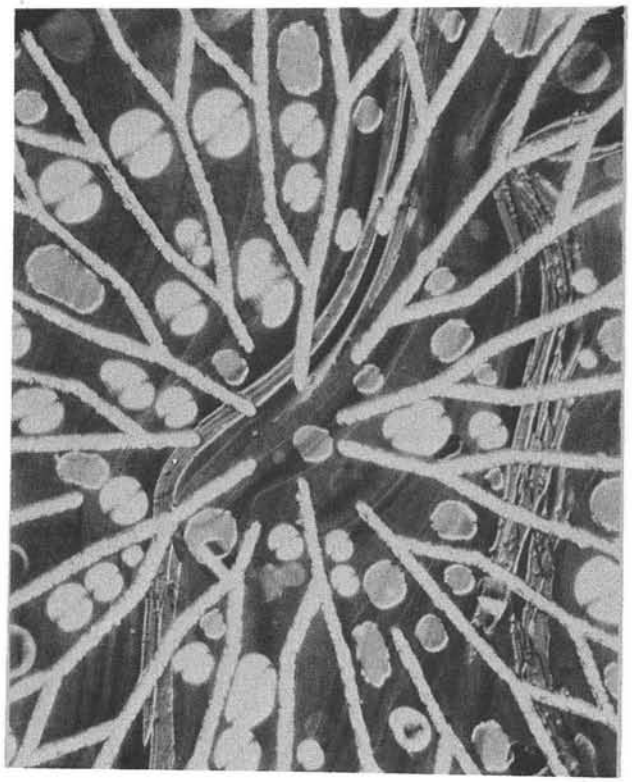

(b) 0.5-hour thermal storage

Fig. 2-67 Photomicrograph of center of cell A6 for thermal storage times from 0 to 10.7 hrs. in air at 320°C. This cell was treated with Freon cleaning gas prior to Si_3N_4 deposition.

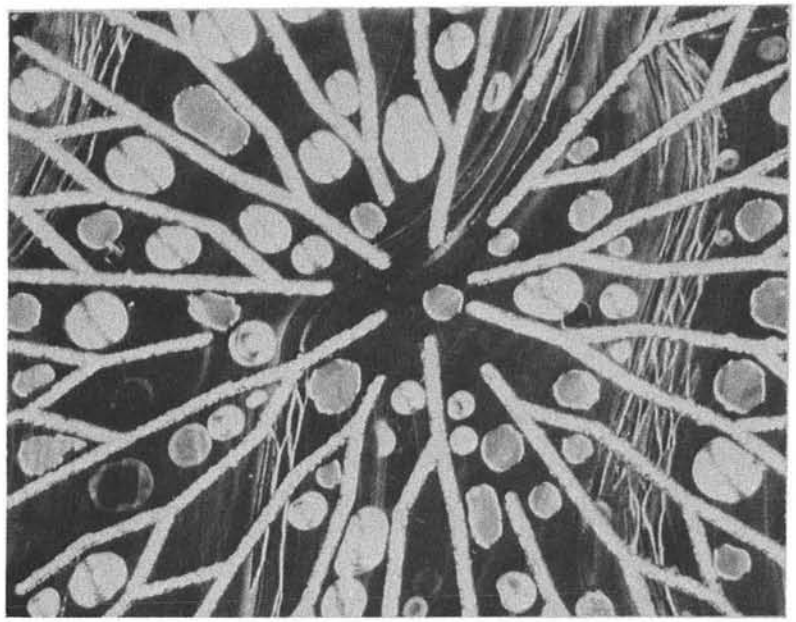

(c) 10.7 hours thermal storage

Fig. 2-67 (continued)

III. OTHER THERMAL STORAGE TESTS

A. Ohmic Contacts

1. Test Patterns

The ohmic contact test pattern is shown in Fig. 3-1a; it consists of a set of source-drain patterns with variable spacing from a FET mask set. By measuring the resistance-versus-spacing characteristic, it is possible to determine the contact resistance, as described below. An attempt was made to automate the ohmic contact testing. To that end, test structures were made by cutting the test pattern into 20 x 20-mil chips, with one set of pads per chip, and soldering the chips to metallized ceramic trays. The individual contact patterns were then wire bonded to pads which could be contacted by a test jig wired to the 9835 computer. Unfortunately, measurements on these test structures produced inconsistent data that could not be used for ohmic contact measurements. A likely cause of this problem was the difficulty in achieving good wire bonds. Furthermore, the test structures were quite time-consuming to fabricate, so their use was abandoned. Measurements were made for the test described below by probing the patterns by hand. An effort is being made to develop an ohmic contact pattern that can be automatically tested, or at least requires less tedious probing for testing.

2. Ohmic Contact Data Analysis

The circuit model for an ohmic contact is shown in Fig. 3-2a. It consists of distributed elements corresponding to the substrate sheet resistivity, R_s, and the contact resistance R_c. The active layer is assumed to be electrically isolated from the substrate, so that current flow is essentially one dimensional.

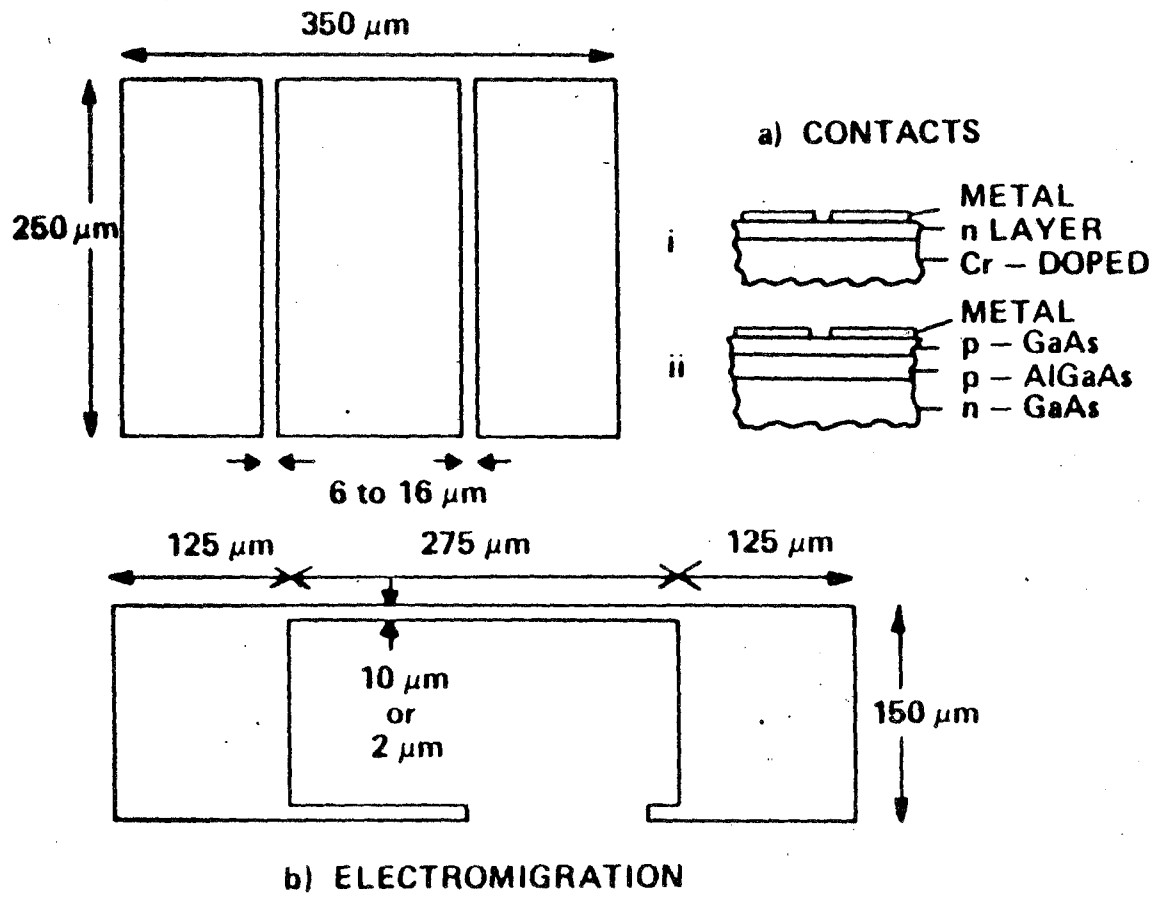

Fig. 3-1 Test Patterns

Figure 3-2

(a) CROSS-SECTION REPRESENTATION OF METAL-EPITAXIAL FILM CONTACT SHOWING SPECIFIC CONTACT RESISTANCE, R_C, AND FILM SHEET RESISTANCE, R_S.

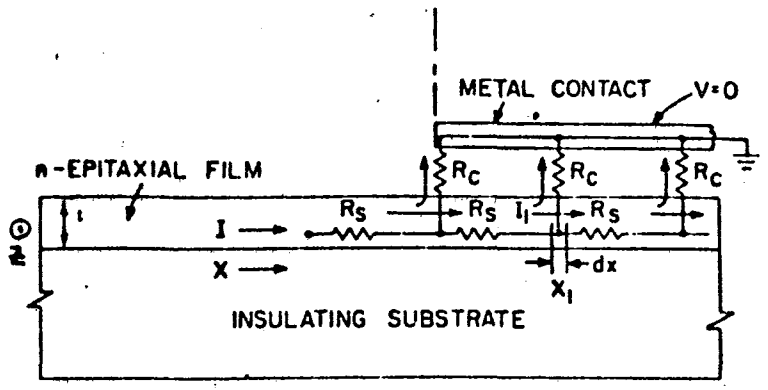

(b) POTENTIAL DISTRIBUTION

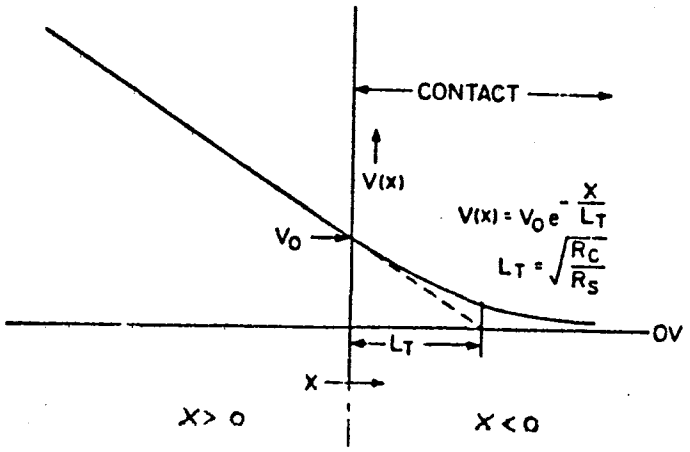

By inspection, the current loss along the substrate is

$$\frac{dI}{dx} = -\frac{V(x)}{R_c} \quad . \tag{1}$$

The voltage drop under the contact is

$$\frac{dV}{dx} = -R_s I(x) \quad . \tag{2}$$

Differentiating (2) and substituting (1) gives the potential distribution under the contact,

$$\frac{d^2V}{dx^2} - \frac{R_s}{R_c} V = 0 \quad . \tag{3}$$

The solution with a potential V_o at the contact edge is

$$V(x) = V_o \exp - \left[\frac{X}{L_T}\right] \tag{4}$$

with

$$L_T = \sqrt{\frac{R_c}{R_s}} \quad . \tag{5}$$

Figure 3-2 shows this distribution. In the channel, before the contact, the potential drops linearly. Under the contact, the potential drops exponentially as Eq. (4). As an example, for $R_c = 4 \times 10^{-4}$ ohm-cm^2 and $R_s = 40$ ohms, L_T is 30 microns. This is considerably shorter than the pad width.

Finally, it is seen that the intercept of the straight line with the x axis lies at $x = L_T$. This can be shown by realizing that the channel current is

$$I = \left(\frac{V_a - V_o}{R_s}\right) \frac{Z}{L} = \frac{MZ}{R_s}$$

where V_a is the applied voltage, Z the width, and L the length of the channel, and M = dV/dx in the channel. The contact current equals the channel current. The contact current is found from integrating (1):

$$I = \frac{Z}{R_c} \int_0^\infty V(x)dx = \frac{Z\,V_o}{R_c} \int_0^\infty e^{-\frac{X}{L_t}} dx = \frac{Z\,L_T\,V_o}{R_c} \qquad (7)$$

Comparison of (6) and (7) yields $M = V_o/L_T$, so that the x intercept lies at $x = L_T$.

This technique can be used to determine both R_c and R_s. We take a number of contact patterns fabricated on the same wafer, of identical geometry except that the channel length, L, is varied from pattern to pattern. Plotting the channel resistance as a function of channel length in effect gives a plot of the x > 0 region of Fig. 3-2b. The intercept at $R = R_o$, from Eq. (7), gives

$$R_o = \frac{V_o}{I} = \frac{\sqrt{R_C\,R_s}}{Z} \qquad (8)$$

The slope of the plot gives the active layer sheet resistivity from

$$m = \frac{d\,R_{ch}}{d\,L} = \frac{\rho_S}{tZ} = \frac{R_S}{Z} \qquad (9)$$

where R_{ch} is the channel resistance, t the thickness, and ρ_S the layer resistivity. Combining (8) and (9) gives the contact resistance,

$$R_C = \frac{Z\,R_o^2}{m} \qquad (10)$$

(Note: For R_o measured from a symmetric pattern of two pads separated by a channel, R_c calculated from Eq. (10) is twice the true contact resistance.)

Figure 3-3 shows a typical fit for a sample undergoing life test. This particular wafer had four patterns of twelve sets of pads similar to Fig. 3-1a. Each data point represents the average of eight measurements. As can be seen, a straight line fit is obtained. Measurement of the slope and intercept gives the contact resistance, R_C, and the sheet resistivity, R_S. For this particular example, a least-squares fit gives $R_C = 1.06 \times 10^{-4}\ \Omega\text{-cm}^2$ and $R_S = 97\ \Omega$.

3. Ohmic Contact Test Results

Two p-type contact wafers were stored in a N_2 ambient at 400°C. Each wafer had four sets of 16 ohmic contact patterns. Probing was carried out by hand.

Figure 3-4 shows the contact resistance versus time for both samples. These data were obtained with the technique described above. It is seen that while the two samples had considerably different initial contact resistivities, the two samples ended up with essentially identical values. Furthermore, changes occurred in the course of time periods long compared to those required for processing. Thus, we can feel confident about using the 400°C Si_3N_4 system without damaging the top contacts.

The sheet resistivity is plotted versus storage time in Fig. 3-5. Of interest is the steady downward trend observed for both samples. The explanation for this is not at present clear; it could well be due to an annealing effect.

It was planned to perform thermal storage tests similar to those described above on n-type ohmic contacts. A test sample was made using the standard solar cell metallization and alloying schedule. The contact resistance of this sample was found to be considerably higher than expected. Upon further investigation, it was decided that either the

Figure 3-3

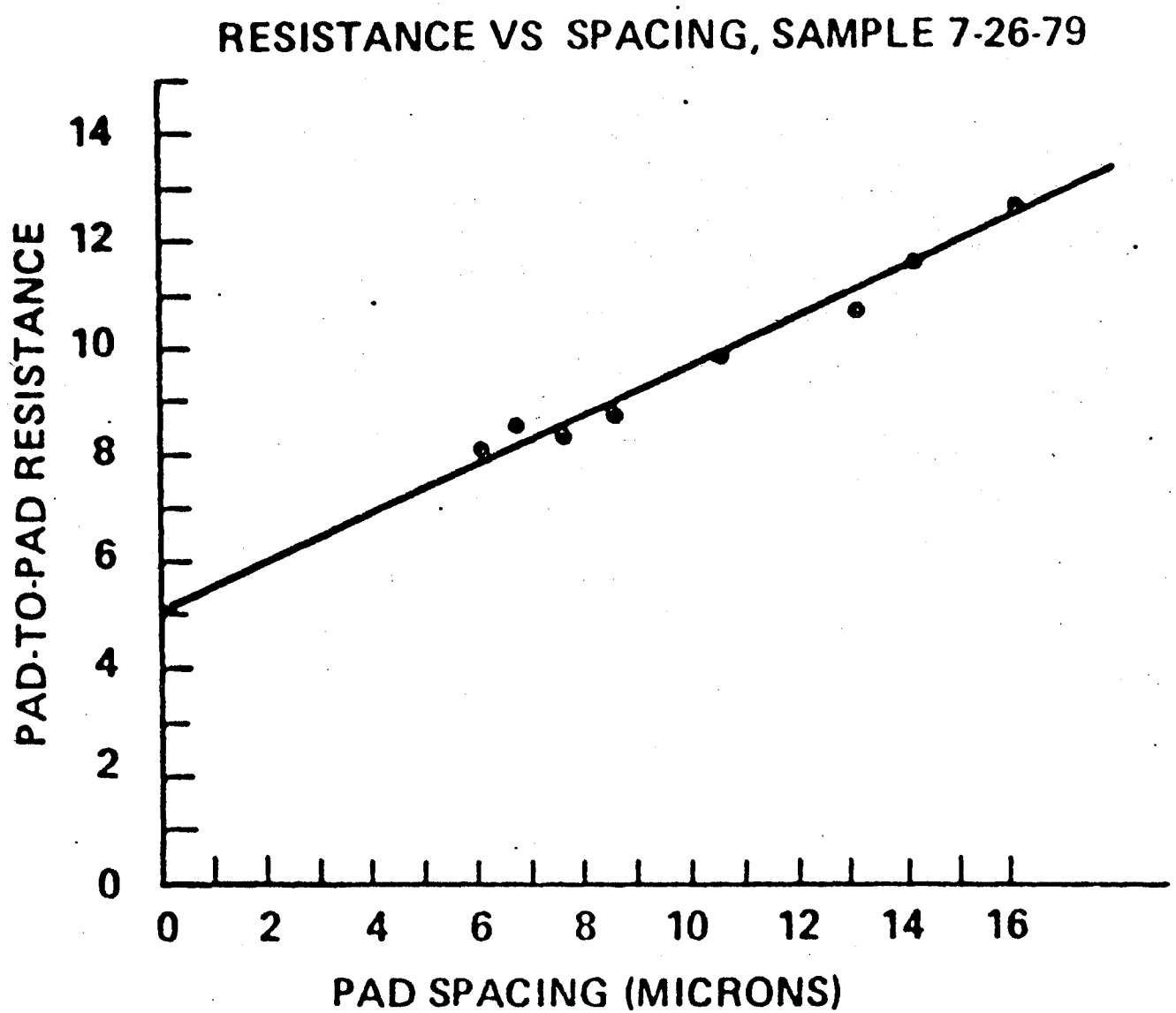
RESISTANCE VS SPACING, SAMPLE 7-26-79
PAD-TO-PAD RESISTANCE
0
2
4
6
8
10
12
14
0
2
4
6
8
10
12
14
16
PAD SPACING (MICRONS)

Figure 3-4

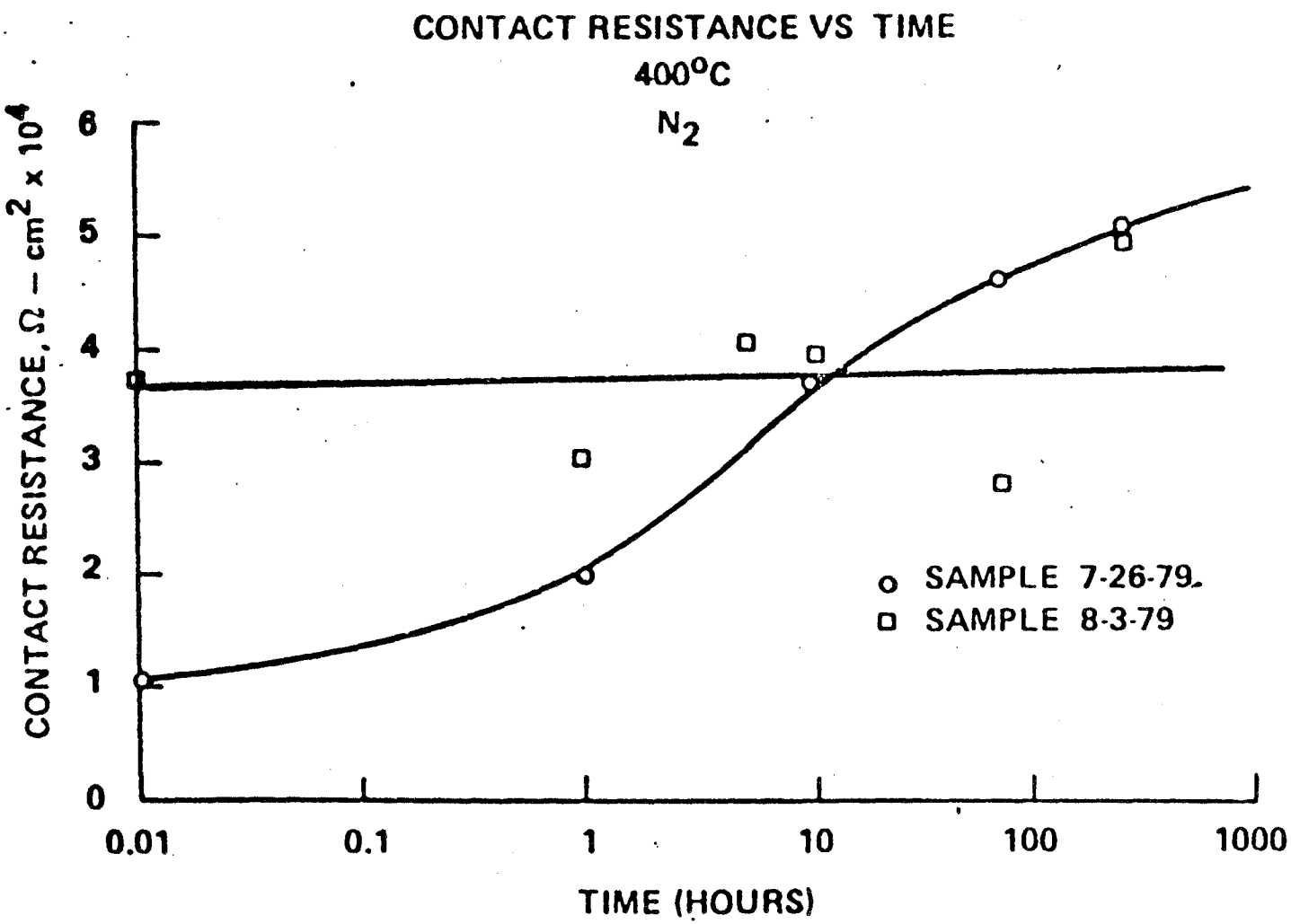
CONTACT RESISTANCE VS TIME
400°C
N_2
CONTACT RESISTANCE, $\Omega - cm^2 \times 10^4$
6
5
4
3
2
1
0
0.01
0.1
1
10
100
1000
TIME (HOURS)
SAMPLE 7-26-79
SAMPLE 8-3-79

Figure 3-5

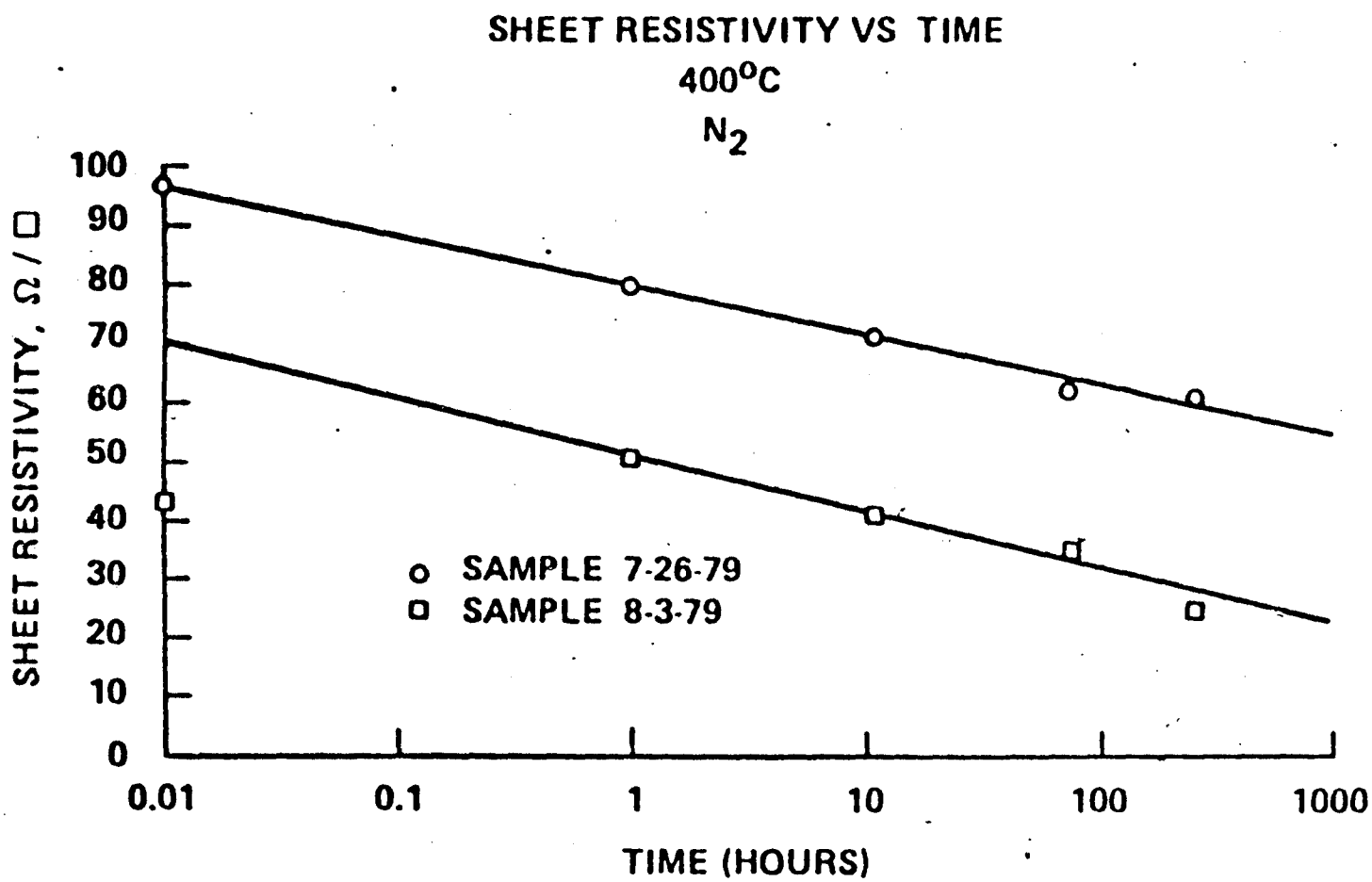
SHEET RESISTIVITY VS TIME
400°C
N2
SHEET RESISTIVITY, Ω/□
100
90
80
70
60
50
40
30
20
10
0
0.01
0.1
1
10
100
1000
TIME (HOURS)
SAMPLE 7-26-79
SAMPLE 8-3-79

alloying schedule or metallization scheme were far from optimum. It was then decided to defer the n-type contact storage tests until it was decided if any fundamental changes would be made in the n-type contact. That issue has not yet been resolved.

B. Electromigration

Figure 3-1b shows the pattern to be used for electromigration tests. A test structure similar to the ohmic contact test structure was fabricated. It consisted of 20 x 20-mil chips of Cr-doped GaAs, with one pattern per chip. The chips were soldered to a metallized alumina tray, and connections from the test pattern to pads on the alumina were made with wire bonds. The contact pads on the alumina were to serve both as test points for automated testing and as contacts for applying a bias thermal storage.

Several months passed after the test pattern was fabricated before an oven was ready for the electromigration test. When the test pattern was examined, it was found that most of the patterns had lost electrical continuity. In some cases, the bond wires had lifted the metal pattern off the GaAs chip. In other cases, the chip had come loose from the tray and the wire bonds were either broken or likely to break. The sample was judged to be unusable.

A second attempt was made to fabricate a test sample. A new design was attempted in which the test patterns and the test pads would both be on the same wafer. Since there was no mask available having this pattern, a double exposure was used in the photolithography. It was planned to join the test patterns to the test pads with wire bonds, but the wafer was broken before this step was accomplished, and there was not sufficient time left in the contract period to try another one.

If the experiment is tried again, it would be best to have a special mask made that incorporates the test pattern with pads large enough to make it easy to bias the patterns during thermal stress. That way, the photolithography can be accomplished in one step and the use of rather delicate wire bonds can be avoided.

IV. CORROSION TESTS

Several groups of tests intended to assess the resistance of the cells to AlGaAs corrosion were performed. The first series of tests served to show that a necessary condition for corrosion resistance was that the Si_3N_4 layer be deposited with the cell held at 400°C or above. The second series of tests showed that some corrosion was still possible with 400°C Si_3N_4, but that OM cells were more corrosion resistant than LPE cells. The third group of tests was aimed at understanding the difference in corrosion resistance between OM and LPE cells. This last group of tests is still in progress.

Early in the program, severe corrosion of the AlGaAs window layer was noticed, even at room temperature storage. The quality of the Si_3N_4 antireflection coating was obviously suspect, and the corrosion tests were focused on this problem.

A number of devices were stored in a 65°C/95% relative humidity environment to reproduce the observed degradation. Figure 4-1c shows the surface of one such cell after 22 hours of storage. Note the severity of the degradation indicative of defects in the Si_3N_4 that allowed the AlGaAs layer to see the high humidity environment.

This degradation has been correlated to the deposition temperature of the Si_3N_4. Specifically, when Si_3N_4 is deposited below 400°C, it lacks the chemical resistance required to provide adequate surface passivation. This is consistent with results published for the deposition technique we employ.[8] Figure 4-2 taken from Ref. (8) shows the etch resistance versus temperature for plasma Si_3N_4 films. Note the flatness of the curves for temperatures at or above 400°C.

Cells with the high temperature nitride show no degradation after extended periods in the corrosion test environment. Figures 4-2a and b show the center of such a cell after 22 and 157.5 hours, respectively.

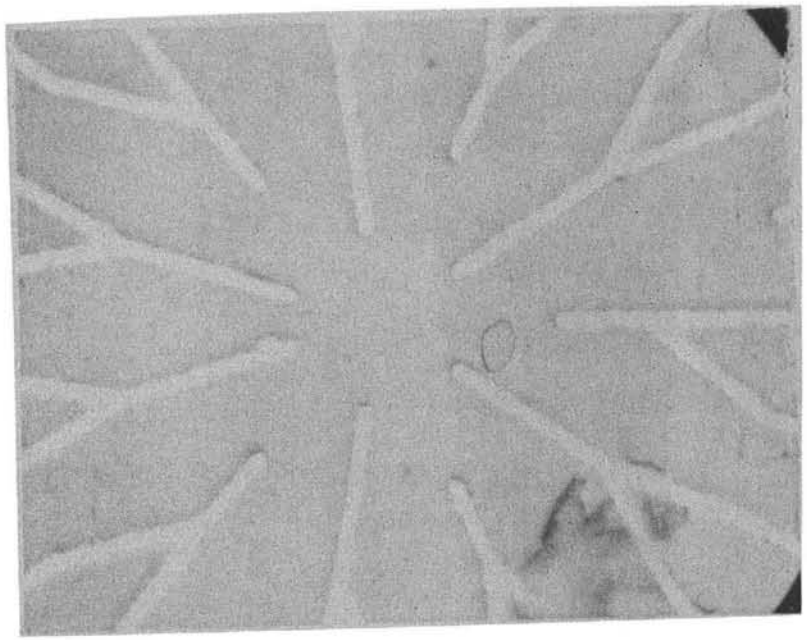

(a)

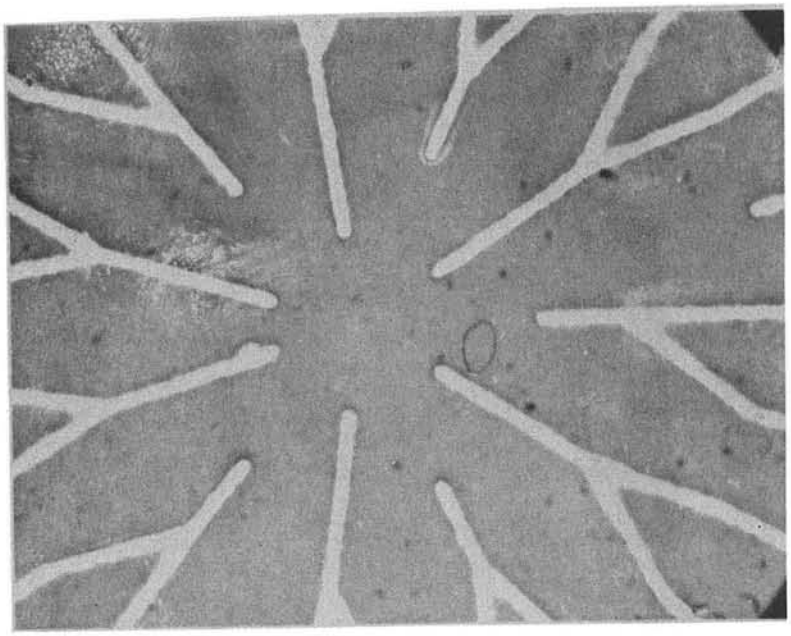

(b)

Fig. 4-1 Photomicrographs of center areas of cells in humidity test; cell (a) with 400°C Si_3N_4 after 22 hours of testing, (b) same cell after 157.5 hours, and (c) cell with 300°C Si_3N_4 after 22 hours of testing.

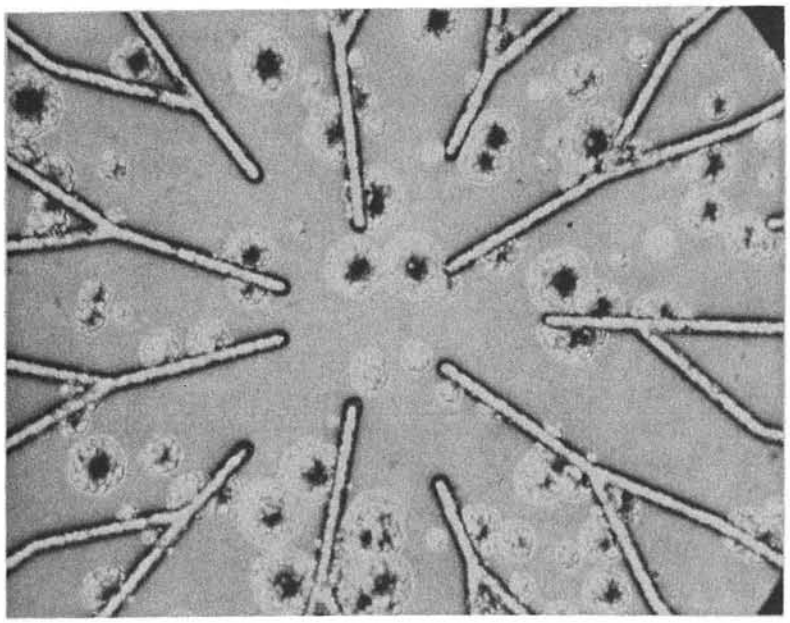

(c)

Fig. 4-1 Photomicrograph of cell with 300°C Si_3N_4 after 22 hours of testing.

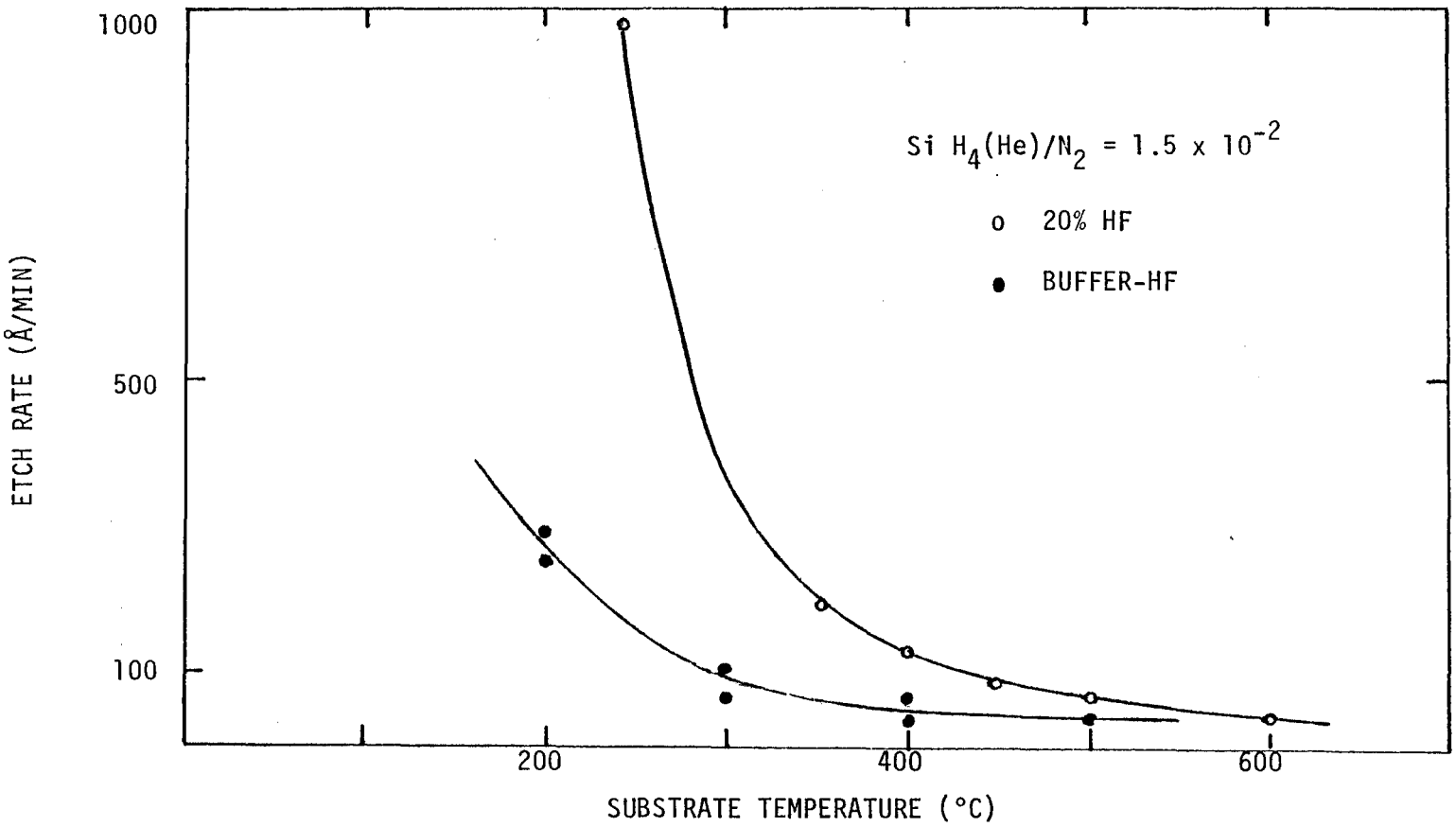

FIGURE 4-2 Etch rate in buffered HF and in 20% HF as a function of substrate temperature (from Ref. 8).

The only cosmetic marks are due to residue left from water drying on the cell surface. Short circuit current measurements confirm that, within experimental error, degradation is nonexistent. Some of these electrical data are shown in Fig. 4-3. Such results were seen consistently on cells with the 400°C Si_3N_4, and indicated that the AlGaAs degradation problem had been substantially overcome at that time.

Unfortunately, the corrosion problem arose again in connection with a program to build two photovoltaic concentrator modules, under Sandia Contract No. 42-7248. Cells were again exposed to the 65°C, 95% relative humidity thermal/humidity test. The cells used in this test were 1/2-inch packaged cells, all with a Si_3N_4 layer which had been deposited at 400°C.

After a 50-hour exposure in the humidity chamber, most of the LPE-grown solar cells exhibited some AlGaAs corrosion. However, organometallic-grown solar cells showed no AlGaAs corrosion, even after 285 hours of exposure in the humidity chamber. Figure 4-4 shows photographs of the surface of an LPE solar cell before and after 50 hours in the humidity chamber. The light-colored areas on the cell surface after exposure are areas of AlGaAs corrosion.

In order to speed up the corrosion testing, a more severe test was employed: the solar cells were boiled in water. LPE cells showed AlGaAs corrosion after one hour of boiling, while none of the organometallic solar cells showed AlGaAs corrosion even after 8 hours of boiling, in addition to the humidity chamber test which had been performed on the same organometallic cells. AlGaAs corrosion on an LPE cell after 1 hour of boiling is shown in Fig. 4-5. No AlGaAs corrosion could be seen on the organometallic cells after boiling, even under high magnification with the SEM.

Figure 4-3

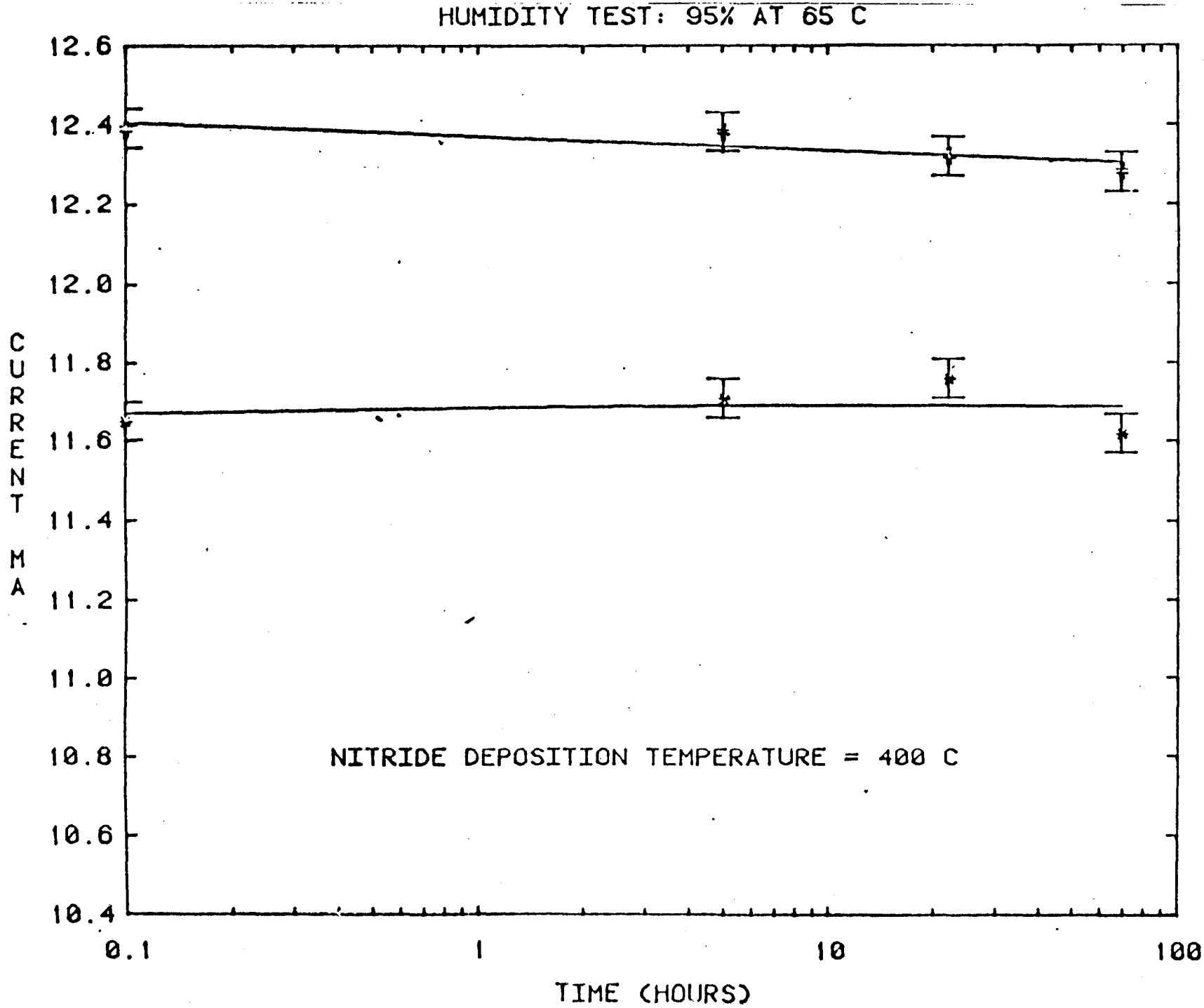
HUMIDITY TEST: 95% AT 65 C
12.6
12.4
12.2
12.0
11.8
11.6
11.4
11.2
11.0
10.8
10.6
10.4
CURRENT MA
NITRIDE DEPOSITION TEMPERATURE = 400 C
0.1
1
10
100
TIME (HOURS)

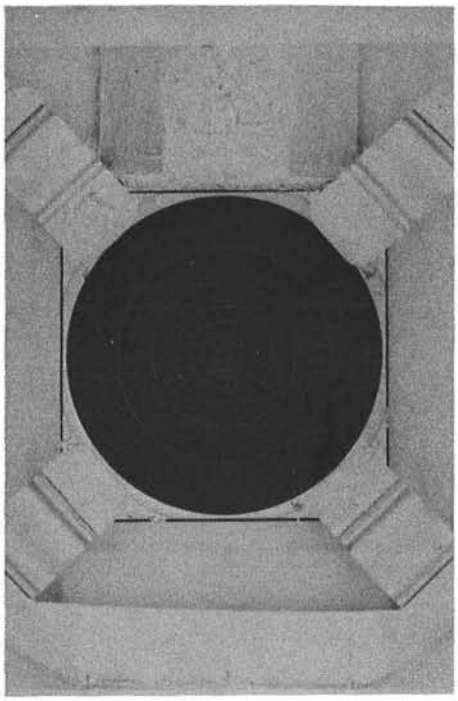

Before

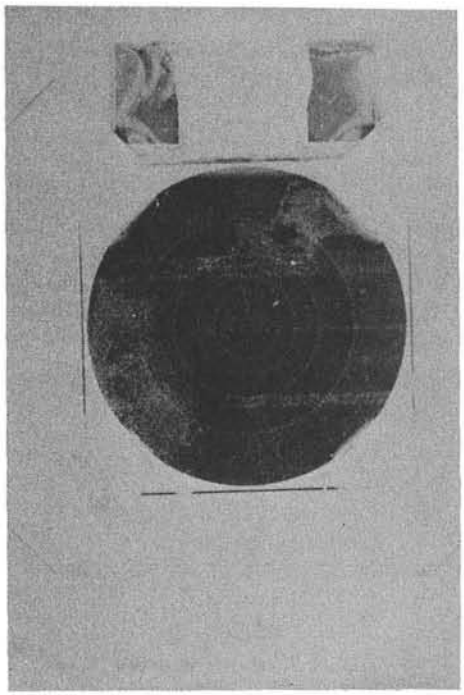

After

Fig. 4-4 Surface of LPE solar cell #2-22-80 IRFG #2 before and after 50 hours in the thermal/humidity chamber.

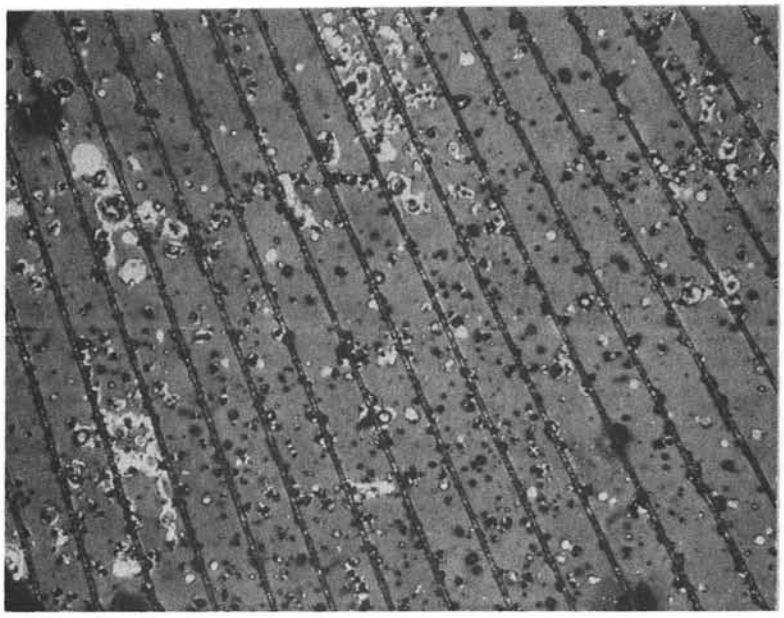

Fig. 4-5 Photomicrograph of the surface of LPE solar cell #2-22-80 HRF #2 showing AlGaAs corrosion after one hour of boiling in water.

There are two differences between the organometallic and LPE solar cells which might account for their remarkable difference in AlGaAs corrosion resistance: the organometallic cells typically have a smoother surface than the LPE cells, and the AlGaAs layer is thinner on the organometallic cells (typically 7000 Å thick for LPE cells, 1500 Å for organometallic cells). The smoother surface on the organometallic cells probably allows the deposition of a more continuous Si_3N_4 layer than on the LPE cells. The thicker AlGaAs layer on the LPE cells may cause the AlGaAs corrosion to spread by a self-propagating mechanism: the AlGaAs layer increases in thickness during corrosion, and this swelling cracks the Si_3N_4 layer around the site of corrosion, thus exposing more AlGaAs to corrosion. The thinner AlGaAs on the organometallic cells may not swell enough to crack the Si_3N_4, thus inhibiting the spread of corrosion.

This mechanism of corrosion propagation was suggested by an SEM examination of corroded cells, but awaits further experimental verification. Figure 4-6 shows an SEM picture of the surface of an LPE cell after one hour of boiling. The pyramidial structure is an area of AlGaAs corrosion and suggests that the corroded AlGaAs is pushing up under the Si_3N_4. Figure 4-7 shows an SEM photograph of another LPE solar cell after exposure in the humidity chamber. There are bands around the corroded region, suggestive of regions of successive corrosion spreading due to breaking off of the Si_3N_4 layer.

The fact that AlGaAs corrosion was seen in the second group of tests with Si_3N_4 is in conflict with the earlier results. A possible explanation for the difference is that several modifications were made in the Si_3N_4 deposition system after the initial measurements. The modifications included mass flow controllers on the gas-feed lines and an accurate vacuum gauge so that the deposition conditions could be established more reproducibly. Also, the baseplate of the deposition

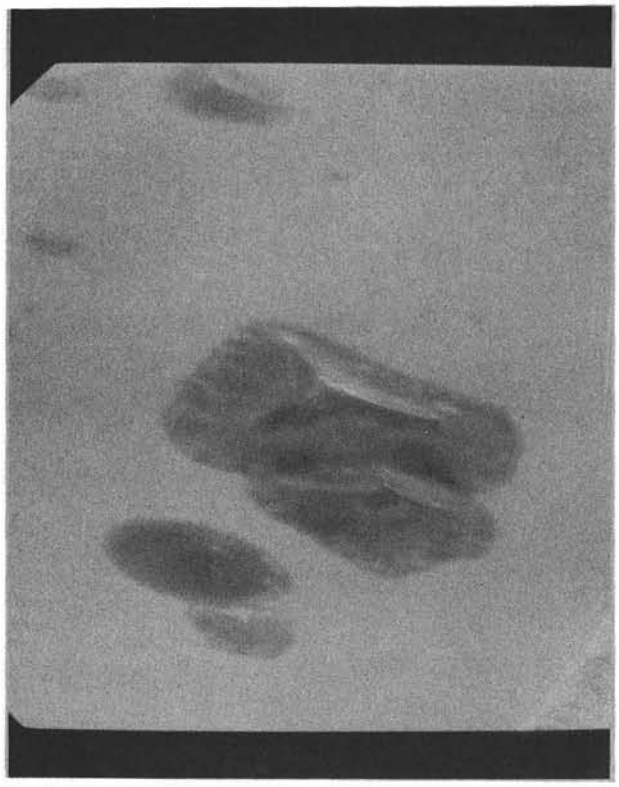

Fig. 4-6 SEM picture at 1350X of an LPE solar cell after one hour of boiling. The pyramidal structure is an area of AlGaAs corrosion.

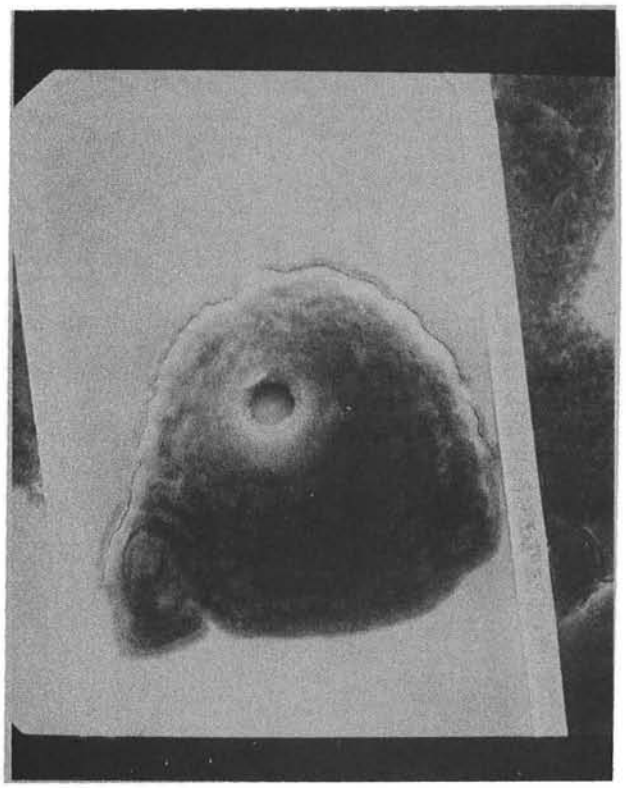

Fig. 4-7 SEM picture at 400X of an LPE solar cell after exposure in the humidity chamber, showin AlGaAs corrosion.

chamber was redesigned and rebuilt to eliminate several rather large leaks. The changes in the system could well have changed the deposition conditions enough so that the Si_3N_4 properties were somewhat different in the two separate tests.

Two experiments were performed that were intended to provide a test of the above explanation of the corrosion resistance of the OM cells. In both experiments, wafers with AlGaAs layers of varying thicknesses were prepared with a standard Si_3N_4 coating over the AlGaAs. The corrosion resistance of the wafers was then tested by immersing the wafers in boiling water.

In one experiment, solar cells were grown by LPE with AlGaAs layers varying from 0.21 μm to 0.85 μm in thickness. After 40 minutes of boiling, small isolated spots of corrosion several microns in diameter formed on all the wafers. Most of the spots were attached to grid lines. After a total of 80 minutes, the corroded areas had grown, but the corrosion was still not severe.

Severe corrosion appeared when the samples were accidentally allowed to boil dry. The corrosion followed the grid lines on the cells with the 0.21- and 0.28-μm AlGaAs layers, but extended between the grid lines on the cells having thicker AlGaAs layers.

The grid lines obviously had an influence on the results of that test. Furthermore, the technique used to grow the different thickness AlGaAs layers caused each wafer with a different thickness to also have a different surface morphology and to have thicker GaAs cap layers on wafers with thicker AlGaAs layers. To eliminate both those points of confusion, another experiment was performed with wafers grown by OM and with no contact grid. Wafers with AlGaAs thicknesses of 0.1, 0.2, 0.3, and 0.4 μm were prepared and coated with Si_3N_4. Corrosion testing was by boiling water, as before.

The surface on the 0.4-μm wafer degraded almost immediately. It was later found that the heater had burned out in the Si_3N_4 deposition system when that wafer was being coated; the deposition was apparently carried out far below 400°C, possibly at room temperature.

The wafer having the 0.1-μm AlGaAs layer survived over 9 hours of boiling with only a few very small spots of corrosion appearing. On the other hand, the other two wafers had significant corrosion after between 3-1/2 and 4-1/2 hours of boiling. The corrosion did not completely cover the surface of either wafer, however.

The results with the OM wafers lend support to the hypothesis that it is the thin AlGaAs layer which gives the OM cells their corrosion resistance. As a further test, we plan to repeat the test with the OM cells described above, but to deposit the Si_3N_4 simultaneously on a set of pieces with the full range of AlGaAs thicknesses under study. Thus any variation in quality of Si_3N_4 will be eliminated from the experiment.

When it became apparent that the LPE cells still had a problem with AlGaAs corrosion, several encapsulating techniques were tried. The one which gave the best results was a technique to bond a cover glass to the cell. Limited testing of the cover glass indicated that the cover glass did prevent AlGaAs corrosion on the LPE cells, and that they could withstand concentrated sunlight. Cover glasses were installed on the cells used in the spectral splitter module built under Sandia Contract No. 13-0308, and successfully withstood several months of module testing on the roof of Varian's Building 7 in Palo Alto. Thus it appears that the AlGaAs corrosion problem can be overcome either by use of the OM cells or cover glasses, or both. The cover glasses are desirable in any event to provide mechanical protection for the cells.

V. ROOF TESTS

Equipment was designed and built to perform two accelerated life tests of solar cells under actual concentrated sunlight. The two tests were to be testing cells under highly concentrated sunlight (up to 9000x) and testing cells at 1000x concentration but at a temperature much higher than the normal operating temperature. An extensive amount of design and fabrication went into preparing for these tests. Unfortunately, by the time the tests were ready to begin, the contract period had ended.

The major parts on hand for these tests are mirrors and secondary optics for high-concentration testing, thermal spacers for the high-temperature illumination test, and cell holders for the improved 1/3-inch cell package. Also, rapid computer-controlled cell testing has been set up, both for cells on the roof under actual insolation and in the laboratory with a flash tester. The only remaining items needed for the tests are mounts for the high-concentration mirrors and a supply of 1/3-inch cells. There should be no problem in fabricating both of these items if it is desired to perform the experiments.

Details of the equipment for these tests are given in the following sections.

1. Illumination-Only Tests

This test exposes a small spot of the cell to extremely high illumination levels. It is possible to evaluate the subsequent effects by comparison to adjacent areas of the cell that did not receive intense illumination.

An important constraint in the design of the concentrators was cost, since suitable parabolic mirrors can run from $2,000 to $5,000 each; a system based on spherical optics was developed. This system is described in Fig. 5-1. The basic element is a spherical mirror designed to reach about 4000 suns. This upper limit arises from spherical aberrations.

Examination of the inset in Fig. 5-1 shows the problem. A ray at a small angle (ray 2) hits the axis at a focal point about $R_C/2$ from the center of the mirror, where R_C is the radius of curvature. A ray at a steeper angle (ray 1) hits the axis nearer the center of the mirror.

Such an aberration can be corrected with a meniscus element as shown in the inset. The steeper ray is bent away from the axis, thus hitting nearer the focus for shallow-angle rays. Thus the overall design philosophy is to use a large spherical mirror to reach about 4000 suns. Even higher concentrations are achieved through the insertion of a meniscus element in the optical path.

The optical elements were designed through the use of several Monte Carlo ray trace computer programs. Each of these worked by choosing a random spot on the sun, weighted by the sun's radial intensity distribution, and drawing a ray to a random spot on the mirror aperture. By tracing a suitable number of these rays, it was possible to find the radial intensity distribution on the cell for any given optical configuration. Programs were written for systems with either a spherical or parabolic mirror and an arbitrary number of spherical refracting surfaces after the mirror, each with a single antireflection coating.

Figure 5-2 shows the computer output for a 12" spherical mirror with a 50" radius of curvature and a 93% front surface reflective coating. The triangle in the upper right shows the point of origin of each ray

Figure 5-1 **OPTICS DESIGN**

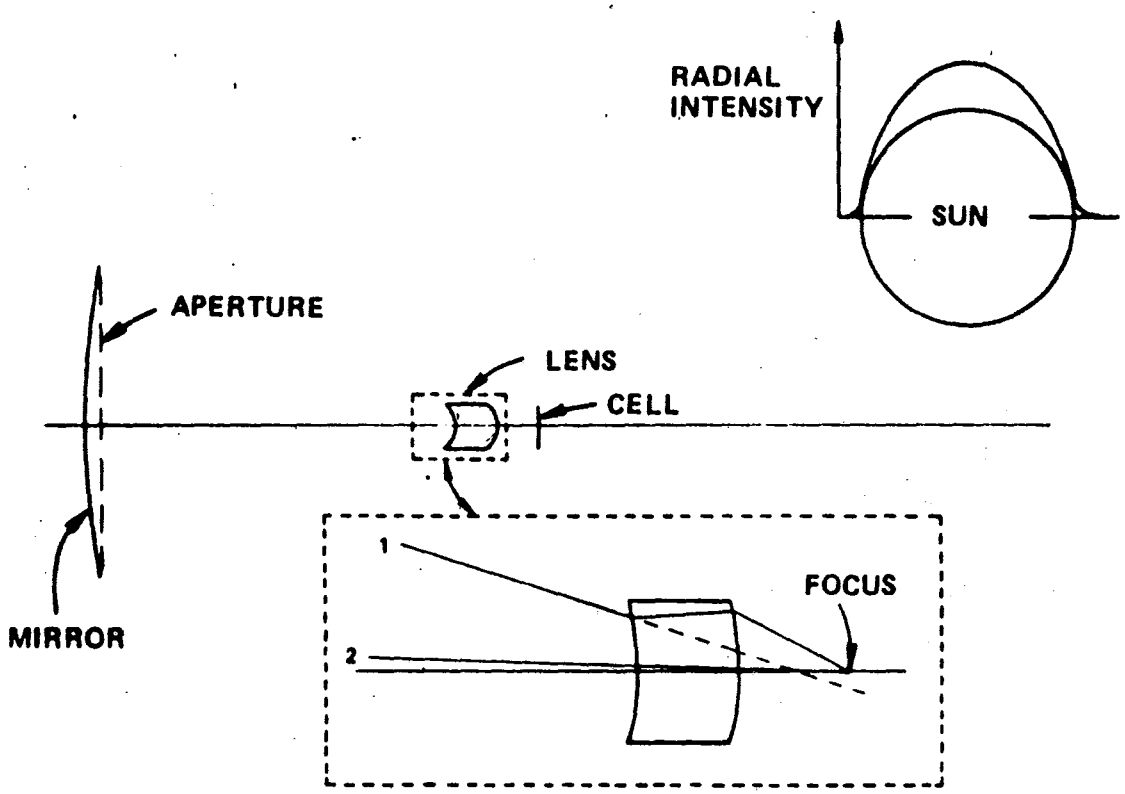

0 LENS SECONDARY CONCENTRATOR

SPHERICAL MIRROR/SECONDARY LENS MCRT

DIAM (IN.)=12.00
RADIUS (IN.)=50.00
CELL Z=24.86
CELL Z-APP Z=24.50
CELL DIAM= .30
REFL= .93

NO. OF RAYS=20000
AVERAGE TRANS = .930
FRAC MISS. CELL=0.0000
14.05 DEG MAX INCIDENCE ANGLE
9.20 DEG AVG INCIDENCE ANGLE
FRAC >45 DEG=0.0000

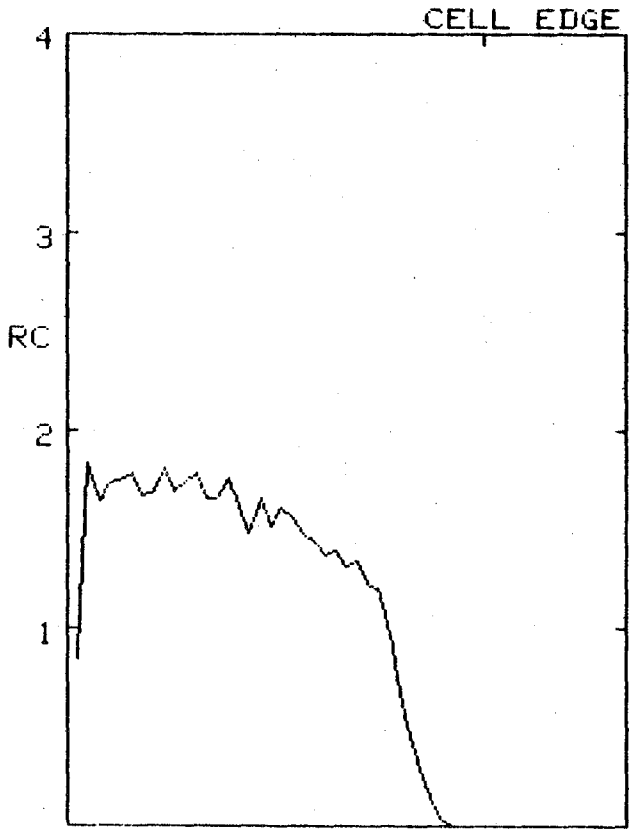

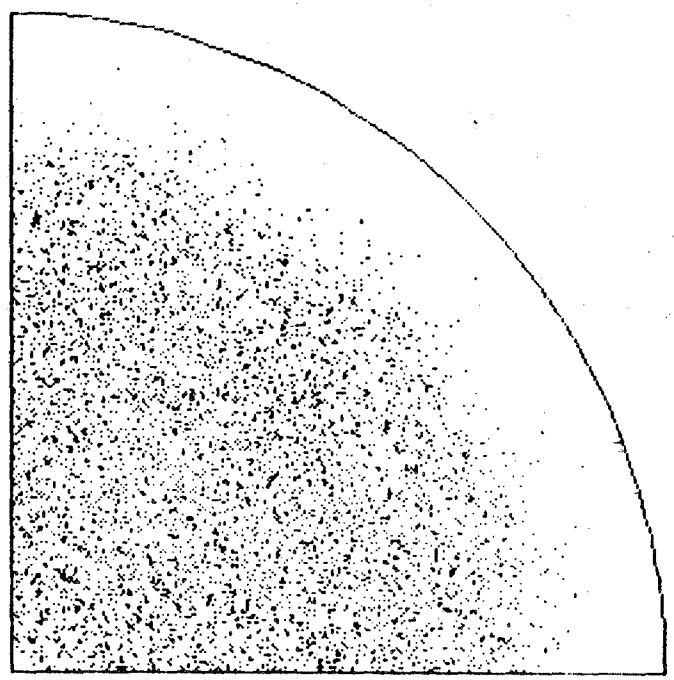

Figure 5-2

from the sun. The circle in the upper center shows the point of intersection with the aperture. This distribution is seen to be random. The quarter circle on the lower right shows where the rays hit the cell. The program keeps track of the radial locations and plots them normalized to the square of the radial location. This radial concentration distribution is seen in the plot at the lower left. This particular mirror provides a peak concentration of about 3700 suns.

The effect of the meniscus element is seen in Fig. 5-3. The element has a concave front surface with a radius of curvature of 1", a convex back surface with a radius of curvature of 1.5", an element thickness of 1" and a diameter of 1.5". The spot is about 0.12" in diameter, and the peak concentration is about 9000 suns.

The mirror and lens designs just described are those that were purchased and received. Ten lenses and 10 mirrors were purchased at a cost of about $700 for each lens and mirror unit.

2. Combined Thermal-Illumination Tests

In this test, cells are exposed to about 1000 suns illumination, while the temperature is raised. The approach here is to use mirrors already in-house for the illumination. Thermal standoffs between the cell and the water-cooled mount provide the elevated temperatures. The mirrors are fifteen square, spherical surface mirrors that were used in a 1977 demonstration experiment. These have recently been recoated with aluminum and protected with an epoxy coating.

The design of the thermal standoffs is shown in Figs. 5-4a, b, and c. Normally, the cell is fastened to a water-cooled mount, maintaining its temperature at 50°C. As seen in Fig. 5-4a, the thermal spacers have a length L, diameter D_S, a temperature at the bottom equal to that of the cooling water, and a power incident of P_{in}. P_{in} is the difference between the insolation and the electrical power generated.

1 LENS SECONDARY CONCENTRATOR

LENS 1; 1.000 IN. THICK, RADIUS OF .750 IN. 24.00 IN. IN FRONT OF MIRROR.
RADII OF CURVATURE (INCHES): FRONT= -1.00 BACK= -1.50
LENS INDEX OF REFRACTION= 1.500 ; dn/df (/eV)= 0.00000

THE LENS HAS A SINGLE LAYER AR COATING ON FRONT AND BACK SURFACES.
90.00 DEGREES THICK (1148.0 ANGSTROMS); E MINIMUM (eV)=2.000
INDEX OF REFRACTION=1.350; dn/df (/eV)=0.00000

SPHERICAL MIRROR/SECONDARY LENS MCRT

DIAM (IN.)=12.00
RADIUS (IN.)=50.00
CELL Z=24.60
CELL Z-APP Z=24.24
CELL DIAM= .20
REFL= .93

NO. OF RAYS=10000
AVERAGE TRANS = .856
FRAC MISS. CELL=0.0000
29.10 DEG MAX INCIDENCE ANGLE
16.31 DEG AVG INCIDENCE ANGLE
FRAC >45 DEG=0.0000

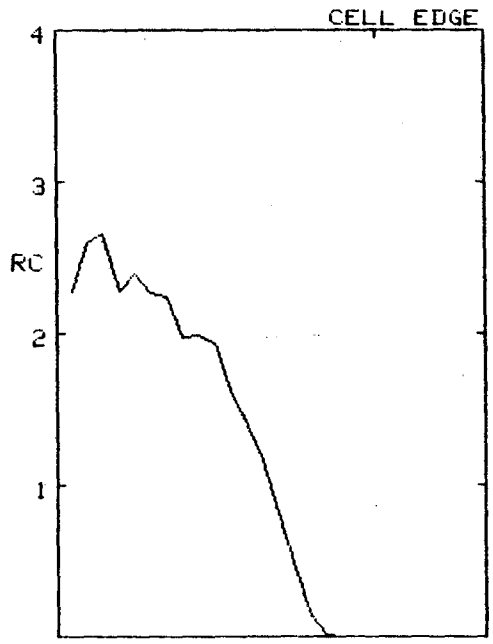

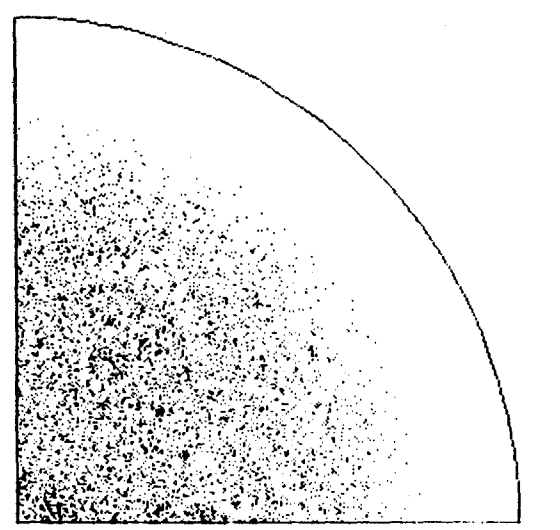

Figure 5-3

Figure 5-4

THERMAL DESIGN

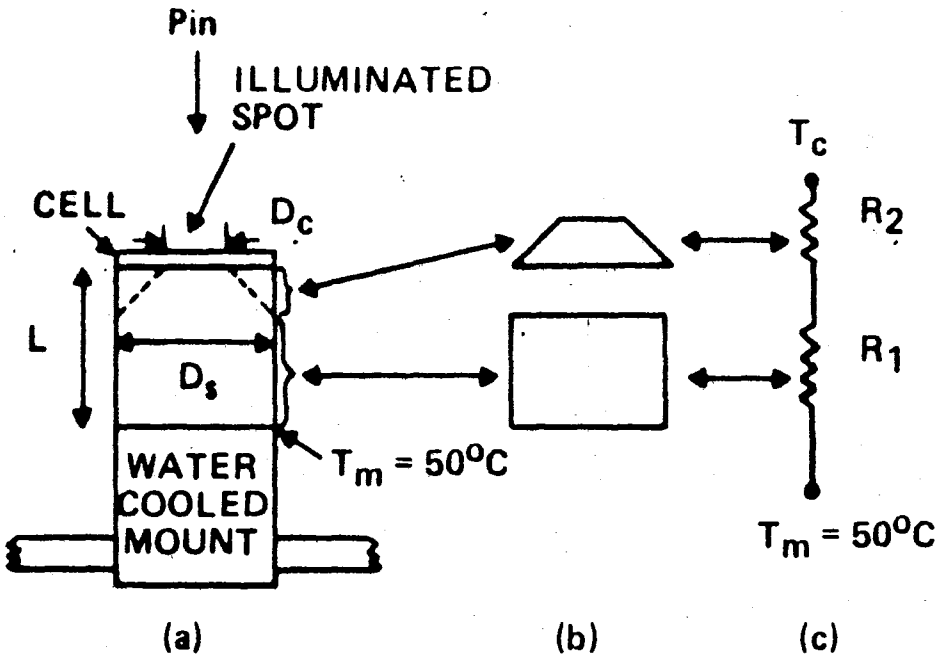

This is modeled as two thermal resistances in series, as seen in Fig. 5-4b and c. R_2 corresponds to the portion of the standoff in which the heat spreads. R_1 corresponds to the rest of the standoff. The cell temperature, T_C, is given by

$$(R_1 + R_2) \cdot P_{in} = T_C - T_m \quad ,$$

where T_m is the mount temperature.

Simple analysis gives

$$R_1 = \frac{2(D_S - D_C)}{\pi K D_S D_C}$$

$$R_2 = \frac{4\left(L + \frac{(D_C - D_S)}{2}\right)}{\pi K D_S^2}$$

where K is the thermal conductivity of the standoff.

For the design chosen, the standoff diameter, D_S, is 2.54 cm. The spot diameter on the cell is D_C = .85 cm. For stainless steel cylinders with L = 2.54 cm and K = 0.16 W/cm °K, R_1 = 7.84°K/W and R_2 = 1.83°K/W. For P_{in} = 35 watts, corresponding to about 1000 suns and 20% cell efficiency, $T_C - T_m$ = 340°C.

Since a gold-germanium solder system has not yet been developed for the cell, the spacers would have to be shortened to avoid melting the solder in the cell package.

3. Computer Interfacing

The 9835A computer has been connected to a programmable load on the laboratory roof, allowing cell performance to be automatically measured. The test setup is similar to that described below for the flash tester. The test setup has been extensively used in testing the

Varian GaAs cell module and the Varian spectral splitter module. The system can obtain a cell or module I-V curve in less than a minute.

4. Array Control

To improve the array reliability, it was decided to replace the existing analog tracking electronics with a microprocessor-based system. This is based on a Motorola MC-6800 board, driving stepping motors for both azimuth and elevation control. Battery backup ensures operation during power failure.

Interfacing the microprocessor to the stepping motors and sun sensors was more difficult than originally expected. The system was completed and appears to function properly. However, while the interfacing was being developed, the old analog tracking electronics were substantially rebuilt. The reliability of the improved analog system has been quite good. Due to the heavy demand on the array for module testing, there has not been enough time to install the microprocessor-controlled system. It is planned to install the microprocessor system whenever a lull in array use develops.

5. Flash Testing

It was necessary to develop a facility for quickly testing packaged cells under concentration with reproducible conditions, in order to assess changes in performance of cells undergoing the accelerated aging tests on the roof. To accomplish this, a computer-controlled flash test system was developed. The flash unit itself had been in use for several years, with cell current and voltage read manually from a storage oscilloscope. The manual system was very tedious and subject to error.

Reference to Fig. 5-5 shows how the computer-controlled flash tester works. A Norman 202 photographic strobe unit is mounted about 20 cm above the cell. This unit is triggered by a computer-generated relay closure. The flash intensity is variable from less than 400 to over 1200 suns, with better than 3% uniformity over the cell area, and reproducibility within the measurement limits of the detection electronics.

The cell is in series with a 5-mΩ current-sensing resistor, and with a germanium power transistor which serves as an active load controlled by the 9835 computer. The peak cell current and voltage are measured with two channels of peak detectors. The detector outputs are read sequentially into a DVM and are then read into the 9835A. The program causes the computer to vary the load resistance to pick out the open circuit voltage and short circuit current, and then to search out the peak power point, flashing the strobe once each time the load is changed.

Considerable effort was expended to show that this transient measurement gives results that accurately represent the solar cell's dc characteristics. This aim has been accomplished; a good correlation has been found between the flash test measurement and measurements of the same cells under concentrated sunlight, both at Varian and Sandia.

Figure 5-5 FLASH TESTER

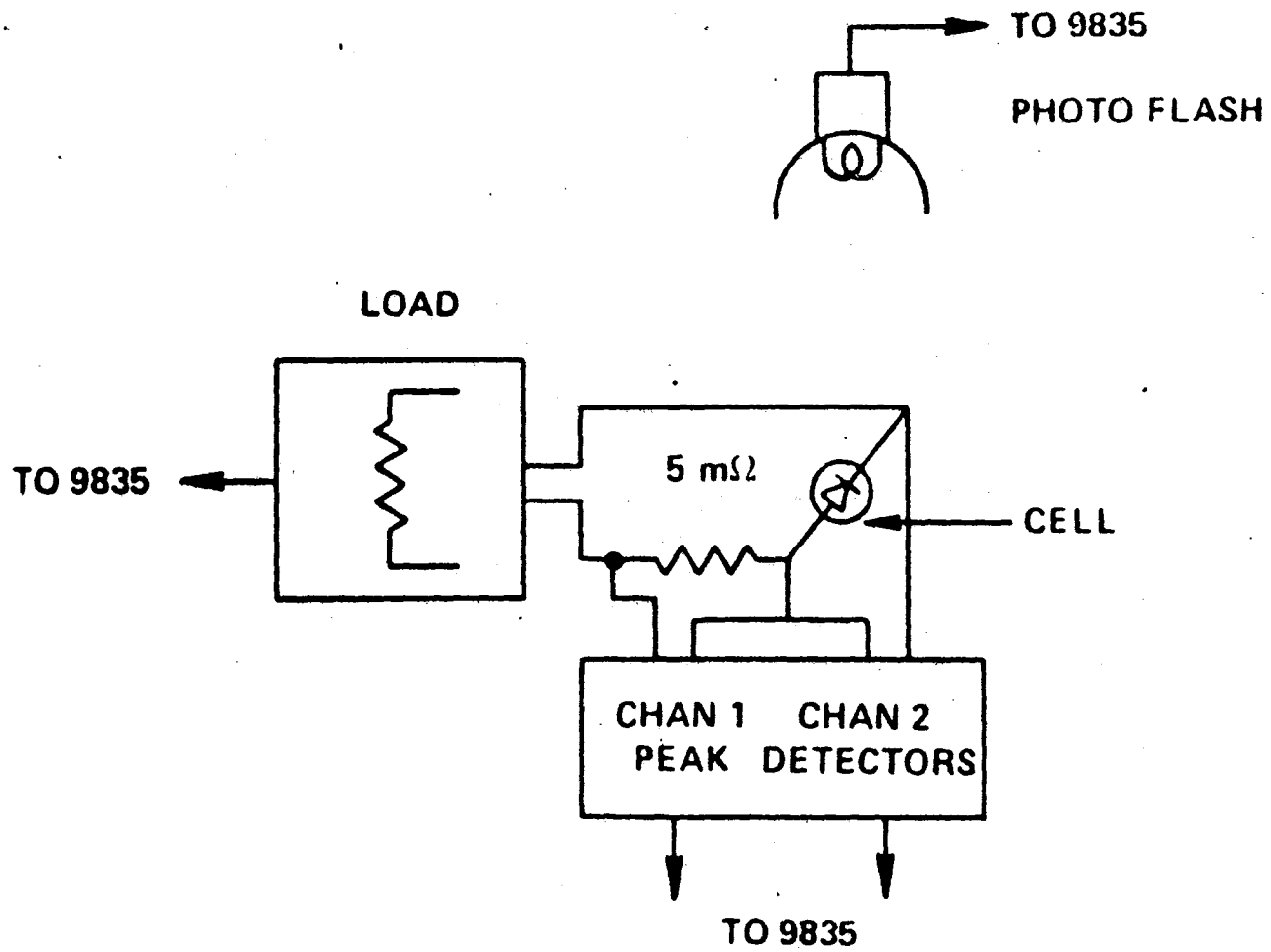

VI. SOLAR CELL FABRICATION

Sixty-four solar cells were produced under this contract and delivered to Sandia, in addition to the 53 cells that were used in the tests described in Section II. Of the cells sent to Sandia, half were 1/3-inch LPE cells and half were 1/2-inch OM cells. The efficiency, short circuit current, open circuit voltage, and fill factor for these cells -- measured with the flash tester at ~400 AM2 suns -- are given in Tables III and IV.

TABLE III

Flash test characteristics of packaged, 1/3-inch LPE GaAs solar cells delivered to Sandia under this contract.

	CELL	E	Isc	Voc	F
1.	8/13/80 BLR6	20.65	4.30	1.153	.764
2.	8/13/80 CLR3	20.48	4.41	1.155	.738
3.	4/28/80 ARF#4	19.89	3.88	1.141	.805
4.	8/13/80 BLR3	19.85	4.35	1.150	.729
5.	4/29/80 ARF#6	19.55	3.90	1.131	.793
6.	4/28/80 ARF#7	19.38	3.88	1.131	.791
7.	8/12/80 BLR1	19.34	4.12	1.150	.739
8.	4/29/80 BRF7	19.24	3.78	1.131	.806
9.	8/13/80 BLR2	19.17	4.36	1.153	.700
10.	4/28/80 ARF#6	19.10	3.80	1.132	.795
11.	4/28/80 ARF#8	18.88	3.88	1.130	.770
12.	4/28/80 ARF#5	18.78	3.86	1.127	.774
13.	4/28/80 ARF3	18.69	3.83	1.129	.785
14.	4/28/80 BRF#2	18.62	3.77	1.133	.775
15.	4/29/80 ARF#1	18.29	3.73	1.136	.773
16.	8/13/80 ALR5	18.26	4.36	1.143	.673
17.	8/13/80 ALR1	18.19	4.23	1.128	.690
18.	4/29/80 CRF#8	18.10	3.49	1.138	.815
19.	1/25/80 IRF#2	17.73	3.65	1.132	.765
20.	4/29/80 CRF#4	17.47	3.52	1.139	.780
21.	4/29/80 BRF4	17.15	3.68	1.126	.740
22.	8/12/80 ALR1	16.79	3.80	1.135	.704
23.	4/29/80 ARF#5	16.66	3.54	1.126	.749
24.	5/1/80 ARF#1	16.60	3.46	1.135	.758
25.	5/1/80 BRF9	16.59	3.69	1.107	.737
26.	8/13/80 CLR2	16.55	4.17	1.128	.645
27.	5/1/80 ARF#3	16.12	3.54	1.140	.715
28.	8/12/80 ALR6	15.95	3.59	1.116	.721
29.	5/1/80 BRF#2	15.89	3.86	.957	.764
30.	5/1/80 BRF#4	15.69	3.80	1.088	.679
31.	1/25/80 IRF#3	15.44	3.70	1.075	.694
32.	8/13/80 ALR2	14.57	4.37	1.037	.583

TABLE IV

Flash test characteristics of packaged, 1/2-inch OM GaAs solar cells delivered to Sandia under this contract.

	CELL	S#	E	Isc	Voc	F
1.	OM797 #2	49	22.42	9.79	1.162	.754
2.	OM729 A2	40	22.10	9.14	1.160	.805
3.	20M194 B2	25	21.89	8.87	1.164	.824
4.	OM796 #2	47	21.83	9.73	1.154	.744
5.	OM729 A1	39	21.53	9.12	1.160	.786
6.	OM798 #1	50	21.29	9.46	1.155	.745
7.	OM775 #2	42	21.20	8.93	1.165	.779
8.	OM799 #1	53	20.94	9.98	1.152	.697
9.	20M187 #1	33	20.52	8.86	1.136	.782
10.	OM794 #3	36	20.44	9.67	1.146	.707
11.	OM794 #2	46	20.43	9.60	1.153	.706
12.	20M194 B3	26	20.37	8.99	1.159	.772
13.	OM775 #3	43	20.37	8.33	1.153	.811
14.	20M194 F3	23	20.25	9.37	1.144	.729
15.	OM775 #4	44	20.10	8.98	1.162	.737
16.	20M192 A1	20	20.08	9.80	1.142	.688
17.	OM798 #3	51	20.05	9.93	1.153	.670
18.	OM797	52	19.84	9.83	1.156	.668
19.	20M194 F2	22	19.74	9.42	1.143	.708
20.	OM728 A2	32	19.63	8.27	1.153	.794
21.	20M185 D1	6	19.49	8.08	1.144	.810
22.	OM799 #2	54	19.38	9.93	1.146	.652
23.	20M185 C1	5	18.98	8.88	1.141	.720
24.	20M183 B2	3	18.87	7.61	1.156	.808
25.	OM728 A1	31	18.87	8.32	1.154	.758
26.	OM725 #1	27	18.78	9.34	1.140	.681
27.	OM799 #3	55	18.76	10.00	1.146	.626
28.	20M183 F2	1	18.47	7.51	1.156	.801
29.	OM728 B1	37	18.39	7.67	1.156	.801
30.	20M185 B1	4	18.35	8.32	1.136	.746
31.	20M183 B1	2	18.25	7.65	1.151	.790
32.	OM825 B1	56	18.12	8.77	1.137	.695

VII. CONCLUSIONS AND RECOMMENDATIONS

The tests described above have shown the basic GaAs cell to be rugged. The projected lifetimes from the thermal stress experiment at a cell temperature of 100°C show that thermally-activated degradation mechanisms within the cell should not be a limit to cell performance in practical photovoltaic systems. The studies of AlGaAs corrosion show that with a properly applied Si_3N_4 protective coating, the cell can withstand high temperature/humidity stressing. The OM cell was shown to be more resistant to AlGaAs corrosion than are LPE cells. Encapsulation of the cell with a cover glass gives further protection, insuring that degradation due to AlGaAs corrosion can be prevented.

The major limitations of tests performed so far are that they have relied on one-sun testing for characterization of the cells, and that the cell was in a passive state during testing. The reliance on one-sun testing means that any increases of resistivity within the cell that would only show up under concentrated sunlight evaluation may have been missed. The testing was restricted to one-sun illumination because testing under concentration requires packaged cells, and the cell package cannot withstand the ~400°C temperatures required to produce a significant number of failures. The fact that the cells were passive during thermal stressing (i.e., no current was flowing through them) means that any degradation mechanisms activated by both current and temperature were missed in the tests.

The rooftop tracking concentrator tests that were planned would complement well the thermal stress tests that were performed. Since the roof tests would test fully packaged cells, the cells would be evaluated with concentrated sunlight testing, or with the flash tester at high equivalent concentration levels. Since neither roof test relies on thermal stressing alone, the cell can be stressed without exceeding the

temperature at which the solder in the package will melt. In particular, the high-intensity illumination experiment would test cells for any degradation activated by higher than normal photon flux or current density. The combined thermal/illumination experiment would test for any degradation activated by the combination of current and high temperature.

Both of the roof tests could be started with little additional effort. Mirrors and cell holders are on hand for both experiments. Corrector lens elements for the high-intensity illumination test have been received, and the thermal standoffs for the combined thermal/illumination experiment have been fabricated. The only remaining requirements for the experiments are the production of a sufficient number of 1/3-inch cells, and fabrication of mounts for the high-concentration mirrors and corrector lens elements. Neither requirement should pose any problems.

The study of ohmic contact degradation and electromigration in the contact grid was intended to complement the one-sun evaluation of the thermally-stressed cells, since those tests would point up likely sources of increased series resistance in the cell that would limit performance at high concentration levels. The ohmic contact aging studies that were performed did not show any serious degradation of the p-type contact. While it would be useful to perform more studies of the ohmic contacts and to perform the electromigration study, it would probably be best to postpone those studies until results of the roof tests became available and perform them only if it appeared that they would be useful in interpreting the results of the roof tests.

Another technique for applying current and temperature stressing to a cell is to pass a forward current of, say, 20 amps through the cell while it is heated in an oven. This technique has the advantage over

the combined thermal/illumination test in that it holds the cell temperature constant, rather than the fluctuating cell temperature that would be developed in the roof tests. The major disadvantage of this technique is the fact that the current flow through the cell is in the reverse direction from that produced under illumination. That fact might make the results of the test difficult to relate to normal cell operation. However, this test could be useful if performed in conjunction with the roof tests.

In summary, we feel that the most useful results of further accelerated aging studies would come from the roof tests, since those tests stress the cells in a way that is closely related to actual cell operating conditions in a photovoltaic system.

REFERENCES

1. H. A. Vander Plas, L. W. James, R. L. Moon and N. J. Nelson, 13th Photovoltaic Specialists' Conf. (IEEE, New York, 1978), p. 934.

2. P. W. Chye, I. Lindau, P. Pianetta, C. M. Garner, C. Y. Su and W. E. Spicer, Phys. Rev. B 18, 5545 (1978).

3. H. B. Kim, G. G. Sweeney and T. M. S. Heng in Gallium Arsenide and Related Compounds, Inst. Phys. Conf. Ser. 24, 307 (1975).

4. J. Gyulai and J. W. Mayer, J. Appl. Phys. 42, 3578 (1971).

5. W. Nelson, IEEE Trans. Elec. Insulation EI-6, 165 (1971).

6. G. J. Hahn and W. Nelson, IEEE Trans. Reliability R-23, 2 (1974).

7. D. S. Peck and O. D. Trapp, Accelerated Testing Handbook (Technology Associates, 1978).

8. R. Gereth and W. Scherber, J. Electrochem. Soc. 119, 1248 (1972).

DISTRIBUTION LIST:

Acurex Corporation (2)
George Sutton
Bob Spencer
485 Clyde Avenue
Mountain View, CA 94042

Aerospace Corporation
Attn: Ed Simburger
2350 El Segundo Blvd.
El Segundo, CA 90266

Applied Solar Energy Corp. (3)
Attn: Steve Olah
Frank Ho
Ken Ling
15251 E. Don Julian Road
City of Industry, CA 91746

Arizona State University (2)
Attn: Charles Backus
Robert Sanderson
College of Engineering
Tempe, AZ 85261

Battelle
Attn: Don Carmichael
505 King Avenue
Columbus, OH 43201

BDM Corporation (3)
Attn: Tim Lambarski
Wayne Kauffman
Bill Schwinkendorf
1801 Randolph Road SE
Albuquerque, NM 87111

Chevron Research (2)
Attn: John Cape
R. Creek
576 Standard Avenue
Richmond, CA 94802

Cyro Industries
697 Route 46
Clifton, NJ 07015

U. S. Dept. of Energy (2)
ALO
Attn James Morley
Ethan Walker
P. O. Box 5400
Albuquerque, NM 87115

U. S. Dept. of Energy (7)
Division of PV Energy Systems
Attn: M. B. Prince (5)
L. A. Barrett
A. Scollaro
1000 Independence Ave. SW
Washington, DC 20585

E-Systems (2)
Attn: Mark O'Neill
A. J. McDanal
P. O. Box 226118
Dallas, TX 75266

General Electric Co.
Attn: Ron Hodge
P. O. Box 527
King of Prussia, PA 19406

International Rectifier
Attn: Harold Weinstein
235 Kansas Street
El Segundo, CA 91214

Intersol Power Corp.
Attn: John Sanders
7400 W Radcliff Avenue
Littleton, CO 80123

Jet Propulsion Lab (2)
Attn: K. Shimada
R. Ferber
4800 Oak Grove Drive
Pasadena, CA 91109

Martin Marietta (4)
Attn: S. Broadbent
M. Imamura
D. Hughes
J. Baumann
P.O. Box 179
Denver, CO 80201

Microwave Associates
Attn: Jonathon Chapple-Sokol
South Avenue MS-116
Burlington, MA 01803

3M
Attn: Sanford Cobb
Industrial Optics
235 2D15
3M Center
St. Paul, MN 55144

Motorola
Attn: Keith Kingston
GED
8201 E. McDowell
Scottsdale, AZ 85252

NASA, HQ
Attn: John Loria
Code RET-1
Washington, DC 20546

New Shelter Home Magazine
9317 Shoshone
Albuquerque, NM 87111

Oak Ridge National Lab
Attn: Steve Kaplan
P. O. Box X
Oak Ridge, TN 37830

Oklahoma University
571 South University Blvd.
Norman, OK

Photowatt (2)
Attn: William Taylor
Mike Keeling
2414 W. 14th Street
Tempe AZ 85281

Power Hybrids
Attn: Jeff Meyer
1742 Crenshaw Blvd.
Torrance, CA 90501

PRC
Attn: E. Stirewalt
5201 Leesburg Pike
Suite 400
Falls Church, VA 22070

Purdue University (2)
Attn: Richard Schwartz
Mark Lundstrom
Electrical Engineering Dept.
West Lafayette, IN 47907

Ray Bahm & Associates
Attn: Ray Bahm
2513 Kimberly Court NW
Albuquerque, NM 87130

Research Triangle Institute
Attn: Mayrant Simons
Box 12194
Research Triangle Park, NC 27709

Rockwell International
Microelectronics Research &
Development Center
Attn: Stan Zehr
1049 Camino Dos Rios
Thousand Oaks, CA 91360

SERI (3)
Attn: Gene Blakeslee
Lee Cole
John Benner
1617 Cole Blvd.
Golden, CO 80401

SERI, Library (2)
1536 Cole Blvd., Bldg. #4
Golden, CO 80401

Southern Cal Edison
Attn: Spencer Carlisle
2244 Walnut Grove Ave.
Rosemead, CA 91770

Spectrolab
Attn: Brian Elm
12500 Gladstone Avenue
Sylmar, CA 91342

Star Light Energy
Attn: J. Furber
1717 18th Street NW
Washington, DC 20009

Strategies Unlimited
201 San Antonio Circle
Suite 205
Mountain View, CA 94040

Solar Works
Attn: Paul Wilkins
Route 2, Box 274
Santa Fe, NM 87501

Thermo Electron
Attn: Ron Scharlack
45 First Avenue
Waltham, MA 02154

UNM/NMERI
Attn: G. Leigh
Campus Box 25
Albuquerque, NM 87131

Varian & Associates (2)
Attn: Peter Borden
N. Kaminar
611 Hansen Way K-219
Palo Alto, CA 94303

Wright Patterson AFB
Attn: Jack Geis
AFWAL/POOC
Wright Patterson AFB, OH

Wyle Labs (2)
Attn: Dave Christenson
George Meares
7800 Governors Drive West
Huntsville, AL 35807

Alliance Tool Corp.
Attn: Helmut Walter
1300 Mt. Read Blvd.
Rochester, NY 14606

Spire (3)
Attn: S. Tobin
M. Nowlan
R. Little
Patriots Park
Bedford, MA 01730

2146	B. Hanson
2146	B. Nasby
2146	J. Rodriguez
2146	B. Rose
2146	H. Weaver
4700	E. Beckner
4720	D. Schueler
4721	H. Gerwin
4721	W. Schimmel
4723	E. Burgess
4724	D. Arvizu
4724	L. Beavis
4724	E. Boes
4724	C. Chiang
4724	M. Edenburn
4724	D. King
4724	A. Miash
4724	M. Rios
5133	R. Chaffin
5133	J. Wiczer
5811	R. Assink
8214	M. Pound
3141	L. Erickson (5)
3151	W. Garner (3)
3154-3	C. Dalin (25) for DOE/TIC Unlimited Distribution